

**Westinghouse Non-Proprietary Class 3**



**Westinghouse Improved  
Performance Analysis and Design  
Model (PAD 4.0)**

**Westinghouse Electric Company LLC  
Nuclear Fuel Business Unit**

**WCAP-15064  
Revision 1**



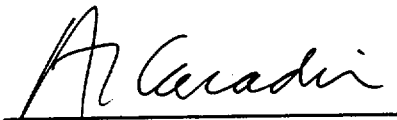
**Westinghouse Improved  
Performance Analysis and Design Model  
(PAD 4.0)**

June 1998 original  
November 1999 revision

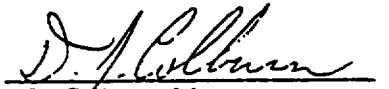
Authors:  
J. P. Foster  
S. Sidener

Edited by:  
W. H. Slagle

APPROVED:

  
A. L. Casadei, Manager  
Core Engineering  
Nuclear Fuels Business Unit

APPROVED:

  
D. Colburn, Manager  
Materials and Fuel Rod Design  
Nuclear Fuels Business Unit

**Westinghouse Electric Company  
Nuclear Fuel Business Unit  
P. O. Box 355  
Pittsburgh, Pennsylvania 15230**

## Table of Contents

### Section 1: Westinghouse In-Reactor Creep Model

<u>Sub-section</u>	<u>Title</u>	<u>Page</u>
1.0	Introduction & Background . . . . .	1
1.1	Purpose . . . . .	1
1.2	Discussion of PAD 3.4 Creep Model . . . . .	1
1.3	Evaluation of PAD 3.4 Creep Model - Need for Change . . . . .	2
2.0	New PAD In-Reactor Creep Model . . . . .	4
2.1	In-reactor Thermal Creep Overview . . . . .	4
2.2	Irradiation Enhanced Creep Overview . . . . .	5
3.0	Creep Model Detailed Justification . . . . .	7
3.1	Out-of-Reactor (Laboratory) Thermal Creep . . . . .	7
3.2	In-reactor Thermal Creep . . . . .	9
3.2.1	Irradiation Hardening . . . . .	9
3.2.1.1	Model Development . . . . .	9
3.2.1.2	Model Evaluation . . . . .	11
3.2.2	Irradiation Creep . . . . .	12
3.2.2.1	Modeling of the B&W/EPRI Data . . . . .	12
3.2.2.2	Normalization of B&W/EPRI Irradiation Creep to Westinghouse Behavior . . . . .	14
3.2.2.3	Irradiation Creep Temperature Dependence . . . . .	16
4.0	Application to ZIRLO™ . . . . .	17
5.0	Summary and Conclusions . . . . .	18
6.0	References for Section 1 . . . . .	19

## Table of Contents

### Section 2: Other PAD Model Changes

<u>Sub-section</u>	<u>Title</u>	<u>Page</u>
1.0	Revised PAD Code Summary of Changes . . . . .	44
1.1	Revised Creep Model . . . . .	44
1.2	Revised Rod Irradiation Growth Model . . . . .	45
1.3	Updated Zr-4 and ZIRLO™ Clad Thermal Conductivity Values . . . . .	45
1.4	Updated Zr-oxide Thermal Conductivity Values . . . . .	45
1.5	Equation of State (EOS) Gas Model . . . . .	46
1.6	Variable Oxide-Metal Ratio Model . . . . .	46
1.7	Gas Absorption in Cladding Effect . . . . .	47
2.0	Revised Rod Irradiation Growth Model . . . . .	48
2.1	Model Background and Justification . . . . .	48
2.2	PAD Revision . . . . .	48
3.0	Updated Zr-4 and ZIRLO™ Clad Thermal Conductivity Values . . . . .	50
3.1	Model Background and Justification . . . . .	50
3.2	Pad Revision . . . . .	50
4.0	Updated Zr-oxide Thermal Conductivity Values . . . . .	53
4.1	Model Background and Justification . . . . .	53
4.2	PAD Revision . . . . .	56
5.0	Equation of State (EOS) Gas Model . . . . .	57
5.1	Model Background and Justification . . . . .	57
5.2	Summary . . . . .	59
5.3	PAD Revision . . . . .	60
6.0	Variable Oxide-Metal Ratio Model . . . . .	63
6.1	Model Background and Justification . . . . .	63
6.2	Variable O/M Ratio Model Details . . . . .	63
7.0	Gas Absorption in Cladding Effect . . . . .	66
7.1	Model Background and Justification . . . . .	66
7.2	PAD Change . . . . .	67
8.0	References for Section 2 . . . . .	68

## List of Tables

### Section 1: Westinghouse In-Reactor Creep Model

<u>Table</u>	<u>Title</u>	<u>Page</u>
1	IMP Zr-4 Out-of-Reactor (Laboratory) Thermal Creep Data . . . . .	22
2A	Calculated STD Zr-4 Out-of-Reactor Creep Rate Values as a Function of Time . . . . .	23
2B	Out-of-Reactor Creep Rate Normalization Factor for IMP Zr-4 Data Relative to STD . . . . .	23
3	Evaluation of Zr-2.5Nb Out-of-Reactor Thermal Creep Irradiation Hardening . . . . .	24
4	Comparison of Oconee-2 In-Reactor and Out-of-Reactor (Laboratory) Creep Rate . . . . .	25
5	Average Diameter Creepdown of IMP Zr-4 and ZIRLO™ Fuel Rod in the High Power Region of North Anna Advanced Material Demonstration Assemblies . . . . .	25
6A	Westinghouse 1-Cycle Fuel Rods . . . . .	26
6B	Westinghouse High Burnup Fuel Rods . . . . .	26

## List of Tables

### Section 2: Other PAD Model Changes

<u>Table</u>	<u>Title</u>	<u>Page</u>
3-1	Thermal Conductivity as a Function of Temperature . . . . .	51
4-1	Summary of Conductivity Values From First Set of Ramps . . . . .	54
4-2	Summary of Conductivity Data . . . . .	54
5-1	Peng-Robinson EOS Component Properties List for PAD . . . . .	61

## List of Figures

### Section 1: Westinghouse In-Reactor Creep Model

<u>Figure</u>	<u>Title</u>	<u>Page</u>
1	Out-of-Reactor Thermal Creep Steady State Rate - Tin Dependence . . . . .	27
2	CW Zr-2.5Nb Pressure Tube Diameter Data (the flux data are not accurate) . . . Figure 8 of Reference 11	28
3	Creep Components - CW Zr-2.5Nb Pressure Tube . . . . . 650 K, 43 MPa Hoop Stress	29
4	CW Zr-2.5Nb Pressure Tube Diameter Data . . . . . Figure 4 of Reference 13	30
5	CW Zr-2.5Nb Pressure Tube Diameter Data . . . . . Figure 7 of Reference 14	31
6	Saturated Out-of-Reactor (Laboratory) Thermal Creep Reduction Factor . . . . .	32
7	CWSR Zr-4, B&W/EPRI, Lot S-1, 577-578 K, 69 MPa . . . . .	33
8	CWSR Zr-4, B&W/EPRI, Lot S-1, 577-578 K, 86 MPa . . . . .	34
9	CWSR Zr-4, B&W/EPRI, Lot S-1, 577-578 K, 103 MPa . . . . .	35
10	CWSR Zr-4 Saturated Transient Component, B&W/EPRI, Lot S-1, 577-578 K . .	36
11	CWSR Zr-4 Steady State Component, B&W/EPRI, Lot S-1, 577-578 K . . . . .	37
12	Comparison of Measured and Calculated Strain for CWSR Zr-4 . . . . . Lot S-1, B&W/EPRI, 577-578 K	38
13	CWSR Zr-4, Lot S-1, B&W/EPRI, 581-582 K, 103 MPa . . . . .	39
14	CWSR Zr-4 Apparent Temperature Dependence . . . . . Lot S-1, B&W/EPRI, 103 MPa	40
15	Comparison of In-Reactor and Out-of-Reactor Creep Rates . . . . . B&W/EPRI, 86 MPa	41

## List of Figures (cont.)

### Section 1: Westinghouse In-Reactor Creep Model

<u>Figure</u>	<u>Title</u>	<u>Page</u>
16	CW Zr-2 Irradiation Creep Temperature Dependence, 207 MPa . . . . . From Reference 16	42
17	CWSR IMP Zr-4 In-Reactor Creep . . . . . $1.08 \times 10^{22}$ n/cm <sup>2</sup> (E > 1 MeV), 41 MPa (6.0 ksi) Hoop Stress	43

## List of Figures

### Section 2: Other PAD Model Changes

<u>Figure</u>	<u>Title</u>	<u>Page</u>
2-1	G/G <sub>0</sub> versus Temperature . . . . .	49
3-1	Thermal Conductivity as a Function of Temperature . . . . . for Zircaloy-4 and ZIRLO™ (1st Order Fit)	52
5-1	Idea Gas Equation of State DP/P versus He Mol Fraction . . . . .	58
5-2	Peng-Robinson Equation of State DP/P versus He Mol Fraction . . . . .	59
5-3	Pen-Robinson Equation of State Measured versus Predicted Pressure . . . . .	60
6-1	Best Estimate O/M Ratio Model . . . . .	65

# **Westinghouse Improved Performance Analysis and Design Model**

## **(PAD 4.0)**

### **Executive Overview**

This revised topical report addresses all model changes made to the Westinghouse Performance Analysis and Design (PAD) model. The original topical report, submitted to the NRC in June 1998, addressed only changes made to the creep model used in the PAD model, but as the model development progressed, additional changes were identified. These additional changes were formally presented to the NRC in September 1998. Since all of these changes have been formally reviewed by the NRC, it has been requested by the NRC that the originally submitted topical report be revised to encompass all the model changes made to PAD. Therefore, the revised topical report has been divided into two sections: Section 1 (the originally submitted in-reactor creep model), and Section 2 (other model changes made to PAD and submitted to the NRC in September 1998).

PAD is a best estimate fuel rod performance model used for both fuel rod performance and safety analysis inputs. The last version of PAD that was reviewed by the NRC was PAD 3.4. The changes made to PAD 4.0 will be related to changes made from this previously licensed version (i.e., PAD 3.4).

**Section 1**  
**Westinghouse In-Reactor Creep Model**

# Westinghouse In-Reactor Creep Model

## 1.0 Introduction & Background

The Westinghouse Performance Analysis and Design (PAD) model is a best estimate fuel rod performance model used for both fuel rod performance analysis and safety analysis inputs. The PAD code consists of several fuel rod performance models integrated to predict fuel temperature, rod pressure, fission gas release, cladding elastic and plastic behavior, cladding growth, cladding corrosion, fuel densification, and fuel swelling as a function of linear power and time. Many of the fuel rod performance models were first introduced to the NRC (then AEC) in the 1972-1973 time frame<sup>(1)(2)(3)(4)</sup>. Subsequent to the original model introduction, two specific revisions have been submitted for review and approval (i.e., PAD 3.3<sup>(5)</sup> and PAD 3.4<sup>(6)</sup>). With respect to the creep model used in PAD, the original model form remains in effect except for a revision that occurred to the irradiation enhanced creep portion of the model in PAD 3.4. The thermal creep portion of the model has remained the same since the model's inception in 1972.

### 1.1 Purpose

The purpose of this section is to introduce the new creep model to be used in the overall PAD fuel rod performance model. The new creep model accounts for advances in the understanding of in-reactor creep that have occurred between 1972 and 1998, and represents a description of in-reactor creep relative to the information and data that are available in 1998. This model enhancement is projected to restore rod internal pressure limit margin to the fuel rod design criterion.

### 1.2 Discussion of the Current PAD Creep Model (PAD 3.4)

The total in-reactor creep rate,  $de/dt$ , in PAD 3.4 is evaluated as the sum of the out-of-reactor (laboratory) thermal creep rate,  $de/dt(out-rx tc)$ , plus the irradiation enhanced creep rate,  $de/dt(ic)$ .

$$de/dt = de/dt(out-rx tc) + de/dt(ic) \quad (1)$$

The out-of-reactor (laboratory) thermal creep rate,  $de/dt(out-rx tc)$ , is a function of clad temperature, clad equivalent or effective stress and time. [

] <sup>a, c</sup>.

The irradiation enhanced creep rate,  $de/dt(ic)$ , is a function of neutron flux and fluence. [

] <sup>a, c</sup>.

### 1.3 Evaluation of PAD 3.4 Creep Model - Need for Change

With the current generation of fuel and the enhanced operational performance requirements placed on the fuel (i.e., increased cycle lengths, higher operating system temperatures, higher operating power levels, higher peaking factors, and higher burnup levels), enhanced modeling and prediction capabilities are necessary to demonstrate the continued acceptable performance of the fuel to the original fuel rod design criteria. As such, new post-irradiation examination (PIE) data needs to be accounted for and incorporated into the fuel rod performance models. This new PIE data has already demonstrated a need to revise the fuel rod corrosion model in PAD<sup>(7)</sup>. In addition, other material property characteristics exist that previously had not been accounted for, either due to the lack of available data or the level of sophistication of the mechanics. With new data now available and the level of sophistication of the mechanics reaching closer to the phenomenological level, significant improvements to the fuel rod performance models can be achieved.

A review of current in-reactor creep models and methods was performed by Westinghouse relative to the state-of-the art mechanics of fuel rod behavior. This involved a detailed review of work performed by AECL and reported in 1996 by Christodoulou et al.<sup>(8)</sup>. The subsequent work performed at AECL, reported by Christodoulou, has demonstrated that the PAD 3.4 in-reactor creep model is overly conservative and needs to be revised. Christodoulou presented the formulation and results of a fundamental-empirical model describing the in-reactor creep of cold-worked (CW) Zr-2.5Nb for pressure tube application. Some of the many models proposed to describe the in-reactor creep of zirconium alloys are described in References 8, 9 and 10. The Christodoulou model is considered to be the most fundamental model that is also based on the largest in-reactor data set to date. The model includes the effects of texture, grain shape, anisotropy and the relative contributions of prismatic, basal and pyramidal planes to dislocation climb assisted glide. This in-reactor model includes data from creep measurements of pressure tubes in power reactors, pressure tubes in test reactors, small pressurized tubes in test reactors and beam stress relaxation samples in test reactors. The test data includes samples with thermal creep strain. In addition, the test data includes textures typical of both pressure and fuel-cladding tubes. As

a result, the framework of this model was selected by Westinghouse to formulate a new in-reactor creep model for fuel rod application.

According to the Christodoulou model, the in-reactor creep rate is the sum of the in-reactor thermal creep rate,  $de/dt(tc)$ , and the irradiation enhanced creep rate,  $de/dt(ic)$ .

$$de/dt = de/dt(tc) + de/dt(ic) \tag{2}$$

[

] <sup>a, c</sup>. As a result, the predicted total creep rate from the current PAD model (Equation (1)) is higher than that derived from Equation (2) and is therefore conservative. This effect will be discussed in subsequent sections.

The PAD creep model needs to be revised due to the demonstrated fact that the original PAD 3.4 creep model is conservative; therefore, there is a need to account for new PIE data and material property behavior. Specifically, the PAD 3.4 in-reactor creep model is being replaced for the following reasons:

- [

] <sup>a, c</sup>

- [

] <sup>a, c</sup>

- [

] <sup>a, c</sup> Out-of-reactor and in-reactor creep behavior is dependent on fabrication process parameters such as final area reduction, intermediate anneal temperature, final anneal temperature and time and post-extrusion anneal temperature.

- [

] <sup>a, c</sup>

- [

] <sup>a, c</sup>

## 2.0 New PAD In-Reactor Creep Model

The new in-reactor creep model developed for fuel rod application in PAD is based on [

] <sup>a, c</sup>.

According to Christodoulou, the total in reactor creep rate is the sum of the in-reactor thermal creep rate,  $de/dt(tc)$ , and the irradiation enhanced creep rate,  $de/dt(ic)$

$$de/dt = de/dt(tc) + de/dt(ic) \quad (2)$$

[ ] <sup>a, c</sup>.

The new in-reactor creep model was developed to describe Westinghouse cold-worked stress relieved (CWSR) tubing. The specific material behavior of the new PAD model is based on Westinghouse cladding. [

] <sup>a, c</sup> the new creep model

describe Westinghouse cladding.

### 2.1 In-Reactor Thermal Creep Overview

The in-reactor thermal creep component was developed using Westinghouse cold-worked stress relieved (CWSR) improved (IMP) Zr-4 (low tin Zr-4) tubing. The in-reactor thermal creep is given by the out-of-reactor (laboratory) thermal creep corrected for in-reactor irradiation hardening. This behavior is described by:

$$[ ] \quad ] \sup{a, c} \quad (3)$$

where [

] <sup>a, c</sup>. The equation [

by:  $\dot{\epsilon} = A \sigma^n \exp(-Q/RT) \exp(-k_d D_p)$ . The equation for  $\dot{\epsilon}$  is given

$$\dot{\epsilon} = A \sigma^n \exp(-Q/RT) \exp(-k_d D_p) \quad (4)$$

where  $A$  is a material constant. The equation was [1]  $\dot{\epsilon} = A \sigma^n \exp(-Q/RT) \exp(-k_d D_p)$  IMP  
 Zr-4 thermal creep tests [2]  $\dot{\epsilon}$  according to:

$$\dot{\epsilon} = A \sigma^n \exp(-Q/RT) \exp(-k_d D_p) \quad (5)$$

The irradiation hardening  $\sigma_{IH}$  [3]  $\sigma_{IH}$ . The expression for IH is:

$$\sigma_{IH} = \sigma_0 \exp(k_d D_p) \quad (6)$$

where  $\sigma_0$  is the yield strength of the material. Equation (6) provides a smooth transition with increasing fluence from no irradiation hardening  $\sigma_{IH} = \sigma_0$  to complete irradiation hardening  $\sigma_{IH} = \sigma_0 \exp(k_d D_p)$ . The application of the [4]  $\dot{\epsilon} = A \sigma^n \exp(-Q/RT) \exp(-k_d D_p)$  was supported by an evaluation of the creep activation energy (discussed below) and the in-reactor thermal creep hardening model reported by Limback and Andersson<sup>(10)</sup> for CWSR Zr-4.

## 2.2 Irradiation Enhanced Creep Overview

The new irradiation enhanced creep component was developed using [5]  $\dot{\epsilon} = A \sigma^n \exp(-Q/RT) \exp(-k_d D_p)$ . The irradiation creep behavior [6]  $\dot{\epsilon} = A \sigma^n \exp(-Q/RT) \exp(-k_d D_p)$

$\dot{\epsilon}$ . Since the [7]  $\dot{\epsilon} = A \sigma^n \exp(-Q/RT) \exp(-k_d D_p)$

creep rate equation is given by:  $\dot{\epsilon} = A \sigma^n \exp(-Q/RT) \exp(-k_d D_p)$ . The irradiation enhanced

$$\dot{\epsilon} = A \sigma^n \exp(-Q/RT) \exp(-k_d D_p) \quad (7)$$

where [

] <sup>a, c</sup>. The [ ] <sup>a, c</sup> creep rate equation is given by:

$$[ ]^{a, c} \quad (8)$$

where [

] <sup>a, c</sup>. The [

] <sup>a, c</sup>. The

equation was [

] <sup>a, c</sup> IMP Zr-4

out-of-reactor (laboratory) thermal creep tests [

] <sup>a, c</sup> and the out-of-reactor (laboratory) creep rate equation for

[ ] <sup>a, c</sup> according to:

$$[ ]^{a, c} \quad (9)$$

The [ ] <sup>a, c</sup> measurements were performed at PWR reactor coolant temperature.

Irradiation enhanced creep increases with increasing temperature. The [

] <sup>a, c</sup> in:

$$[ ]^{a, c} \quad (10)$$

where [

] <sup>a, c</sup>. Hence, Equation (10) gives the [

] <sup>a, c</sup>.

A more detailed evaluation of each component of the PAD model is provided in the subsequent sections.

### 3.0 Creep Model Detailed Justification

As stated in the previous section, a more detailed justification for the equations and coefficients follows below for a more thorough understanding of Westinghouse's model development.

#### 3.1 Out-of-Reactor (Laboratory) Thermal Creep

The out-of-reactor (laboratory) creep behavior of CWSR Zr-4 tubing fabricated by Westinghouse was established for [ ]<sup>a, c</sup>. Internal pressure creep tests were conducted using [

] <sup>a, c</sup>. The test samples in each test condition were strained into the secondary creep region. The internal pressure and diametral strain were converted to mid-wall hoop stress and strain. The mid-wall hoop strain data were analyzed by separating the total strain into primary and secondary components. The following equations resulted:

- Total creep strain,  $e$  (fraction):

$$[ ]^{\text{a, c}} \quad (11)$$

where  $t$  is the time (hour).

- Secondary creep rate,  $(de/dt)_s$  (fraction/hour):

$$[ ]^{\text{a, c}} \quad (12)$$

where [

$$]^{\text{a, c}}.$$

- Elastic modulus,  $E_E$  (psi):

$$[ ]^{\text{a, c}} \quad (13)$$

where  $TF$  is the temperature in ( $^{\circ}F$ ).

- Saturated primary strain,  $e_p$  (fraction):

$$[ \quad ]^{a, c} \quad (14)$$

- Time coefficient, K:

$$[ \quad ]^{a, c} \quad (15)$$

The PAD code calculates [

$$]^{a, c}$$

is:

$$[ \quad ]^{a, c} \quad (16)$$

The coefficient [

$]^{a, c}$  is therefore given by:

$$[ \quad ]^{a, c} \quad (17)$$

### 3.2 In-Reactor Thermal Creep

#### 3.2.1 Irradiation Hardening

##### 3.2.1.1 Model Development

The determination of the in-reactor creep components may be illustrated by the CW Zr-2.5Nb pressure tube reported by Fidleris<sup>(11)</sup> as shown in Figure 2. The tube was irradiated for 27,550 hours in the Whiteshell WR-1 test reactor. At the outlet end of the tube the temperature is 650K (711 °F) and the hoop stress is 43 MPa (6.2 ksi), [ ]<sup>a, c</sup>. These temperatures are considerably higher than normal CANDU pressure tube service operation temperatures, because the Whiteshell test reactor used organic coolant.

[

] <sup>a, c</sup>. This clearly shows that irradiation reduces the out-of-reactor (laboratory) thermal creep strain, i.e., that irradiation hardening of out-of-reactor (laboratory) thermal creep occurs.

The irradiation hardening of out-of-reactor (laboratory) thermal creep is further illustrated by [

$\dot{\epsilon}^a, c$ . This clearly shows that irradiation decreases (or "hardens") the out-of-reactor (laboratory) thermal creep. [

$\dot{\epsilon}^a, c$ .

The irradiation hardening effect on the out-of-reactor (laboratory) thermal creep is even noticeable [

$\dot{\epsilon}^a, c$ .

The irradiation enhanced component is [

$\dot{\epsilon}^a, c$ .

[

$\dot{\epsilon}^a, c$

(18)

This is shown in Figure 3 as the irradiation enhanced component.

The irradiation hardening [

$\sigma$  may be described by an equation of the form:

$$\sigma = \sigma_0 \left[ 1 + \frac{K \Phi^n}{1 + K \Phi^n} \right] \quad (19)$$

where  $\Phi$  is the fluence in  $n/cm^2$  ( $E > 1$  MeV). Equation (19) provides a smooth transition with increasing fluence from no irradiation hardening [ $\sigma = \sigma_0$ ] to complete irradiation hardening [ $\sigma = \sigma_0 (1 + K \Phi^n)$ ].

### 3.2.1.2 Model Evaluation

The irradiation hardening factor,  $K$ ,

was determined from the results shown in Figure 3. The results were:

$$K = 1.5 \times 10^{-11} \text{ cm}^2 \text{ n}^{-n} \quad (20)$$

$$n = 1.5$$

The  $K$

was determined. The result was:

$$K = 1.5 \times 10^{-11} \text{ cm}^2 \text{ n}^{-n} \quad (21)$$

These results indicate that the in-reactor irradiation hardening of thermal creep is

$$\sigma = \sigma_0 \left[ 1 + \frac{K \Phi^n}{1 + K \Phi^n} \right]$$

Limback and Andersson<sup>(10)</sup> reported a model that describes the in-reactor creep behavior of CWSR Zr-4 cladding. The  $K$

$\epsilon^{a,c}$ . The

equations are:

$$[\epsilon^{a,c}] \quad (22)$$

where  $\epsilon^{a,c}$  and:

$$[\epsilon^{a,c}] \quad (23)$$

where  $\epsilon^{a,c}$

$\epsilon^{a,c}$  Equation (23) becomes:

$$[\epsilon^{a,c}] \quad (23a)$$

The calculated IH factors using Equation (23a) are presented in Figure 6 as a dashed line. Figure 6 shows that the calculated  $\epsilon^{a,c}$

$\epsilon^{a,c}$ .

### 3.2.2 Irradiation Creep

#### 3.2.2.1 Modeling of the B&W/EPRI Data

The determination of the irradiation enhanced creep component was performed using the reported B&W/EPRI Oconee-2 creepdown data<sup>(15)</sup>. The tabulation presented by Franklin<sup>(20)</sup> is the  $\epsilon^{a,c}$

$\epsilon^{a,c}$ . The hoop strain,  $\Delta D/D$ , was

described by an equation of the form:

$$[\epsilon^{a,c}] \quad (24)$$

where  $\epsilon^{a,c}$

] a, c.

[

] a, c

(25)

[

] a, c

Figure 12 shows that this fit is in excellent agreement with the data.

[

] a, c.

The steady state irradiation creep component is [

] a, c.

The [

] <sup>a, c</sup>.

### 3.2.2.2 Normalization of B&W/EPRI Irradiation Creep to Westinghouse Behavior

The B&W/EPRI in-reactor creep data [

] <sup>a, c</sup>.

The out-of-reactor (laboratory) thermal creep rates may be [

] <sup>a, c</sup>.

The irradiation enhanced creep behavior [

] <sup>a, c</sup> according to Equation (26):

$$[ \quad ]^{a, c} \quad (26)$$

[

$$]^{a, c};$$

$$[ \quad ]^{a, c} \quad (27)$$

Equation (27) may be written as:

$$[ \quad ]^{a, c} \quad (28)$$

For [

] <sup>a, c</sup>. Equation (28) becomes,

$$[ \quad ]^{a, c} \quad (29)$$

which is the form of Equation (26). Hence, Equations (26) and (27) are related by the relationships,

[

] <sup>a, c</sup>. The conversion factors are:

$$[ \quad ]^{a, c} \quad (30)$$

$$[ \quad ]^{a, c}$$

and the resulting equation for [ <sup>a, c</sup> ] is:

$$[ \quad ]^{a, c} \quad (31)$$

where [

$$]^{a, c};$$

$$[ \quad ]^{a, c} \quad (32)$$

The average value for  $C_3$  was

$$[ \quad ]^{a, c} \quad (33)$$

This factor was [   
 ]<sup>a, c</sup>.

### 3.2.2.3 Irradiation Creep Temperature Dependence

The irradiation creep temperature dependence was [

] <sup>a, c</sup>.

The data may be described by a function:

$$[ \quad ]^{a, c} \quad (34)$$

where [   
 ]<sup>a, c</sup>.

#### 4.0 Application to ZIRLO™

The in-reactor creep model developed above to describe CWSR IMP Zr-4 may be applied to ZIRLO™. This application may be accomplished using the Westinghouse IMP Zr-4 and ZIRLO™ fuel rod creepdown data. Generally, after 1-cycle, the cladding is freestanding (i.e., fuel pellet contact has not occurred).

[

] <sup>a, c</sup>.

The irradiation creep behavior exhibited by Westinghouse IMP Zr-4 and ZIRLO™ fuel rods is considered to be consistent with in-reactor irradiation creep data. [

] <sup>a, c</sup>.

Higher burnup Westinghouse IMP Zr-4 and ZIRLO™ fuel rods are available. Table 6B [

] <sup>a, c</sup>. As a result of this ZIRLO™ creep discussion, a multiplier will be used to account for ZIRLO™ creep as compared to IMP Zr-4 creep.

## 5.0 Summary and Conclusions

In summary, the discussion above presented a new in-reactor creep model. The model was developed based on the best available zirconium alloy in-reactor creep models and data available to date. The model is consistent with fundamental descriptions of in-reactor creep. As a result of the mechanistic approach, the model is expected to be much more consistent with in-reactor creep behavior. The model describes the behavior of Westinghouse CWSR tubing. The total in-reactor creep rate is composed of irradiation enhanced and in-reactor thermal components. The irradiation enhanced component is dependent on the stress, flux (and fluence) and temperature. The in-reactor thermal component is dependent on the stress, time, temperature and fluence.

## 6.0 References

1. Letter from R. Salvatori (Westinghouse) to D. F. Knuth (AEC), NS-SL-518, December 22, 1972.
2. Letter from R. Salvatori (Westinghouse) to D. F. Knuth (AEC), NS-SL-521, January 4, 1973.
3. Letter from R. Salvatori (Westinghouse) to D. F. Knuth (AEC), NS-SL-524, January 4, 1973.
4. Letter from R. Salvatori (Westinghouse) to D. F. Knuth (AEC), NS-SL-543, January 12, 1973.
5. Miller, J. V. (Ed.), "Improved Analytical Models Used in Westinghouse Fuel Rod Design Computations," WCAP-8720 (Proprietary), WCAP-8785 (Non-proprietary), October 1976 and letter from J. F. Stolz (NRC) to T. M. Anderson (Westinghouse), "Safety Evaluation of WCAP-8720," February 9, 1979.
6. Weiner, R. A. (Ed.), "Improved Fuel Performance Models for Westinghouse Fuel Rod Design and Safety Evaluations," WCAP-10851-P-A (Proprietary), WCAP-11873-A (Non-proprietary), August 1988.
7. Letter from H. A. Sepp (Westinghouse) to C. M. Craig (NRC), "Transmittal of Presentation Material," NSD-NRC-97-4948, January 17, 1997.
8. N. Christodoulou, A. R. Causey, R. A. Holt, C. N. Tome, N. Badie, R. J. Klassen, R. Sauve and C. H. Woo, "Modeling In-Reactor Deformation of Zr-2.5Nb Pressure Tubes in CANDU Power Reactors," Zirconium in the Nuclear Industry: Eleventh International Symposium, ASTM STP 1295, 1996, 518.
9. D. L. Baty, W. A. Pavinich, M. R. Dietrich, G. S. Clevinger and T. P. Papazoglou, "Deformation Characteristics of Cold-Worked and Recrystallized Zircaloy-4 Cladding," Zirconium in the Nuclear Industry: Sixth International Symposium, ASTM STP 824, ASTM, 1982, pp. 306-339.

10. M. Limback and T. Andersson, "A Model for Analysis of the Effect of Final Annealing on the In- and Out-of-Reactor Creep Behavior of Zircaloy Cladding," *Zirconium in the Nuclear Industry: Eleventh International Symposium*, ASTM STP 1295, ASTM, 1996, pp. 448-468.
11. V. Fidleris, "The Irradiation Creep and Growth Phenomena," *Journal of Nuclear Materials*, Volume 159, 1988, pg. 22.
12. N. Christodoulou, et al., ASTM STP 1175, 1974, pg 1111.
13. R. A. Holt, A. R. Causey and V. Fidleris, "Correlation of Creep and Growth of Pressure Tubes with Operating Variables and Microstructure," *Dimensional Stability and Mechanical Behaviour Irradiated Metals and Alloys*, British Nuclear Energy Society, 1983, 175.
14. A. R. Causey, V. Fidleris, S. R. MacEwen and C. W. Schulte, "In-Reactor Deformation of Zr-2.5 wt% Nb Pressure Tubes," *Influence of Radiation on Material Properties: 13th International Symposium (Part II)*, ASTM STP 956, ASTM, 1987, pp. 54-68.
15. T. P. Papazoglou and H. H. Davis, "EPRI/B&W Cooperative Program on PWR Fuel Rod Performance," EPRI Report NP-2848, Final Report, March 1993.
16. V. Fidleris, "Uniaxial In-Reactor Creep of Zirconium Alloys," *Journal of Nuclear Materials*, Volume 26, 1968, pp. 51-76.
17. Nick Christodoulou, private communication, February 1998.
18. R. P. Tucker, V. Fidleris and R. B. Adamson, "High-Fluence Irradiation Growth of Zirconium Alloys at 644 to 725 K," *Zirconium in the Nuclear Industry: Sixth International Symposium*, ASTM STP 824, ASTM, 1984, pp. 427-451.
19. A. R. Causey, "In-Reactor Stress Relaxation of Zirconium Alloys," *Zirconium in Nuclear Applications*, ASTM STP 551, 1974, pp. 263-273.
20. D. G. Franklin, G. E. Lucas and A. L. Bement, "Creep of Zirconium Alloys in Nuclear Reactors," ASTM STP 815, ASTM, 1983.

21. F. Garofalo, "An Empirical Relation Defining the Stress Dependence of Minimum Creep Rate in Metals," *Trans. AIME*, Volume 227, 1963, pg. 351.
22. H. Kunishi and A. Valvasori, "Final Report on Post-Irradiation Examinations of North Anna Advanced Demonstration Assemblies," Westinghouse CNFD Report Number PPE-97-137 Proprietary Class 2C, August 1997.
23. J. P. Foster, E. R. Gilbert, K. Bunde and D. L. Porter, "Relationship Between In-Reactor Stress Relaxation and Irradiation Creep," *Journal of Nuclear Materials*, Volume 252, 1998, pp. 89-97.
24. A. R. Causey, G. J. C. Carpenter and S. R. MacEwen, "In-Reactor Stress Relaxation of Selected Metals and Alloys at Low Temperatures," *Journal of Nuclear Materials*, Volume 90, 1980, pp. 216-223.

**Table 1**

**IMP Zr-4 Out-of-Reactor (Laboratory) Thermal Creep Data**

**a, c**

A large, empty rectangular frame with a thin black border, spanning most of the page width and height. It is positioned between the title and the page number, indicating that the table content is missing or redacted.

**Table 2A**  
**Calculated STD Zr-4 Out-of-Reactor Creep Rate Values**  
**as a Function of Time**



a, c

**Table 2B**  
**Out-of-Reactor Creep Rate Normalization Factor for IMP Zr-4 Data**  
**Relative to STD**



a, c

**Table 3**  
**Evaluation of Zr-2.5Nb Out-of-Reactor Thermal Creep**  
**Irradiation Hardening**

a, c

\* Minimum diameter near the edge of the fuel.

\*\* Diameter measured about 1 meter from the core edge.

**Table 4**  
**Comparison of Oconee-2 In-Reactor and**  
**Out-of-Reactor (Laboratory) Creep Rates.**

a, c

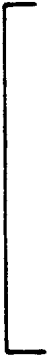


**Table 5**  
**Average Diameter Creepdown of IMP Zr-4 and ZIRLO™ Fuel Rods**  
**in the High Power Region of North Anna Advanced Material Demonstration Assemblies**

a, c



**Table 6A**  
**Westinghouse 1-Cycle Fuel Rods**

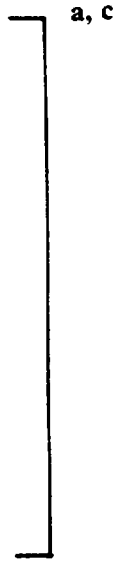


**Table 6B**  
**Westinghouse High Burnup Fuel Rods**



**Figure 1**

**Out-of-Reactor Thermal Creep Steady State Rate - Tin Dependence**

a, c

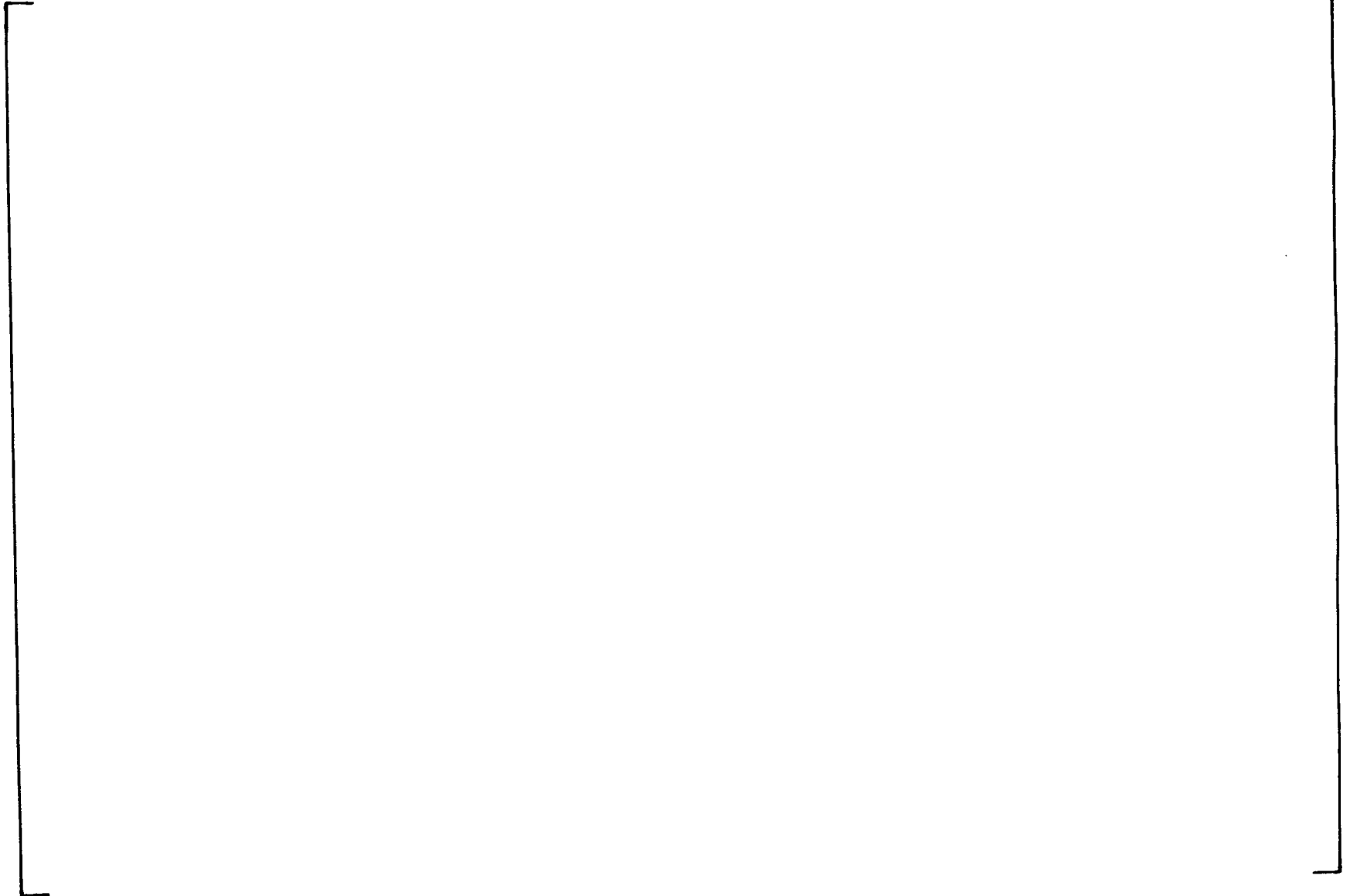


**Figure 2**  
**CW Zr-2.5Nb Pressure Tube Diameter Data (the flux data are not accurate)**  
**Figure 8 of Reference 11**

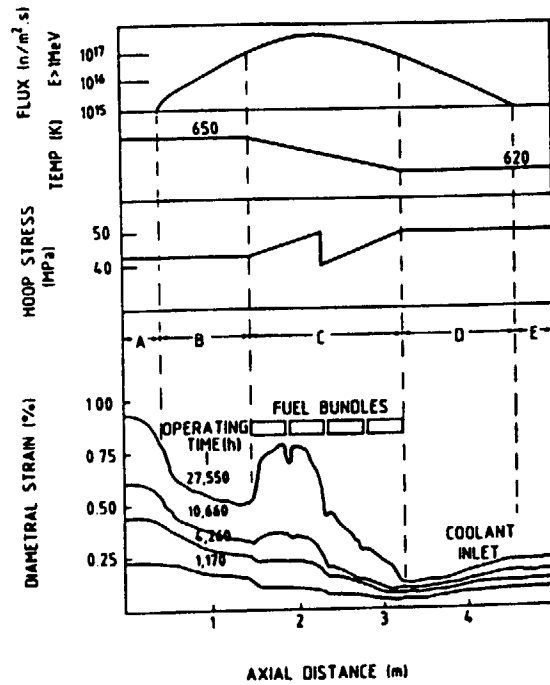
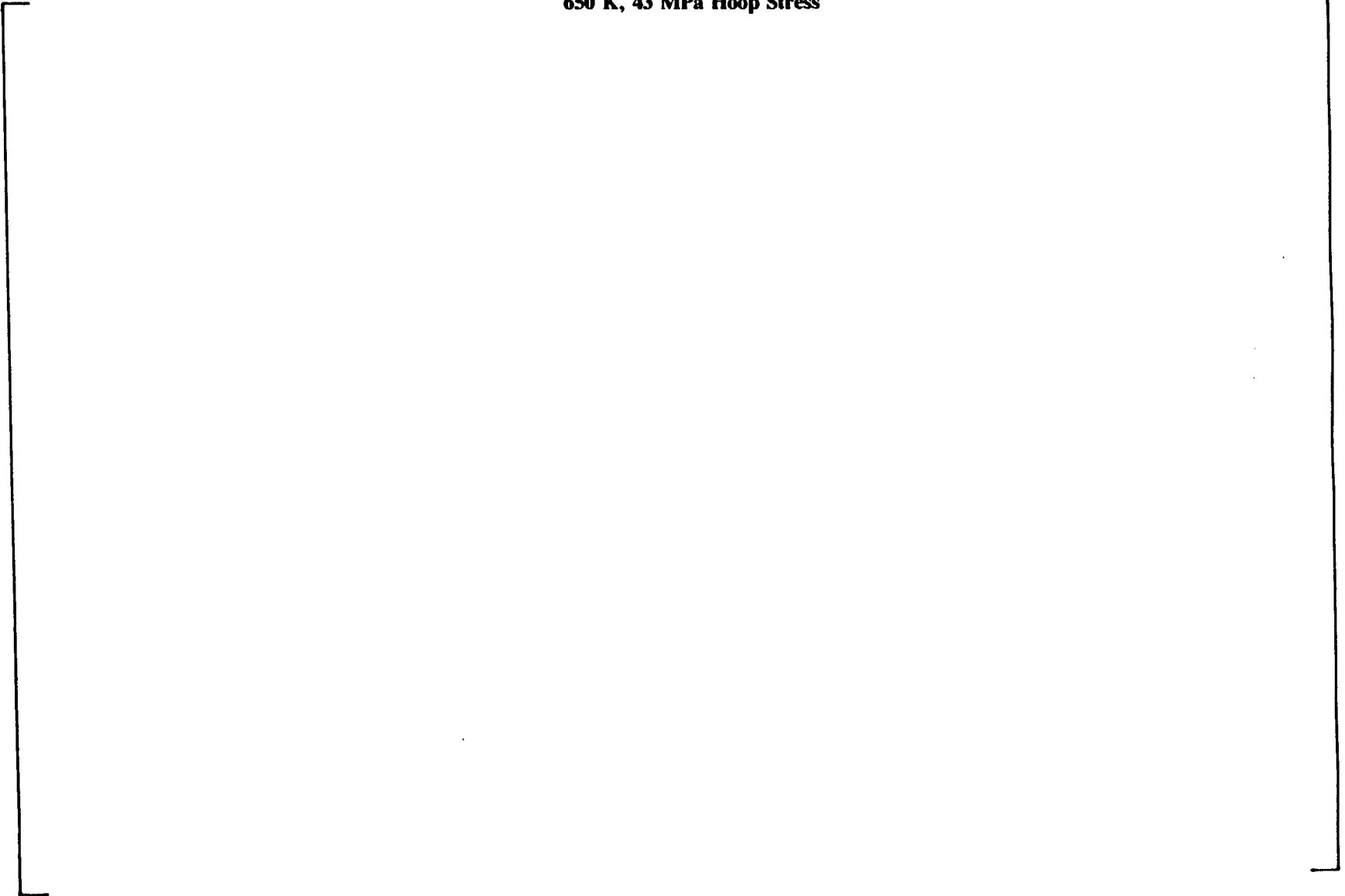


Fig. 8. Diametral creep of cold-worked Zr-2.5Nb loop tube in WR-1 reactor.

Reprinted from Journal of Nuclear Materials, Volume 159,  
 V. Fidleris, "The Irradiation Creep and Growth Phenomena", pp 22-42,  
 Copyright 1988, with permission from Elsevier Science

**Figure 3**  
**Creep Components - CW Zr-2.5Nb Pressure Tube**  
**650 K, 43 MPa Hoop Stress**

a, c



**Figure 4**  
**CW Zr-2.5Nb Pressure Tube Diameter Data**  
**Figure 4 of Reference 13**

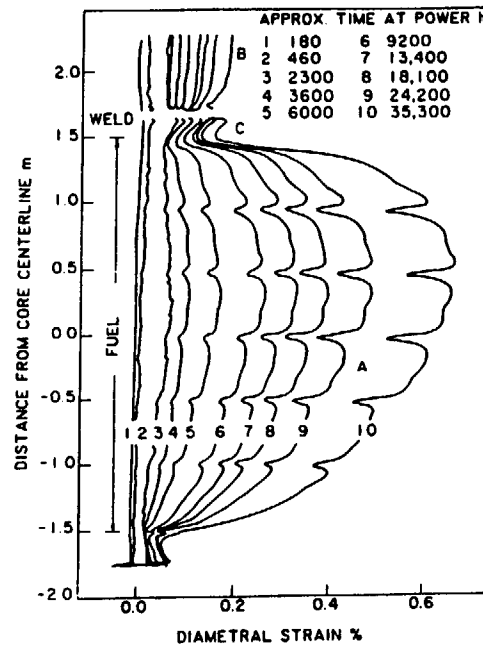


**FIGURE 4** Diametral strain of cold-worked Zr-2.5 wt% Nb pressure tube vs axial location in NRU. Illustrating

A approximate cosine distribution of strain in fueled zone  
 B creep in upper extension, and  
 C suppression of creep near edge of core.

Reprinted from Dimensional Stability and Mechanical Behaviour Irradiated Metals and Alloys, British Nuclear Energy Society,  
 R. A. Holt, A. R. Causey and V. Fidleris, "Correlation of Creep and Growth of Pressure Tubes with Operating Variables and Microstructure",  
 pp. 175-178, Copyright 1983, with permission from Thomas Telford, London.

**Figure 5**  
**CW Zr-2.5Nb Pressure Tube Diameter Data**  
**Figure 7 of Reference 14**

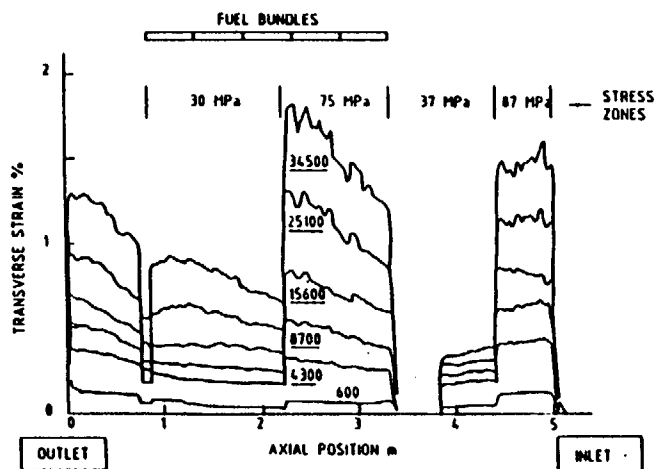


FIG. 7—Transverse strain profiles of a pressure tube in WRT.

Reprinted from Influence of Radiation on Material Properties: 13th International Symposium (Part II), ASTM STP 956,  
A. R. Causey, V. Fidleris, S. R. MacEwen and C. W. Schulte, "In-Reactor Deformation of Zr-2.5 wt% Nb Pressure Tubes", pp 54-68,  
Copyright 1987, with permission from ASTM.

**Figure 6**

**Saturated Out-of-Reactor (Laboratory) Thermal Creep Reduction Factor**

a, c



**Figure 7**

**CWSR Zr-4, B&W/EPRI, Lot S-1, 577-578 K, 69 MPa**

**a, c**



**Figure 8**

**CWSR Zr-4, B&W/EPRI, Lot S-1, 577-578 K, 86 MPa**

**a, c**



**Figure 9**

**CWSR Zr-4, B&W/EPRI, Lot S-1, 577-578 K, 103 MPa**

**a, c**



**Figure 10**

**CWSR Zr-4 Saturated Transient Component, B&W/EPRI, Lot S-1, 577-578 K**

**a, c**



**Figure 11**

**CWSR Zr-4 Steady State Component, B&W/EPRI, Lot S-1, 577-578 K**

**a, c**



**Figure 12**  
**Comparison of Measured and Calculated Strain for CWSR Zr-4**  
**Lot S-1, B&W/EPRI, 577-578 K**

a, c

**Figure 13**

**CWSR Zr-4, Lot S-1, B&W/EPRI, 581-582 K, 103 MPa**

**a, c**



**Figure 14**  
**CWSR Zr-4 Apparent Temperature Dependence**  
**Lot S-1, B&W/EPRI, 103 MPa**

a, c

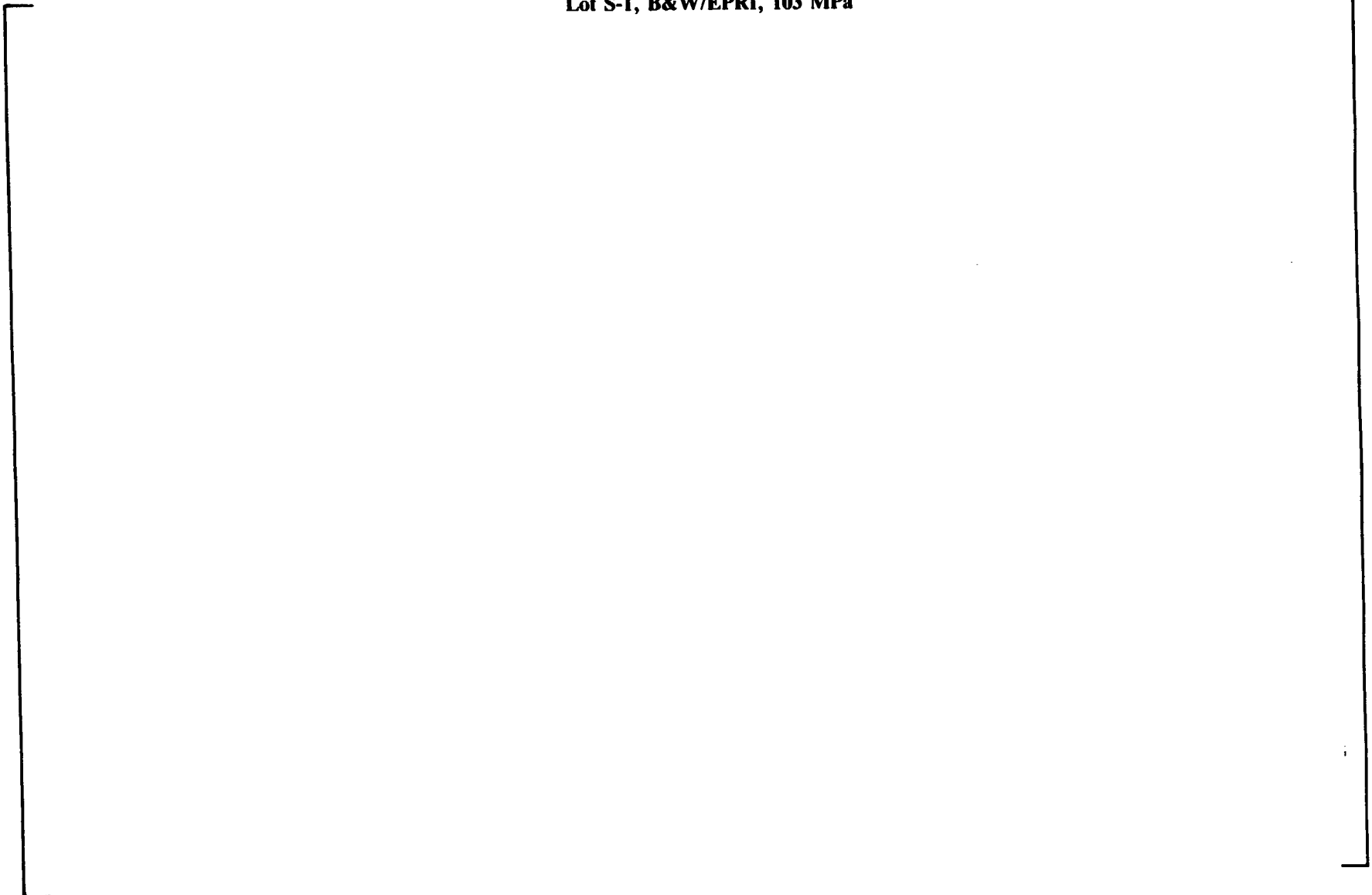
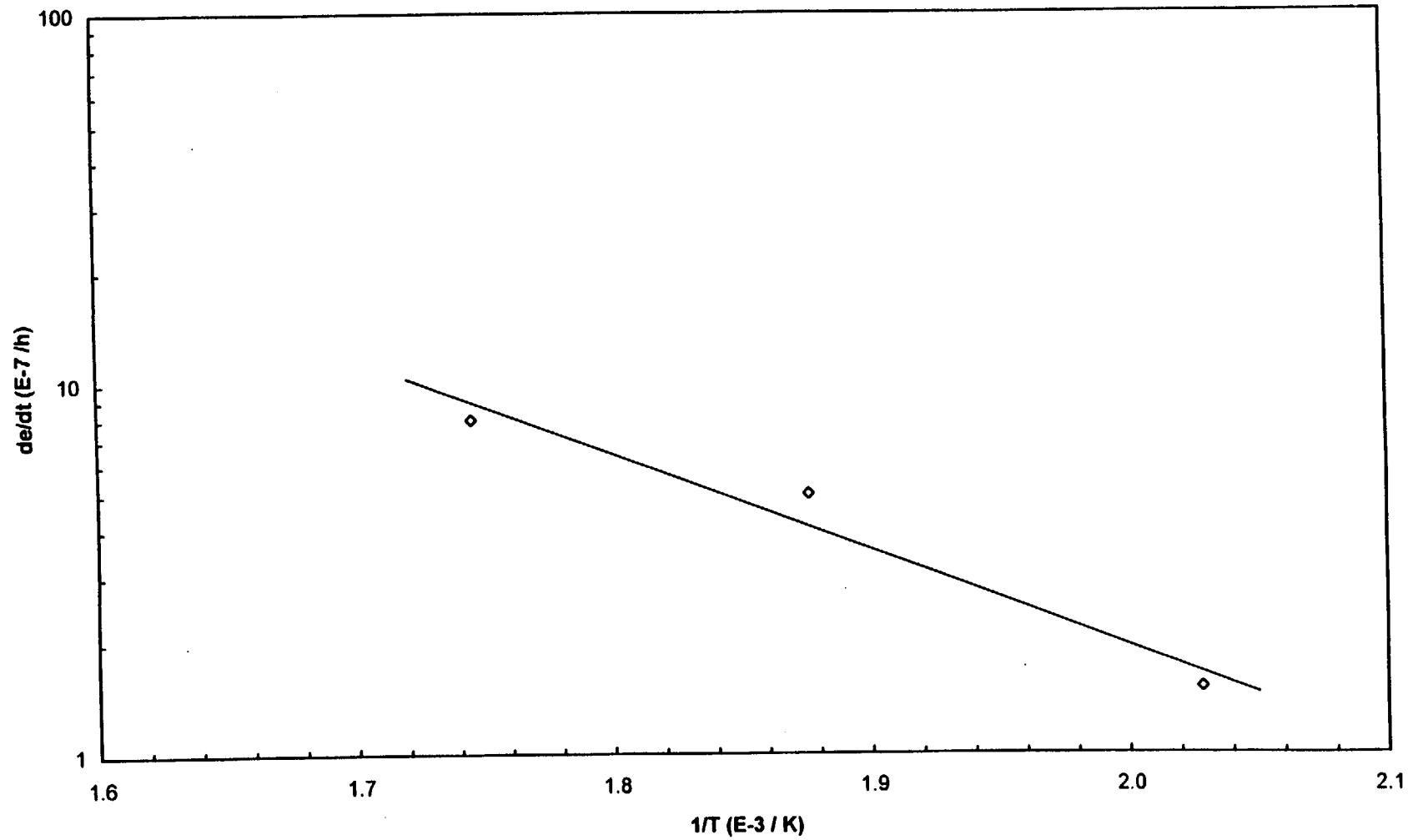


**Figure 15**  
**Comparison of In-Reactor and Out-of-Reactor Creep Rates**  
**B&W/EPRI, 86 MPa**



Figure 16  
CW Zr-2 Irradiation Creep Temperature Dependence, 207 MPa  
From Reference 16



Graphical representation of data from Reference 16  
This figure was not included in Reference 16

**Figure 17**

**CWSR IMP Zr-4 In-Reactor Creep**

**$1.08 \times 10^{22}$  n/cm<sup>2</sup> (E > 1 MeV), 41 MPa (6.0 ksi) Hoop Stress**

**a, c**



**Section 2**  
**Other PAD Model Changes**

## 1.0 Revised PAD Code Summary of Changes

The following changes have been incorporated into the revised PAD code:

- 1) Revised Creep Model (described in Section 1 of this report),
- 2) Revised Rod Irradiation Growth Model,
- 3) Updated Zr-4 and ZIRLO™ Clad Thermal Conductivity Values,
- 4) Updated Zr-oxide Thermal Conductivity Value,
- 5) Updated Equation of State (EOS) Model,
- 6) Variable Oxide-Metal Ratio Model (as discussed during the Westinghouse/NRC meeting on May 5, 1998), and
- 7) Gas Absorption in Cladding Effect.

Item 1 was submitted in the original version of WCAP-15063-P. Items 2 through 7 were presented to the NRC as additional model changes that were being incorporated into the PAD model during a meeting with the NRC and Battelle Northwest Labs (reviewer of the WCAP). These latter items were requested to be incorporated into WCAP-15063-P by the NRC since that had been reviewed along with the revised creep model and would be the basis for the new PAD 4.0 model.

### 1.1 Revised Creep Model

Description: Refer to WCAP-15063-P for creep model details. This is a substantial improvement in the creep model, which is an important model with wide-reaching impacts for all of the subsequent calculations in the revised PAD code.

Why Change?: The revised creep model is fundamentally sound and has a much more rigorous in-reactor data base to support the mechanistic understanding of in-reactor creep. The new model incorporates temperature-dependent irradiation creep and irradiation hardening.

Effect of change: The overall impact of the revised creep model in the revised PAD code on rod internal pressure predictions is favorable.

## 1.2 Revised Rod Irradiation Growth Model

Description: The current PAD model (WCAP 10851-P-A) does not have a temperature dependence for irradiation growth of zirconium alloys. The revised PAD model incorporates this temperature dependence.

Why change?: This change is based on work reported by the industry which has been demonstrated at EBR-II and DIDO that irradiation growth is a strong function of temperature, particularly for temperatures above 660 K (728 °F).

Effect of change: This is a relatively small change which will only effect rod growth when high temperatures are present in the cladding.

## 1.3 Updated Zr-4 and ZIRLO™ Clad Thermal Conductivity Values

Description: PAD (WCAP-10851-P-A) currently uses conductivity values from open literature for Zircaloy-4 and Zircaloy-2, for Westinghouse Zr-4 and ZIRLO™. The revised PAD code uses measured values on Westinghouse fuel products; for both ZIRLO™ and Zr-4.

Why change?: Experimental work was conducted specifically to update the database for Westinghouse product, and when incorporated will substantially improve thermal model accuracy.

Effect of Change: This update has a positive impact on rod internal pressure by slightly lowering clad temperatures for a given power level.

## 1.4 Updated Zr-oxide Thermal Conductivity Values

Description: PAD (WCAP-10851-P-A) currently uses a value for zirconium-oxide thermal conductivity based on work done in 1979 on theoretically-dense zirconium-oxide in a vacuum. Recent EPRI-sponsored work shows that the oxide thermal conductivity is higher than that currently included in PAD. Oxide thermal conductivity has been revised in the new version of PAD based on this work.

Why Change?: Recent in-pile tests indicate that a more conductive thermal oxide layer is formed in PWR environments, which enhances the oxide thermal conductivity. This change will enable more accurate assessments of the rod thermal response characteristics consistent with industry understanding of zirconium-oxide properties.

Effect of Change: This change yields a small reduction in clad average temperature and thus a reduction in fuel centerline temperature.

### 1.5 Equation of State (EOS) Gas Model

Description: PAD (WCAP-10851-P-A) currently uses the ideal gas law for calculating the pressure inside the fuel rods. A review of the available state-of-the-art gas laws, show that a new equation of state (EOS) model is more accurate. The revised PAD code uses the Peng-Robinson EOS model for the calculation of fuel rod internal pressure.

Why change?: Changing the PAD gas model from the ideal gas law to the Peng-Robinson EOS will more accurately represent the internal gas pressure of Westinghouse fuel rods.

Effect of Change: This model causes the predicted rod pressure to increase for a given burnup higher than the current ideal gas law and has a small negative effect on rod internal pressure.

### 1.6 Variable Oxide-Metal Ratio Model

Description: PAD (WCAP-10851-P-A) currently uses a constant theoretical oxide-metal ratio 1.56 to calculate metal wastage. Westinghouse previously identified to the NRC (May 1998) that we would be using a value of [

] <sup>a, c</sup>.

Why change?: The change in oxide characteristics as the thickness increases has been documented in public literature and measured on archive hot cell photomicrographs.

Effect of Change: This change allows for accurate calculation of remaining wall thickness as oxide is generated and thus improves accuracy of the clad stress and creep calculations.

### 1.7 Gas Absorption in Cladding Effect

Description: PAD (WCAP-10851-P-A) currently models that air can contribute to the internal pressure of the fuel rod throughout life. Air is rapidly absorbed into the cladding by forming hydrides, oxides and nitrides of zirconium and is eliminated from gas pressure calculations in the revised PAD code.

Why change?: Published literature on diffusion/reaction rates for gases in zirconium alloys, confirms a rapid consumption of any air or reactive gases is expected at operating fuel temperatures. [

] a, c.

Effect of Change: This change will result in a small reduction in rod internal pressure.

## 2.0 Revised Rod Irradiation Growth Model

### 2.1 Model Background and Justification

Extensive in-reactor testing has been performed in EBR-II (fast neutron spectrum) and DIDO (thermal spectrum). One set of tests reported by Rogerson determined the irradiation growth in DIDO and EBR-II with the same material (RXA Zr-2)<sup>(1)</sup>. The result shows that the growth strain exhibited by the EBR-II sample is within the sample-to-sample scatter exhibited by the DIDO data. This result shows that irradiation growth data measured in a fast neutron spectrum (specifically EBR-II) is applicable to thermal neutron spectra. Therefore, the EBR-II data may be applied to PWRs.

The available CW irradiation growth data covers an extensive parameter range. The temperatures are in the range of 353 to 687 K (176 to 777 °F), and the fluences extend up to values similar or higher than typical end-of-life PWR fuel rods ( $1.7 \times 10^{22}$  n/cm<sup>2</sup>, E > 1 MeV). In the case of the EBR-II tests, large growth strains were observed (strains as large as 2.5%)<sup>(2)</sup>. At high fluences (>  $0.5 \times 10^{22}$  n/cm<sup>2</sup>, E > 1 MeV) and temperatures > 650 K, the irradiation growth strain and strain rate is the same for CW and RXA material. Figures from Reference 2 for 20% CWSR Zr-2 slab material show that this behavior is not texture or temperature dependent (for temperatures > 650 K).

### 2.2 PAD Revision

The revised PAD irradiation growth equation was modified using the irradiation growth rate temperature dependence reported by Fidleris et. al. <sup>(3)</sup>. At temperatures > 660 K, the irradiation growth rate increases rapidly with increasing temperature. The high temperature effect (for temperatures > 660 K), was modeled by [

] <sup>a, c</sup> (see Figure 2-1):

$$[ G/G_0 = 0.0212T(K) - 12.967 \quad \text{for } T > 660 \text{ K} ]^{a, c}$$

[

] <sup>a, c</sup>.

**Figure 2-1**  
 **$G/G_0$  versus Temperature**



### 3.0 Updated Zr-4 and ZIRLO™ Clad Thermal Conductivity Values

#### 3.1 Model Background and Justification

Table 3-1 summarizes the thermal conductivity values calculated as a function of temperature, based on the tests conducted by the "Properties Research Laboratory" in West Lafayette, Indiana, on Westinghouse Zircaloy-4 and ZIRLO™ cladding. [

] <sup>a, b, c</sup>.

A linear fit of the data presented in Table 3-1 yields the following best estimate model for Zircaloy-4, in the temperature range of [

] <sup>a, b, c</sup>.

$$[ \quad ]^{a, b, c} \quad (1)$$

where,  $k$  = Thermal Conductivity in  $Wcm^{-1}K^{-1}$   
 $T$  = Temperature in  $^{\circ}C$

In the case of ZIRLO™, a linear fit of the data presented in Table 3-1 yields the following best estimate model in the temperature range of [

] <sup>a, b, c</sup>.

$$[ \quad ]^{a, b, c} \quad (2)$$

where,  $k$  = Thermal Conductivity in  $Wcm^{-1}K^{-1}$ , and  
 $T$  = Temperature in  $^{\circ}C$

Figure 3-1 represents the linear plots of thermal conductivity versus temperature for Zircaloy-4 and ZIRLO™ as represented by Equations 1 and 2 respectively.

#### 3.2 PAD Revision

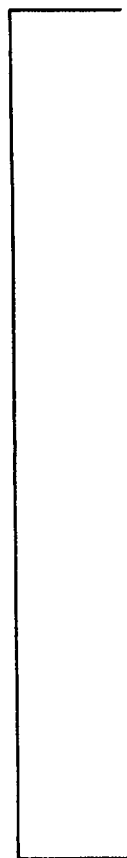
In view of the fact that the maximum allowable clad design temperature for steady state operation for Zircaloy-4 is [ <sup>a, c</sup> ] and for ZIRLO™ is [ <sup>a, c</sup> ] respectively, and for Condition II transients is [ <sup>a, c</sup> ] for Zircaloy-4 and [ <sup>a, c</sup> ] for ZIRLO™, models represented by Equation (1) for Zircaloy-4 and Equation (2) for ZIRLO™ clad will be used for thermal conductivity predictions as a function of temperature for Westinghouse fuel clad in the revised PAD code.

**Table 3-1**  
**Thermal Conductivity as a function of temperature**

**a, c**



**Figure 3-1**  
**Thermal Conductivity as a Function of Temperature**  
**for Zircaloy-4 and ZIRLO™**  
**(1st Order Fit)**



**a, c**

## 4.0 Updated Zr-Oxide Thermal Conductivity Value

### 4.1 Model Background and Justification

A best estimate value of [ ]<sup>a, b, c</sup> has been used in PAD (WCAP-8720) for Zr-4 oxide layers, based on data from Reference 4. Since that time, additional data have become available (References 5 and 6) which indicates that the oxide layer thermal conductivity has a higher value. The purpose of this update is to use the appropriate data from References 5 and 6 to establish a revised best-estimate average value of the Zr oxide layer thermal conductivity.

The first set of new ramp tests (Reference 5) consisted of a set of 12 ramps on four rods with oxide layer thicknesses of 30, 54, 66 and 82 microns. Thermal conductivity values ranged from 1.4 to 3.7 W/mK with an average value of 2.4 W/mK.

The second set of ramp tests, Reference 6, was run because there was no clear dependence of oxide thermal conductivity on oxide layer thickness, and it seemed that crud could have been present on two of the rods and that could have affected the results. The two fuel rods were brushed and the tests were repeated.

During the second set of ramps, it was noted that the rod elongation during up-ramps was greater than contraction during down-ramps. It was postulated that pellet-cladding mechanical interaction could be occurring during the up-ramps, and it was recommended that only the down-ramps be used for thermal conductivity measurements. The oxide layers were re-measured, and it was found that the thickness of the 26 micron layer was actually 30 microns.

A total of seven down ramps were measured during the second set of experiments. The resulting thermal conductivity values are given in Table 3-2 of Reference 6. A summary of the thermal conductivities from the first set of ramps is given in Table 4-1.

**Table 4-1**

**Summary of Conductivity Values From First Set of Ramps**

a, b, c



These data were combined with data from the second set of ramps given in Table 3-1 of Reference 6. The combined data are given in Table 4-2. The variables are the TEST series, 1 or 2, the RAMP number, UP1D2 = 1 for up ramps and 2 for down ramps, t = the oxide thickness, and K = the thermal conductivity.

**Table 4-2**

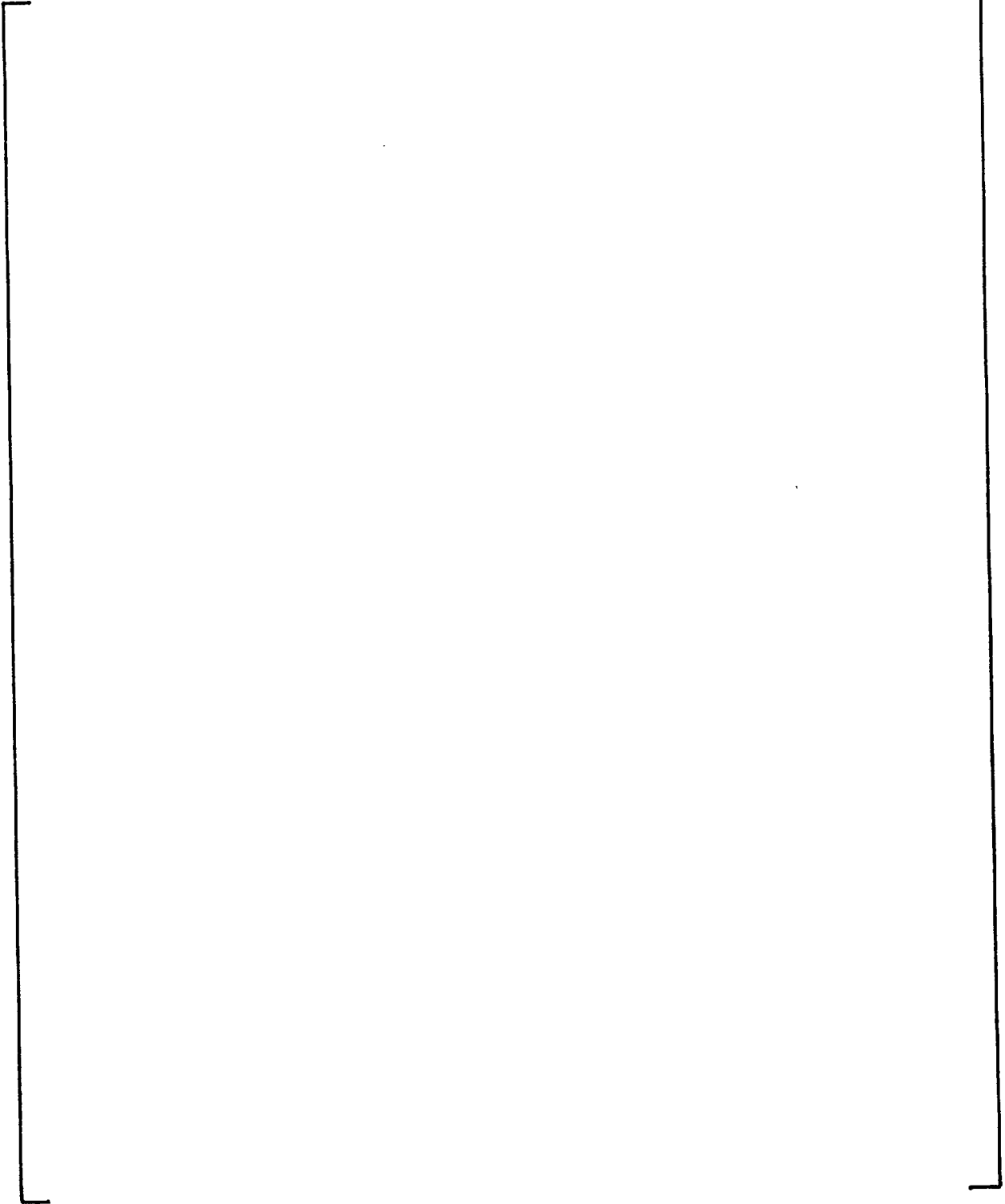
**Summary of Conductivity Data**

a, b, c



**Table 4-2 (cont.)**  
**Summary of Conductivity Data**

**a, b, c**

A large, empty rectangular frame with a thin black border, spanning most of the page width and height. It is positioned between the title and the footer, indicating that the table content is missing or redacted.

**Table 4-2 (cont.)**  
**Summary of Conductivity Data**

a, b, c

--	--

The results of a statistical analysis of the Table 4-2 data for the down ramps are given below:

[	] a, c
[	] a, c
[	] a, c

Tests were performed to determine if the conductivity values are normally distributed. [

] a, c.

**4.2 PAD Revision**

In conclusion, the NFIR conductivity data can be characterized and included in the revised PAD code as follows:

[	] a, c
---	--------

for evaluating cladding temperatures with oxide layers present.

## 5.0 Updated Equation of State Model (EOS)

### 5.1 Model Background and Justification

The relationship between pressure, temperature, and mass for a fission gas in PAD (WCAP-10851-P-A) is based on the Ideal Gas Law,

$$PV = NRT \quad (1)$$

where  $P$  and  $T$  are the pressure and temperature of the gas respectively,  $V$  is the volume occupied by the gas, and  $N$  is the number of moles of gas. The universal gas constant is  $R$ . Equation (1) is equivalent to:

$$Pv = RT \quad (2)$$

where  $v$  is the specific volume and  $R$  is a (particular) gas constant.

The Ideal Gas Law relationship is valid for many gases near room temperature and pressure, and is good for noble gases such as helium, neon, and argon up to moderate pressures (400 - 500 psia). At high pressures ( $P > 500$  psia) however, the Ideal Gas Law becomes increasingly inaccurate. Figure 1 from Reference 8, shows the compressibility of several gases at high pressure, where compressibility  $Z$  is defined as:

$$Z = \frac{Pv}{RT} \quad (3)$$

For an ideal gas, the compressibility  $Z = 1.0$ . Deviation from 1.0 is an indication of non-ideal behavior, and that the use of the Ideal Gas Law will lead to inaccurate results.

Figure 1 from Reference 8, shows that above about 500 psia, inert gases do not exhibit ideal behavior.

At end of life, when the rod internal pressure can exceed 2000 psia, none of these gases will exhibit ideal behavior. Therefore, use of the Ideal Gas Law to estimate rod pressure given the temperature and specific volume will be inaccurate. Since helium makes up the majority of the gas, and the compressibility of helium is greater than 1.0, the Ideal Gas Law will underpredict the actual rod pressure.

A survey was conducted to determine the most appropriate EOS. It was determined that the Peng-Robinson equation, Reference 9, gave the most accurate predictions for the range of interest. For fission gas mixtures even at end of life, helium has the highest mol fraction. To check these EOSs for high He mol fraction, the

results were plotted as DP/P versus helium mol fraction. These results are shown in Figures 5-1 and 5-2. Measured data was obtained from References 10 through 14, for the various gas matrix evaluations.

Note that DP/P is defined as:

$$\frac{DP}{P} = \frac{P_{data} - P_{prediction}}{P_{data}} \quad (4)$$

This quantity is positive when the pressure is underpredicted, and negative when overpredicted.

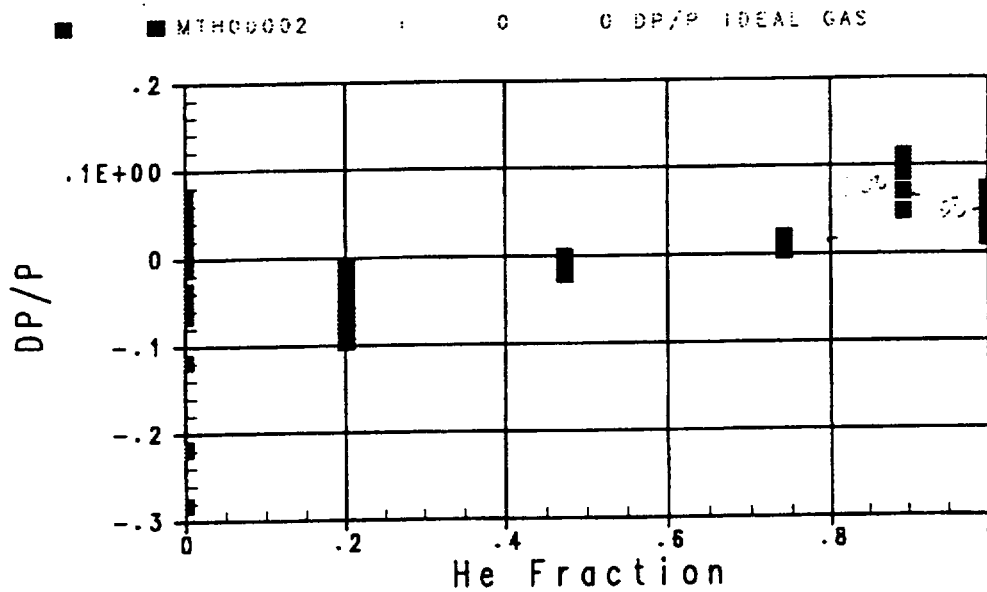


**Figure 5-1**  
**Ideal Gas Equation of State**  
**DP/P versus He Mol Fraction**

From Figure 5-1 it becomes clear that for gas compositions rich in helium, the Ideal Gas Law may underpredict the actual pressures, in some cases by more than 10%.

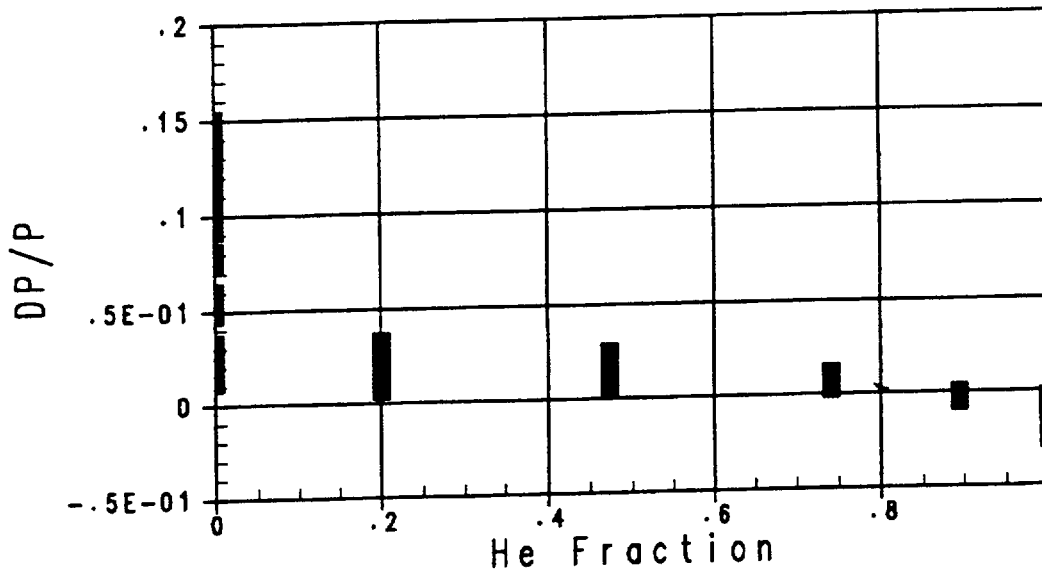


**Figure 5-2**  
**Peng-Robinson Equation of State**  
**DP/P versus He Mol Fraction**

The Peng-Robinson EOSs performs well at high He composition. For mol fractions greater than about 0.2, it predicts the pressure to within +/- 5%. At mol fractions approaching 1.0, the Peng-Robinson EOS overpredicts the pressure slightly, but never by more than 3% as shown in Figure 5-2.

Figure 5-3 shows the Peng-Robinson M-P plot results for various pressures. The pressure predictions for mixtures with high helium mol fractions are always predicted to within 5%.

## 5.2 Summary

The Ideal Gas Law was found to potentially underpredict pressure for compositions with high helium mol fraction. The more complex cubic Equations of State (Redlich-Kwong, Soave, and Peng-Robinson) were more accurate at high helium mol fraction, and tended to overpredict the pressure slightly. Of these three, the Peng-Robinson EOS was found to be slightly better than the other two.

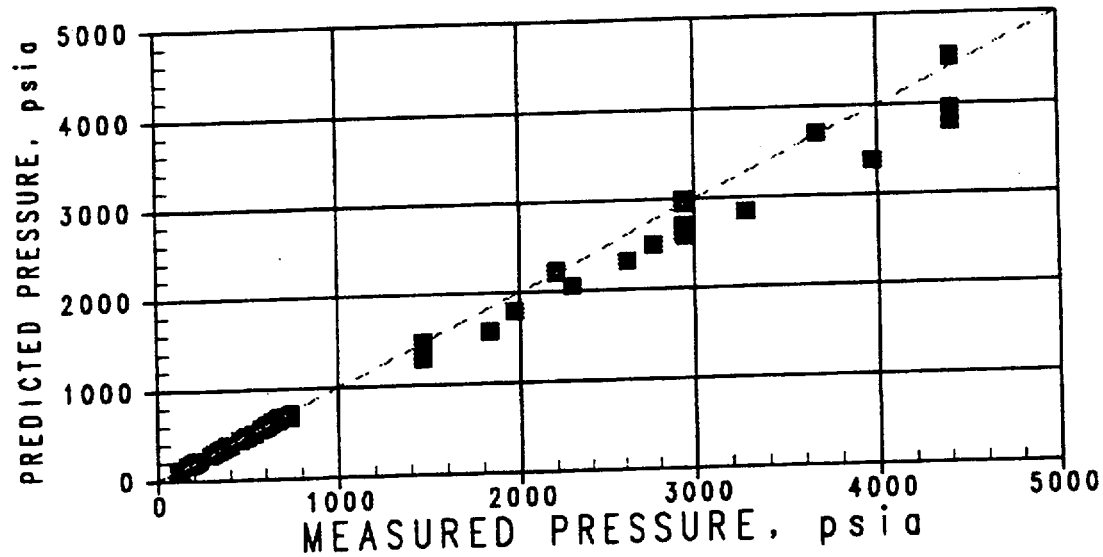


**Figure 5-3**  
**Peng-Robinson Equation of State**  
**Measured versus Predicted Pressure**

### 5.3 Pad Revision

PAD revision investigations of several Equations of State applicable to gas mixtures when compared to available data over a range of pressure, temperature, and composition shows the Peng-Robinson EOS is most accurate and will be used in the revised PAD code.

The pressure-temperature-volume relationship for a pure fluid is often represented by a cubic Equation of State, which has the general form:

$$P = \frac{RT}{v - b} - \frac{a}{v^2 + uv + wb^2} \quad (5)$$

where  $P$  is the pressure,  $T$  is temperature,  $v$  is specific volume, and  $R$  is the Universal Gas constant.

For the Peng-Robinson equation of state.  $u = 2.w = -1$  with

$$b = \frac{0.07780RT_c}{P_c} \quad (6)$$

and

$$a = \frac{0.45724 r^2 T_c^2}{P_c} [1 + f\omega(1 - T_r^{0.5})]^2 \quad (7)$$

where,

$$f\omega = 0.37464 + 1.54226\omega - 0.26992\omega^2 \quad (8)$$

In Equations (6) and (7), the subscript “c” denotes properties at the critical point. The reduced pressure is defined as

$$T_r = \frac{T}{T_c} \quad (9)$$

The function for  $f\omega$  given by Equation (8) uses the acentric factor  $\omega$ , which is a parameter that represents the complexity of a molecule with respect to geometry and polarity. For mono-atomic gases,  $\omega$  is usually zero or very small.

In the revised PAD code up to seven different gases can be present in the gas mixture. The following table lists these components and the properties assigned in the code as taken from Reference 9:

**Table 5-1**  
**Peng-Robinson Equation of State**  
**Component Properties List for PAD**

Component	Tcrit. K	Pcrit, bar	$\omega$
Helium	5.19	2.27	-0.365
Xenon	289.7	58.4	+0.008
Krypton	209.4	55.0	+0.005
Argon	150.8	48.7	+0.001
Nitrogen	126.2	33.9	+0.039
Water Vapor	647.3	221.2	+0.344
Hydrogen	33.2	13.0	-0.281

For gas mixtures, the attraction and repulsion between molecules of different components causes non-linear variation of some properties with composition. To account for this in Equation (5), a set of mixing rules can be defined to this non-linearity. The values of "a" and "b" in Equation (5) are re-defined. Based on the recommendations in Reference 4, the following mixing rules are used in the revised PAD code.

$$a_m = \sum_i \sum_j y_i y_j (a_i a_j)^{0.5} (1 - k_{ij}) \quad (10)$$

$$b_m = \sum_i y_i b_i \quad (11)$$

The  $b_i$  and  $a_i$  for each pure component are given by Equations (6) and (7) respectively. The term  $k_{ij}$  is used for some binary pairs to adjust for strong interactions and is determined from experimental data. In the revised PAD code  $k_{ij} = 0$ , is assumed for all binary combinations.

## 6.0 Variable O-M Ratio Model

### 6.1 Model Background and Justification

In order to accurately model fuel rod clad temperatures and stresses in a fuel performance models as well as 17% metal wastage calculations, an accurate model of Zircaloy-4 oxide to metal ratio is needed for use in design. Due to the differences in densities of the oxide and the base metal, there is a volumetric change from the metal consumed to the oxide formation. This volumetric difference results in a thicker oxide than the metal that was consumed. The ratio of the volumes is characterized by the oxide-to-metal ratio (O/M). The theoretical oxide-to-metal ratio is referred to as the Pilling-Bedworth ratio, and for Zirconium based alloys the value of 1.56 is commonly used. However, during the in-reactor generation of  $ZrO_2$ , different mechanisms occur that cause the oxide density to be less than theoretical resulting in higher O/M ratios at increasing oxide thicknesses. Westinghouse metallographic O/M measurements from fuel rod hot cell programs were evaluated and a predictive model was generated which relates O/M with oxide thickness.

[

] <sup>a, c</sup>. This model was first presented to the NRC by presentation on May 5, 1998.

### 6.2 Variable O/M Ratio Model Details

As the oxide grows, it transitions from a protective to a non-protective structure. The non-protective oxide contains cracks and pores and this transition occurs when the oxide is about [ ] <sup>a, c</sup>. In generating a model which predicts O/M ratio as a function of oxide thickness, the first [ ] <sup>a, c</sup> of oxide should result in a constant theoretical value of O/M ratio. At higher oxide thicknesses, the data presented in the previous section is used to develop the relationship of O/M ratio with increasing oxide thickness.

The equations governing the O/M ratio as a function of oxide thickness are as follows:

$$\frac{O}{M} = \frac{O}{M_{Th}}, \quad t < [ ]^{a, c} \quad (1)$$

$$\frac{O}{M} = [ ]^{a, c} \quad (2)$$

where:  $O/M_{th}$  = theoretical value of  $O/M$  ratio = 1.56

a = fitting coefficient, [

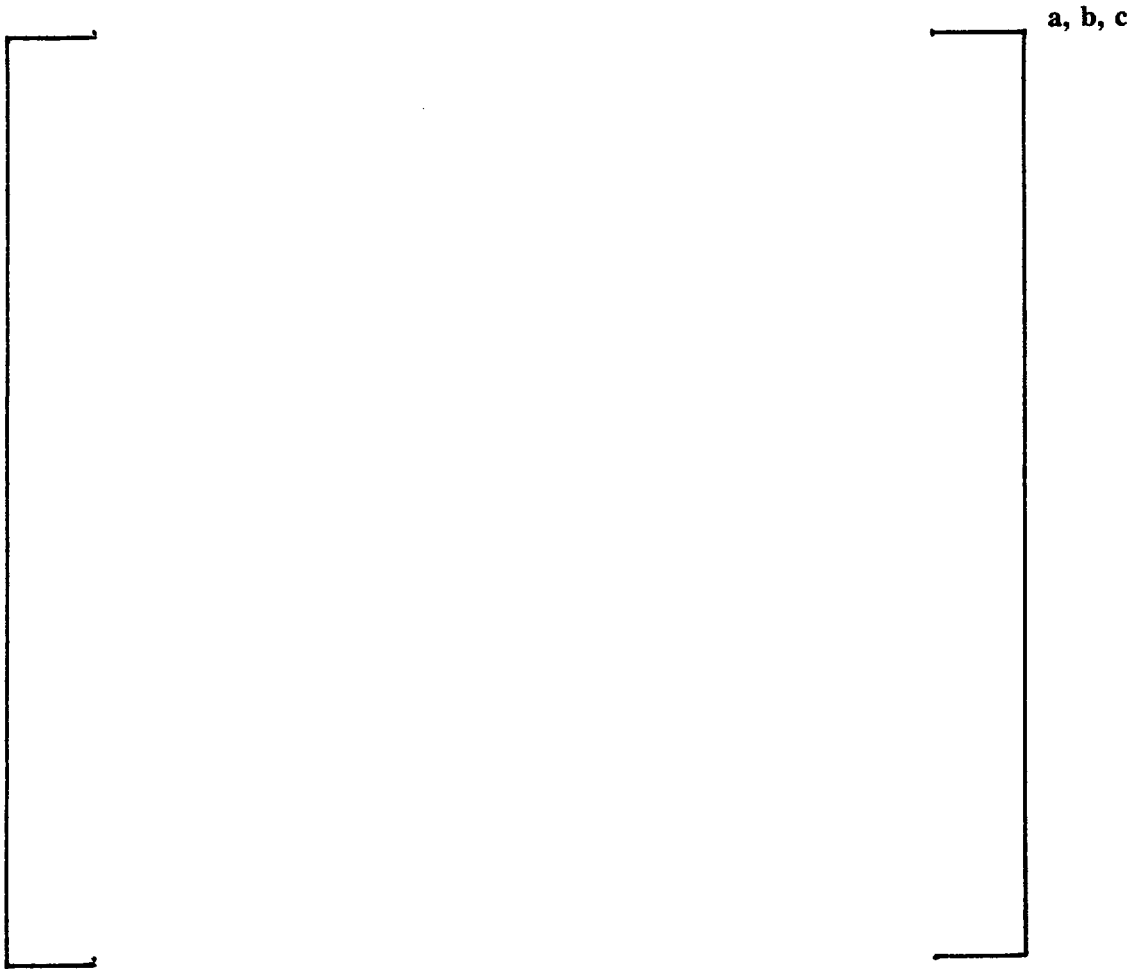
] <sup>a, c</sup>

b = fitting coefficient

t = oxide thickness (mils)

Equations 1 and 2 are combined and plotted against the sorted data from  $O/M$  measurements in Figure 6-1.

**Figure 6-1**  
**Best Estimate O/M Ratio Model**



## 7.0 Gas Absorption in Cladding Effect

### 7.1 Model Background and Justification

The fuel rod internal gas mixture includes: (1) the fission gasses produced during operation, (2) gas from the pellets including the gas from the IFBA coating if present, (3) the gas from the rod pre-pressurization, and (4) the [ ]<sup>a, c</sup>. When the rod is pre-pressurized and sealed during fabrication, the rod [ ]

[ ]<sup>a, c</sup>. Both IFBA and non-IFBA rods contain this equivalent volume [ ]<sup>a, c</sup>. Zirconium alloys are known to react with [ ]<sup>a, c</sup>.

For example, assuming a plenum volume of about [ ]<sup>a, c</sup> and a gas mixture of [ ]

[ ]<sup>a, c</sup>.

With about [ ]<sup>a, c</sup> the corresponding weight gain for total [ ]<sup>a, c</sup>. Based on reaction rates in Reference 16, [ ]<sup>a, c</sup> will occur within [ ]<sup>a, c</sup>; thus, all of the [ ]<sup>a, c</sup>.

Zirconium preferentially reacts with [ ]<sup>a, c</sup> are present. The reaction rate with [ ]<sup>a, c(2)</sup>. When the [ ]<sup>a, c</sup>. The absorption rate of [ ]

[ ]<sup>a, c</sup>. Based upon the weight of [ ]<sup>a, c</sup>. Thus, it will take about [ ]<sup>a, c</sup>. This may be a lower than actual rate since rate is temperature dependent. [ ]<sup>a, c</sup>.

Irradiated rods were punctured in the hot cell and the gas present in the rod was captured and analyzed. In the 22, [ ]<sup>a, c</sup> measured and in 7 other rods from [ ]<sup>a, c</sup> there was [ ]<sup>a, b, c</sup>.

The measurement sensitivity is reported as less than 0.01% by volume. If the [ ]



## 8.0 References

1. A. Rogerson, "Irradiation Growth in Annealed and 25% Cold Worked Zircaloy-2," *Journal of Nuclear Material*, Volume 154, pages 276-285, 1988.
2. R. P. Tucker, V. Fidleris and R. B. Adamson, "High-Fluence Irradiation Growth of Zirconium Alloys at 644 and 725 K," *Zirconium in the Nuclear Industry: Sixth International Symposium*, ASTM STP 824, pages 427-451.
3. V. Fidleris, R. P. Tucker and R. B. Adamson, "An Overview of Microstructural and Experimental Factors that Affect the Irradiation Growth Behavior of Zirconium Alloys," *Zirconium in the Nuclear Industry: Seventh International Symposium*, ASTM STP 939, pages 49-85.
4. "MATPRO- Version 11," NUREG/CR-0497, TREE-1280, Feb. 1979. (Methodology/Calculations)
5. "In-Pile determination of Thermal Conductivity of Oxide layer on LWR Cladding, Part 1: Irradiation Period July - October 1995, Final Report," EPRI-TR-107718-P1, January 1997.
6. Thermal Conductivity of Oxide Layer on LWR Cladding, Part 2: Irradiation Period September - November 1996 and Crud Analysis, Draft Final Report," EPRI Draft Tr-107718-P2, April 1997.
7. Ostle and Mensing, "Statistics in Research, Third edition," The Iowa State University Press, 1975.
8. Cook, G. A., Argon, Helium, and the Rare Gases, Interscience Publishers, New York, 1961.
9. Reid, R. C., Prausnitz, J. M., and Poling, B., "The Properties of Gases and Liquids," 4th Ed., McGraw Hill, 1986.
10. Hurley, J. J., et al., "Virial Equation of State of Helium, Xenon, and Helium-Xenon Mixtures from Speed of Sound and Burnett PrT Measurements," *International Journal of Thermophysics*, Volume 18, No. 3, May 1997.
11. McCarty, R. D., "Thermophysical Properties of Helium-4 From 2 to 1500 K With Pressures to 1000 Atmospheres," COM 75-10334, National Bureau of Standards, Nov. 1972.

12. Matheson, Gas Data Book, 6th Ed.
13. Briggs, T. C., and Howard, A. R., "Compressibility Data for Helium, Nitrogen, and Helium-Nitrogen Mixtures at 0°, 25°, and 50° C and at Pressures to 1000 Atmospheres," Bureau of Mines Report of Investigations 7639, 1972.
14. Gandhi, J. M., and Saxena, S. C., "Correlated Thermal Conductivity Data of Rare Gases and Their Binary Mixtures at Ordinary Pressures," Journal of Chem. and Eng. Data, Volume 13, No. 3, July 1968.
15. Handbook of Chemistry and Physics, 41 Edition, page 3379.
16. Lustman and Kerze, "Metallurgy of Zirconium," McGraw-Hill Book Company, Inc., 1955, pages 578-608.

**PAD 4.0**

**Creep, Thermal, and Fission Gas  
Calibration and Verification Statistics**

## PAD 4.0

### Creep Calibration and Verification Statistics

#### Introduction:

An improved in-reactor irradiation and thermal creep model has been developed<sup>(1)</sup> and has been incorporated into PAD 4.0. The new creep model is substantially different in form from the model used in PAD 3.4. Therefore, a full calibration, verification and uncertainty analysis was conducted in order to incorporate this new model into PAD 4.0.

The equations that govern the irradiation creep and thermal creep were modified to represent the new formulations. The creep model was developed to accurately model Conventional Zr-4, Improved Zr-4, and ZIRLO™; however, to properly calibrate the model, individual irradiation creep rate and thermal creep rate multipliers were determined for the three alloys from measured profilometry data.

#### Procedure:

The process used in performing the creep calibration involves comparing the experimentally measured fuel rod profilometry data, with the PAD 4.0 predicted profilometry for each of the calibration rods. Both the measurements and the PAD results include the corrosion layer on the cladding O.D. No attempt has been made to correct the measured data for the oxide layer thickness, as the uncertainties in these corrections would be relatively large. In addition, the PAD cladding O.D. includes the calculated oxide thickness.

The calibration coefficients which determine the thermal and irradiation components of creep are [ ]<sup>a, c</sup>.

Independent calibrations were performed and values of [ ]<sup>a, c</sup>.

#### Cladding Creep Model Data:

Profilometry data was obtained from [ ]<sup>a, c</sup> and is shown in the table of "List of Creep Data".

Not all of the creep profilometry data can be used for calibration. [

[<sup>a, c</sup>]  
a, b, c

**Statistical Analysis:**

The results of the calibration defined the creep model coefficients for the three alloys are as follows:

*Creep Calibration Coefficients*  
a, b, c

The statistical results for the calibration, validation, and verification (total) data for all three alloys are shown below:

*Statistical results of creep calibration*  
a, b, c

Figure 1.1 shows the predicted creep-down data versus measured creep-down data for [

] <sup>a, c</sup>. Figures 1.2 and 1.3 break down the creep data into the calibration and validation subsets.

Figures 1.4 through 1.7 show the residual dependence of the model on axial elevation, rod average burnup, time averaged temperature, and time averaged stress. [

] <sup>a, c</sup>.

Comparisons of the creep model with individual campaign creep-down data are shown in Figure 1.8 through Figure 1.12 for Conventional Zr-4, Figures 1.13 and 1.14 for Improved Zr-4, and Figure 1.15 for ZIRLO™.

Since the creep model is applicable to both creep-in and creep-out, uncertainties obtained from the verification data will be used in a manner consistent with the creep model. [

] <sup>a, c</sup>.

**Uncertainties:**

[

] <sup>a, c</sup>;

[

] <sup>a, c</sup>

[ ]<sup>a, c</sup>.

The measured, predicted, and weight data are given in tabular form in the List of Creep Data, attached. The weighted standard deviation calculated using the method above was found for both the M/P data and the M-P data.

The results are below: [ ]<sup>a, b, c</sup>.

**Weighted Standard Deviations of Entire Creep Data Set**

[ ]<sup>a, b, c</sup>

[ ]<sup>a, b, c</sup>.

The above standard deviations of M/P could be used to calculate the 95% upper bound and 95% lower bound uncertainties in the creep model; however, the scatter in the creep predictions is subject to other uncertainties in addition to the true creep uncertainty. Since some of these other uncertainties can be quantified, they can be removed from the data before using it to calculate upper and lower bounds.

The uncertainty in the predictions can be defined as follows:

a, c

Where  $\sigma_{meas}$  = The Profilometry Measurement Uncertainty  
 $\sigma_{fab}$  = The Cladding O.D. Fabrication Uncertainty  
 $\sigma_{creep}$  = The True Creep Model Uncertainty  
 $\sigma_{other}$  = All Other Uncertainties

The total uncertainty represented by the standard deviation of the M-P data [

] <sup>a, c</sup> is a result of a combination of many uncertainties. The uncertainty of interest is the true creep model uncertainty which will be used to determine the 95% upper bound and 95% lower bound model uncertainties. The measurement uncertainty and as-built fabrication uncertainties are known and given as [ ] <sup>a, c</sup>, respectively. The "other" uncertainties cannot be explicitly defined and can be lumped together with the creep uncertainty. The above equation was solved for the combination of creep and "other" uncertainties giving a value of [

] <sup>a, c</sup>. This represents a reduction in the total uncertainty by removing quantifiable uncertainties. The reduction is a factor of [

] <sup>a, c</sup>. The uncertainty in the M/P data is what is really needed so it is reduced by this same ratio giving a true creep model M/P uncertainty of [ ] <sup>a, c</sup>.

The 95% upper bound and 95% lower bound uncertainties were then calculated using a standard deviation of [ ] <sup>a, c</sup> along with the individual alloy mean values of M/P. [

] <sup>a, c</sup>. The calculations and bounding uncertainties are shown below.

	a, b, c
--	---------

*Creep Model Uncertainties (ACREEP)*

	a, b, c
--	---------

**Conclusions:**

The creep model has been successfully calibrated for use in PAD 4.0. The multipliers for [ ] <sup>a, c</sup> have been determined and are shown in Creep Calibration Coefficients table. The uncertainties associated with this model are tabulated in preceding table. All of the creep model comparisons show reasonable agreement between measured and predicted data. The results are similar with those determined for the PAD 3.4 creep model.

**List of Creep Data**

a, b, c

**List of Creep Data (cont.)**

a, b, c

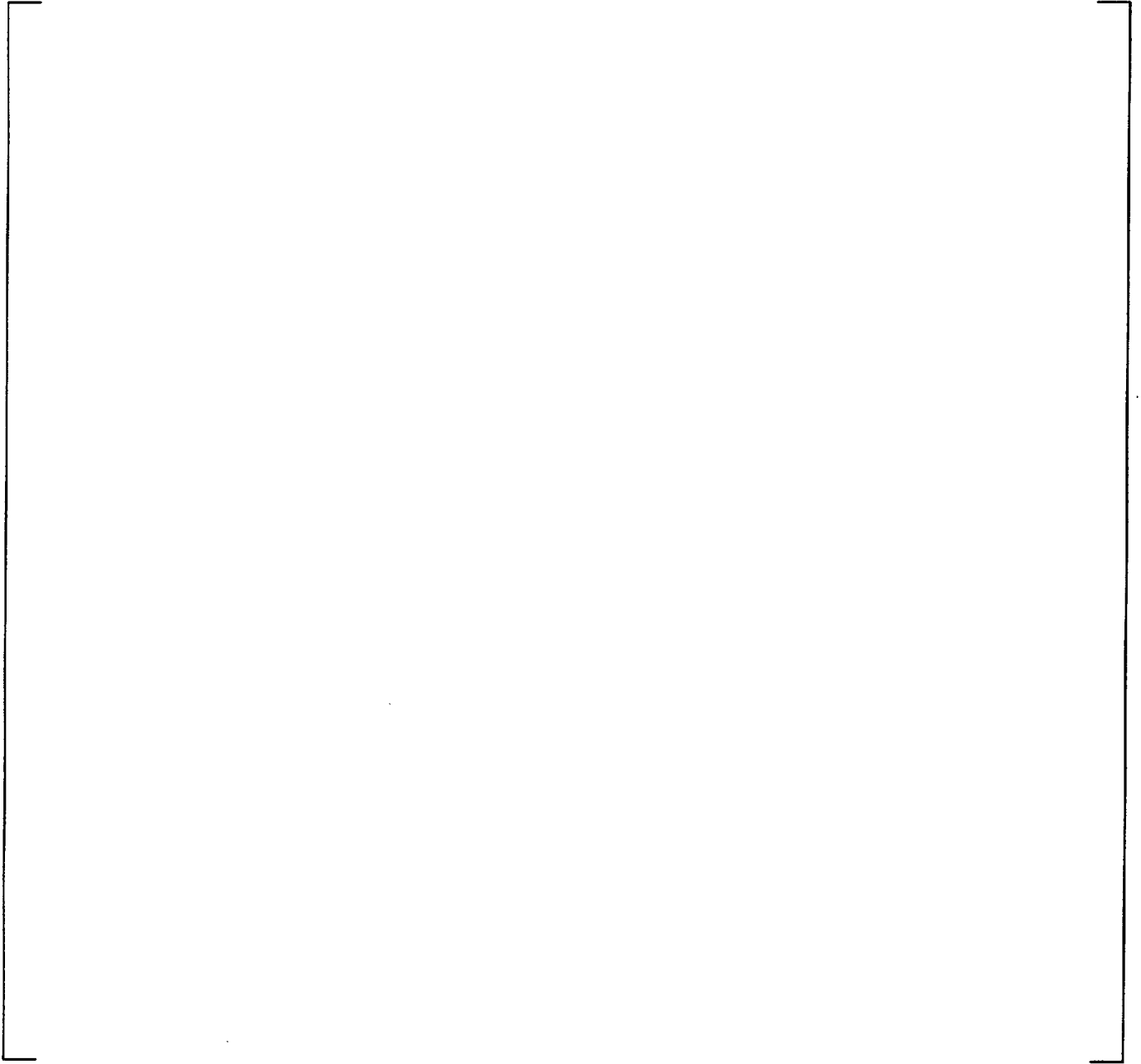


Figure 1.1

**PAD Creep Model Predictions  
(all data)**

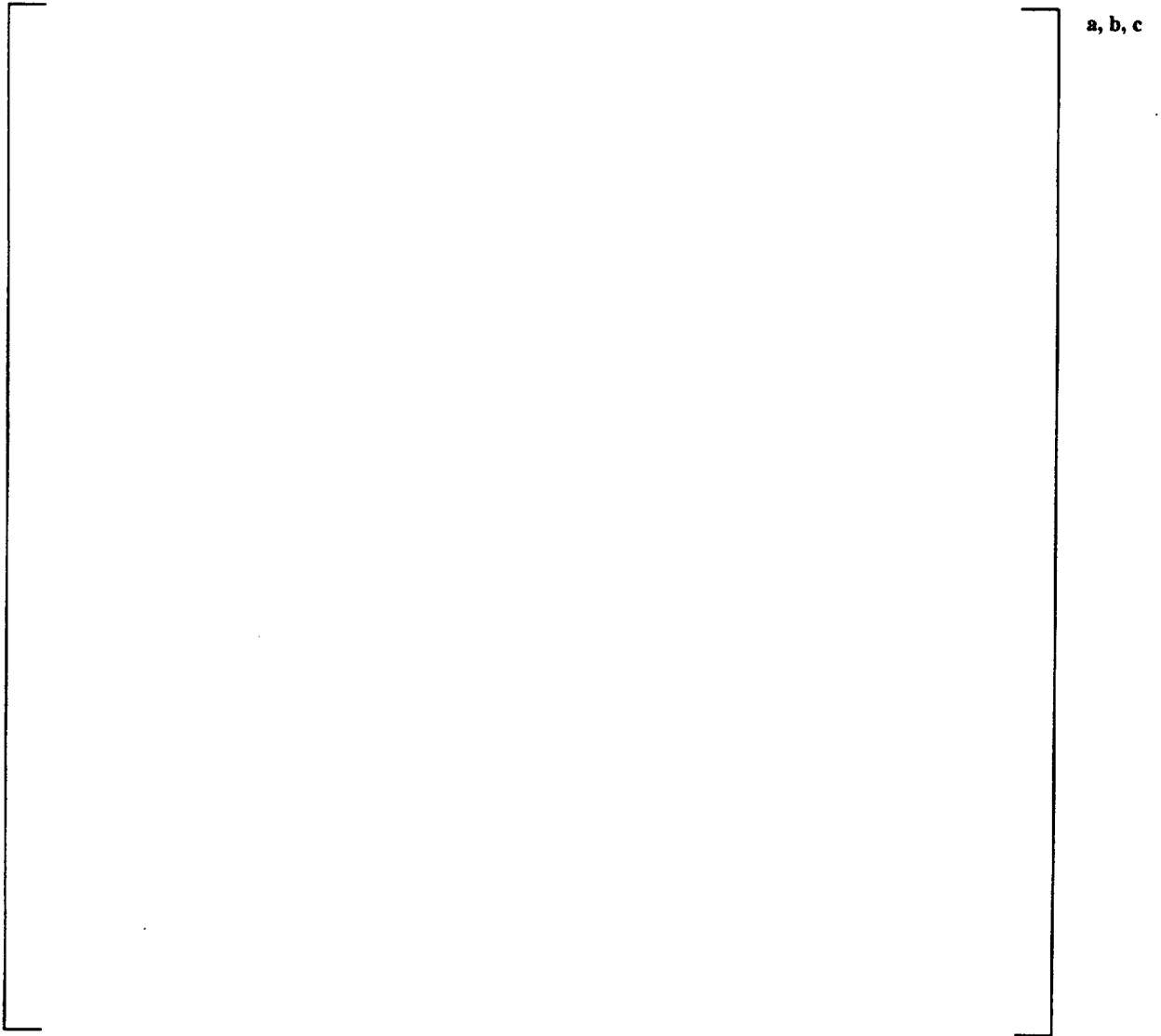


Figure 1.2

**PAD Creep Model Predictions  
(calibration data)**

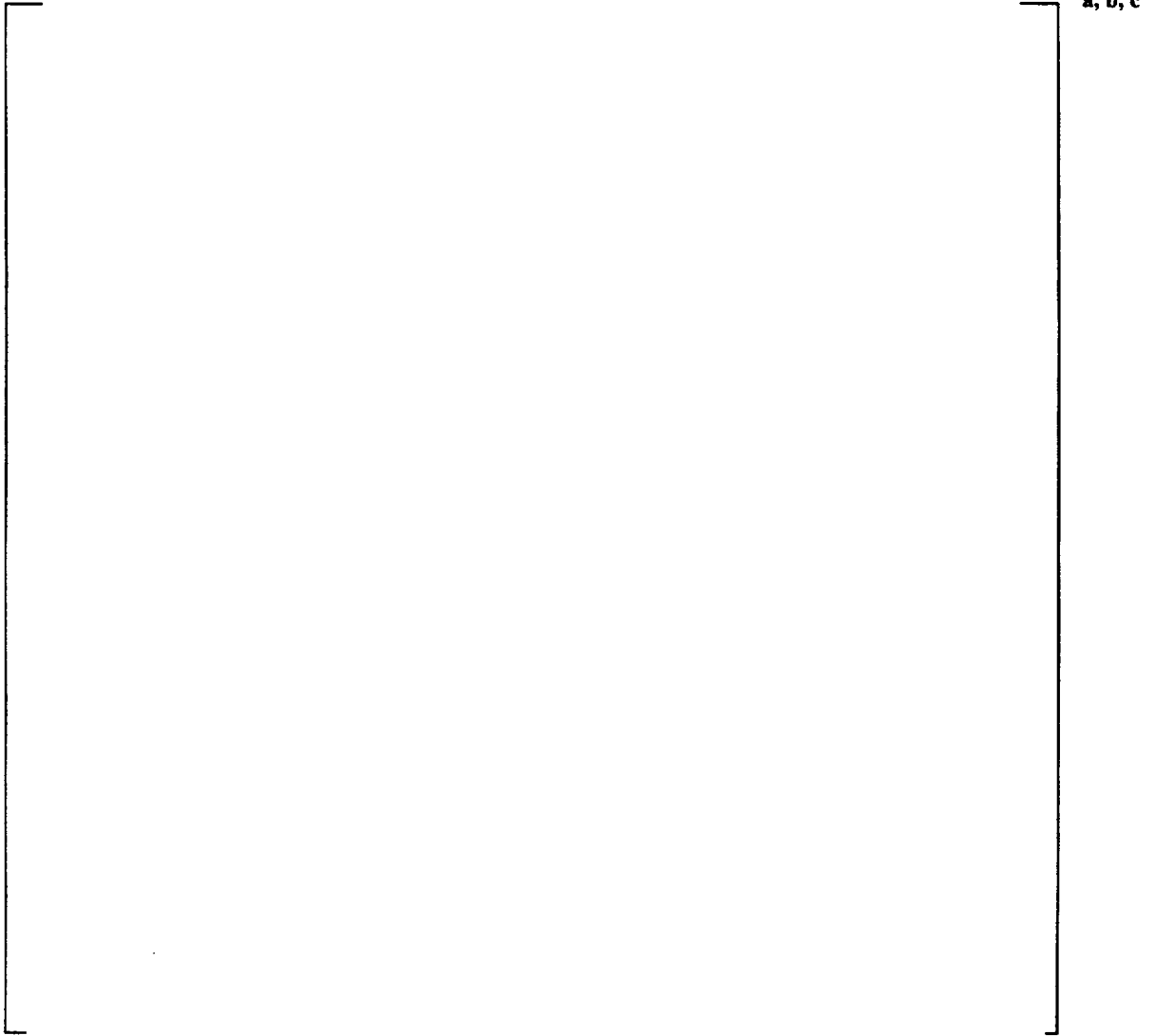
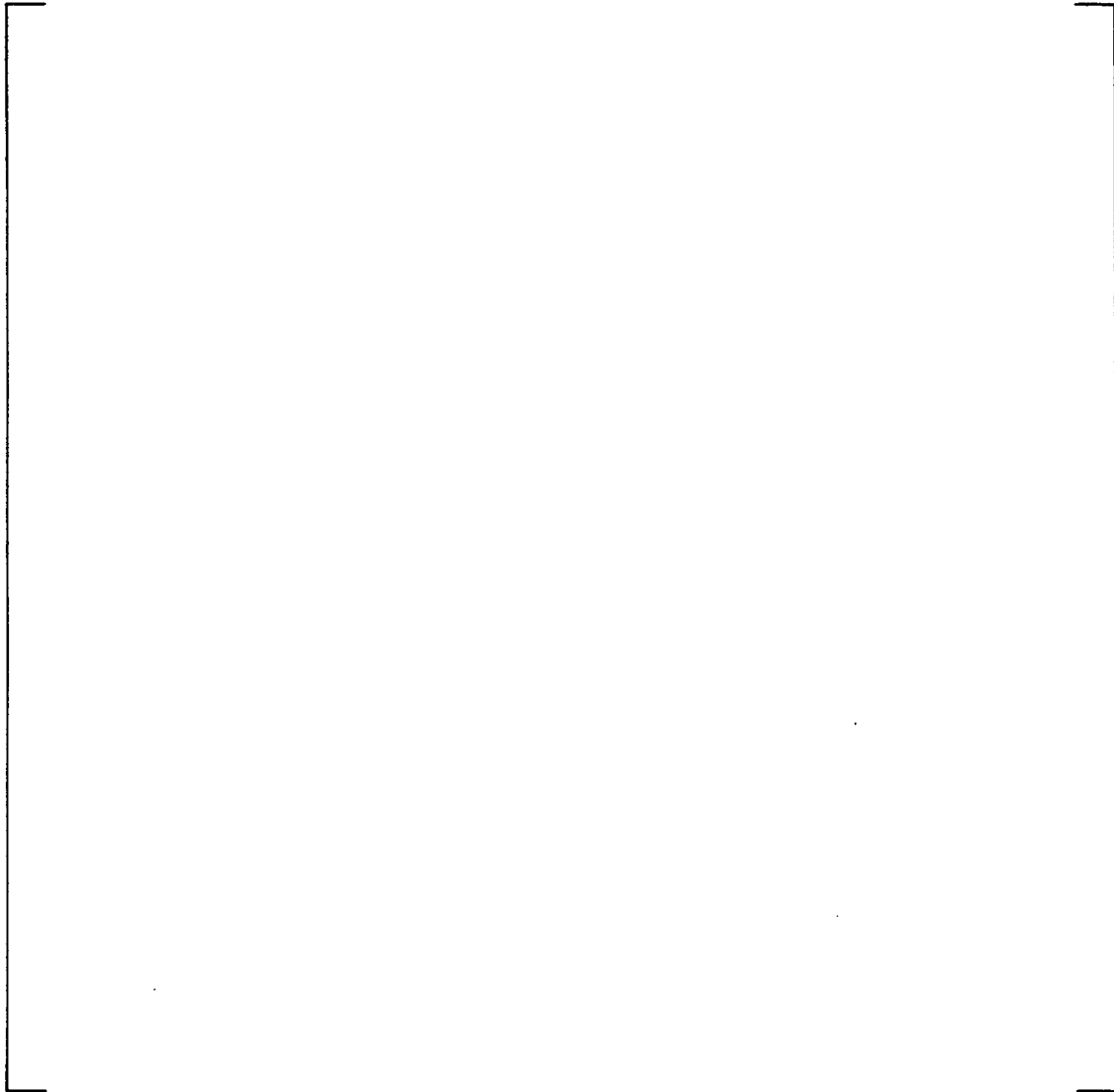


Figure 1.3

**PAD Creep Model Predictions  
(validation data)**



a, b, c

**Figure 1.4**

**PAD Creepdown M-P vs. Axial Elevation  
(all data)**

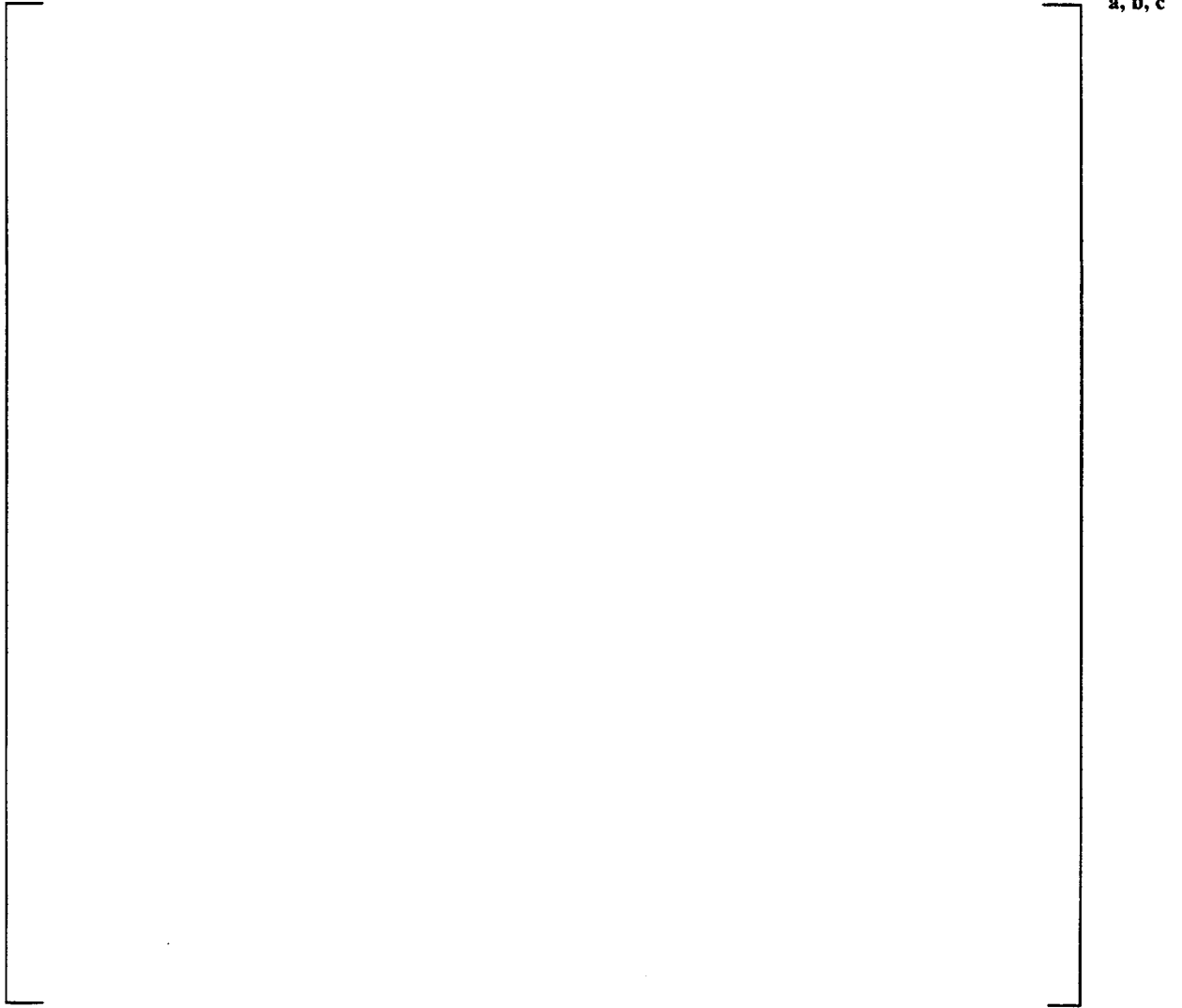


Figure 1.5

**PAD Creepdown M-P vs. Burnup  
(all data)**

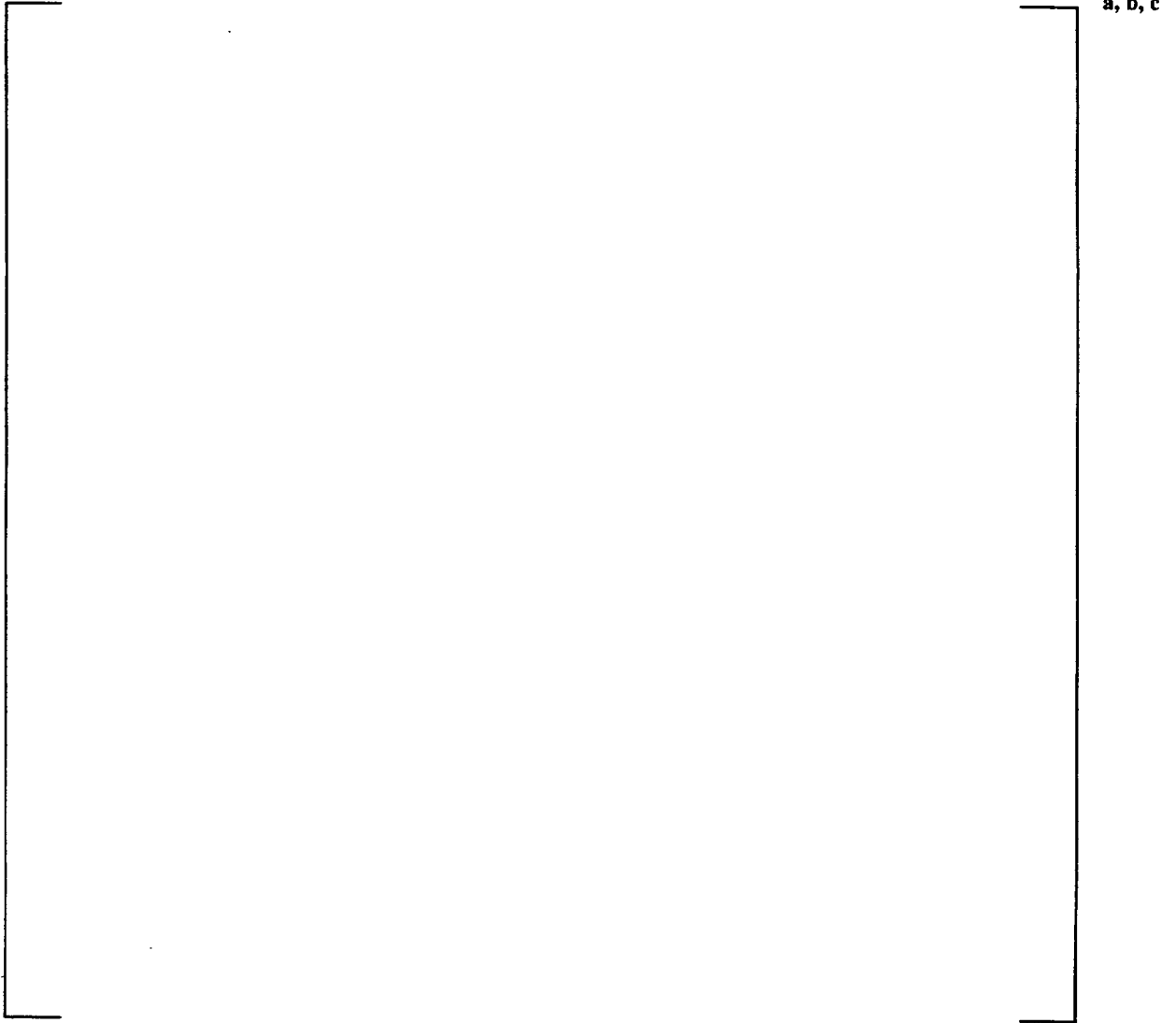


Figure 1.6

**PAD Creepdown M-P vs. Time Averaged Temperature  
(all data)**

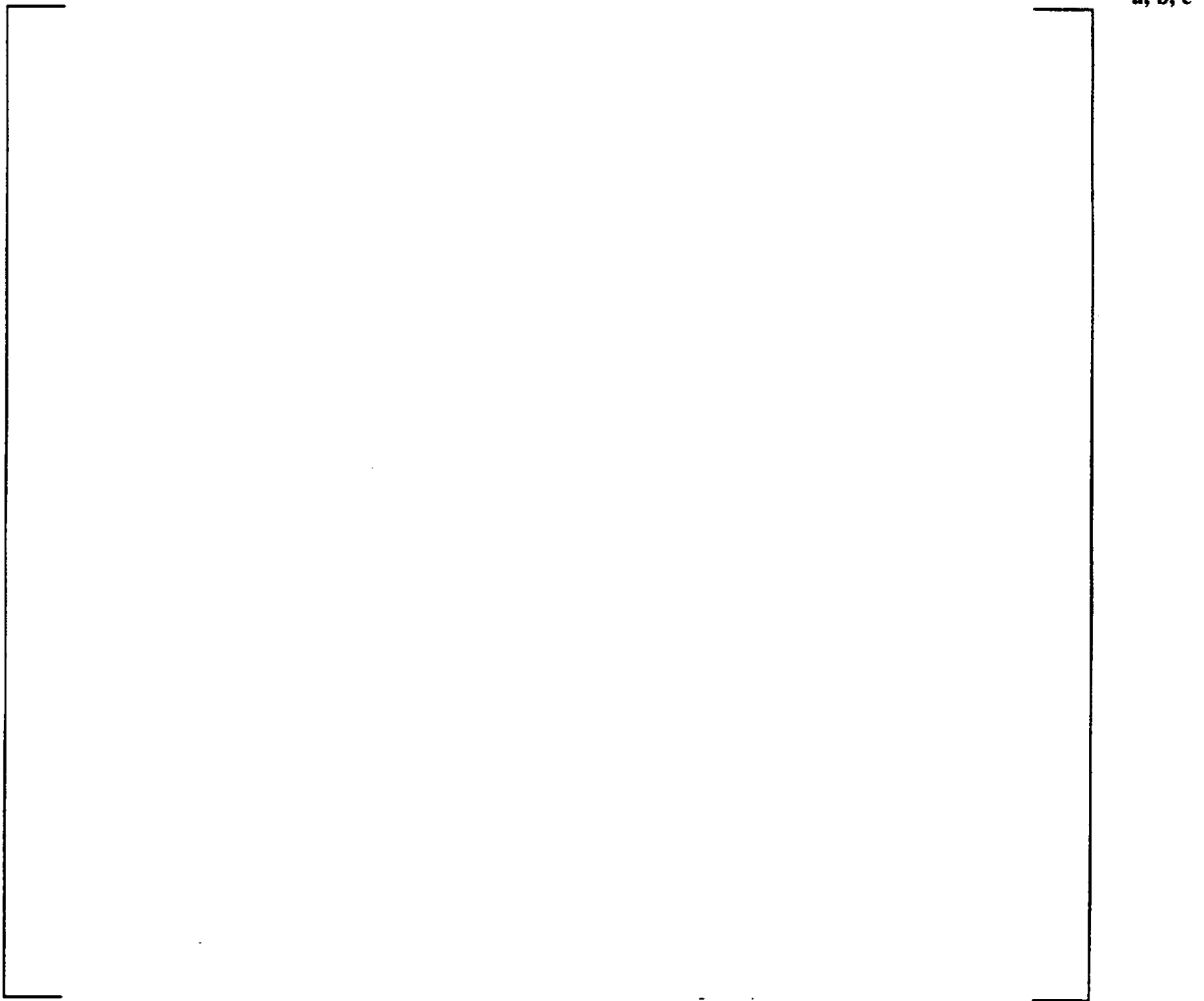
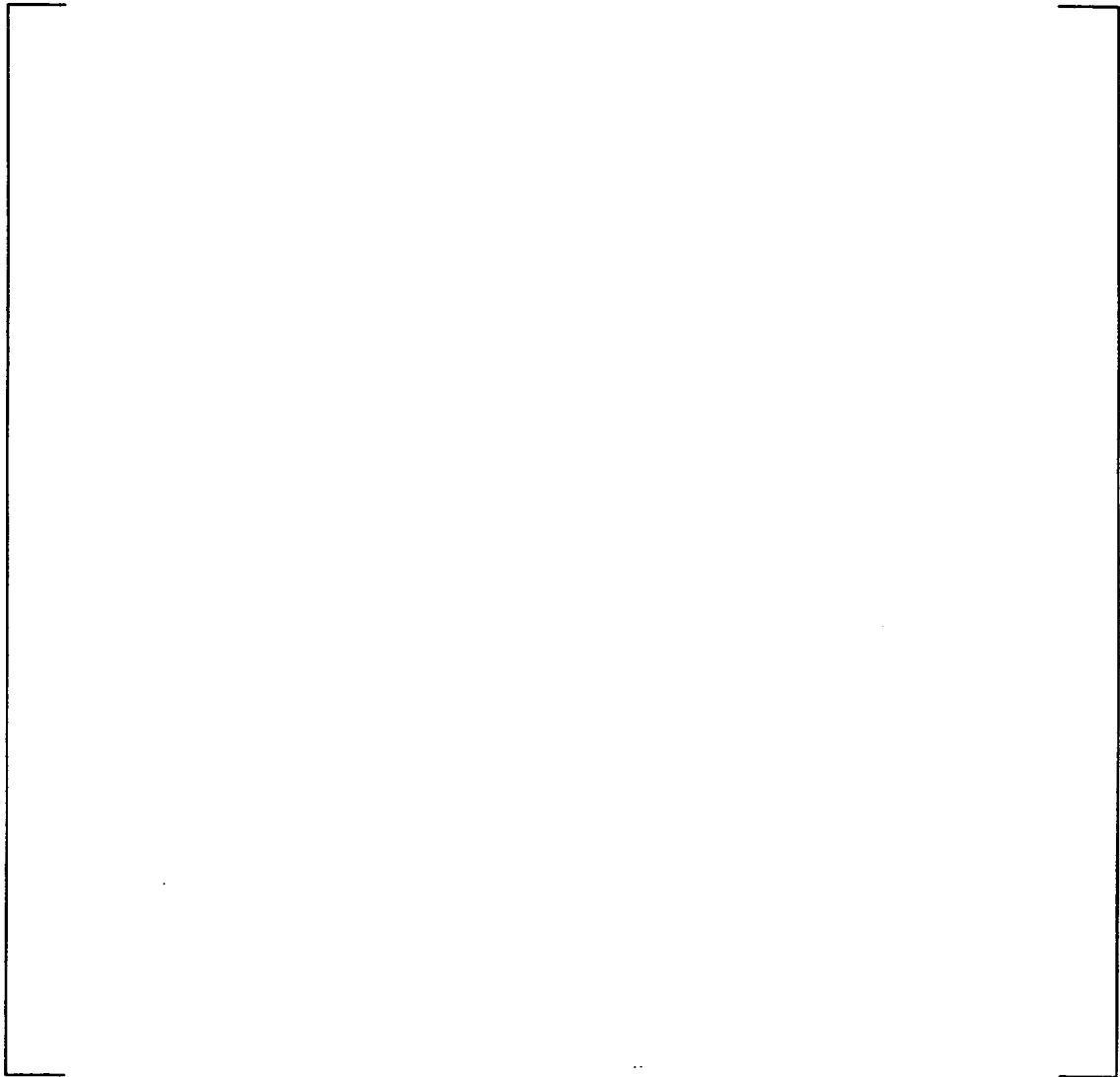


Figure 1.7

**PAD Creepdown M-P vs. Time Averaged Stress  
(all data)**



a, b, c

**Figure 1.8**

**Zion 2,3,4, and 5 cycle Creep Data  
(Conv. Zr-4)**



a, b, c

Figure 1.9

**Surry 1,3, and 4 cycle Creep Data  
(Conv. Zr-4)**

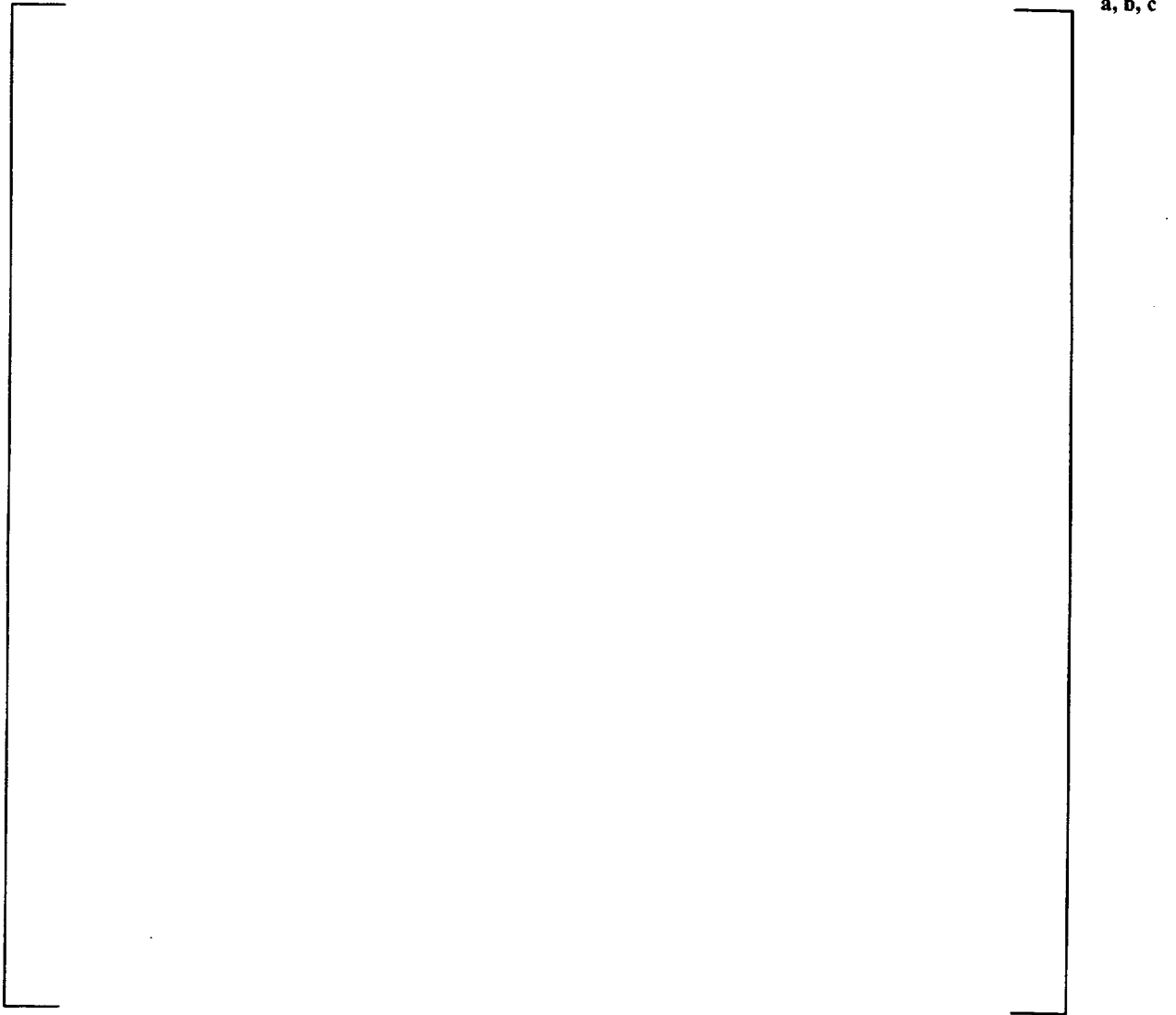


Figure 1.10

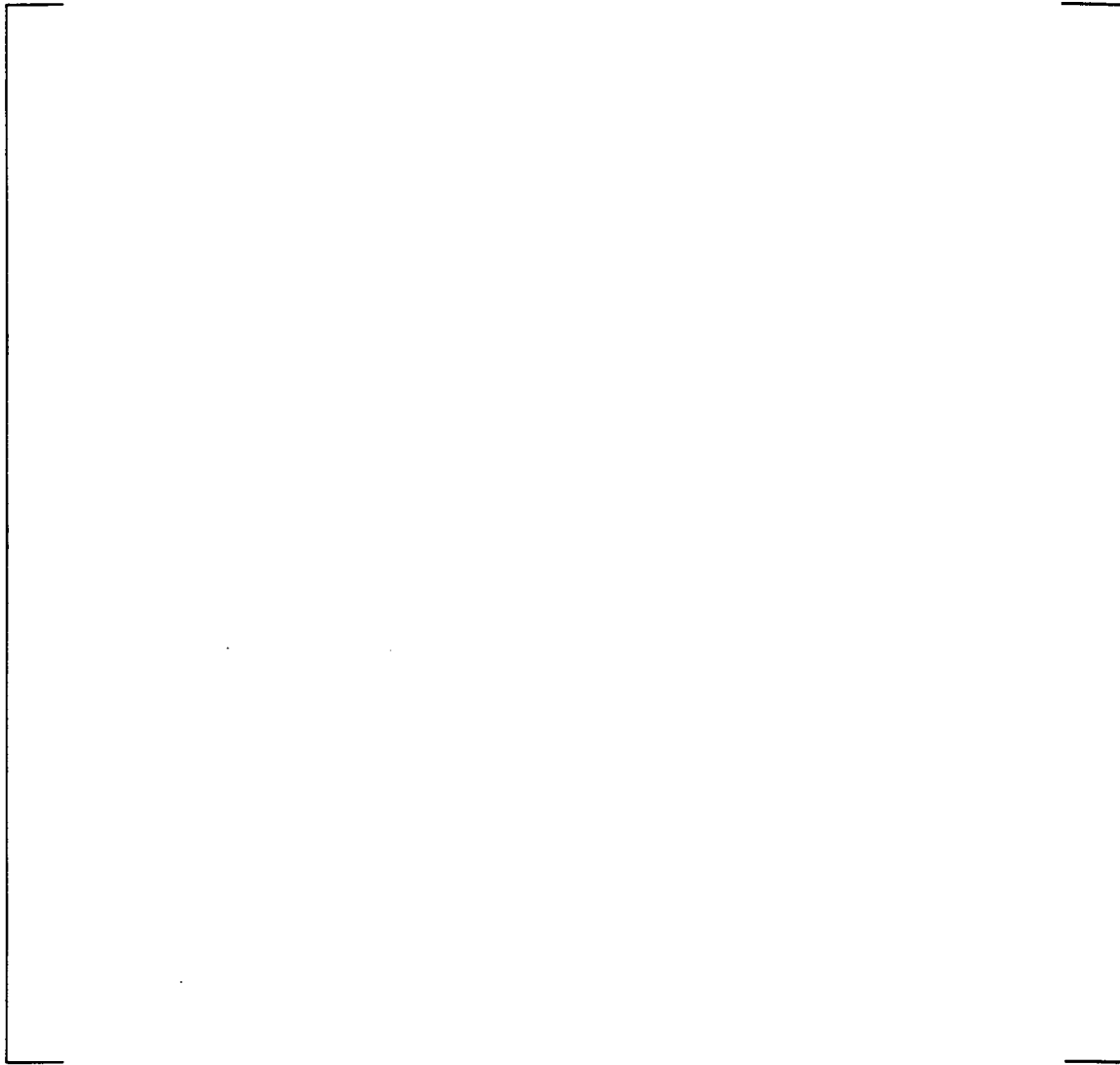
**Trojan 3 cycle Creep Data  
(Conv. Zr-4)**



a, b, c

Figure 1.11

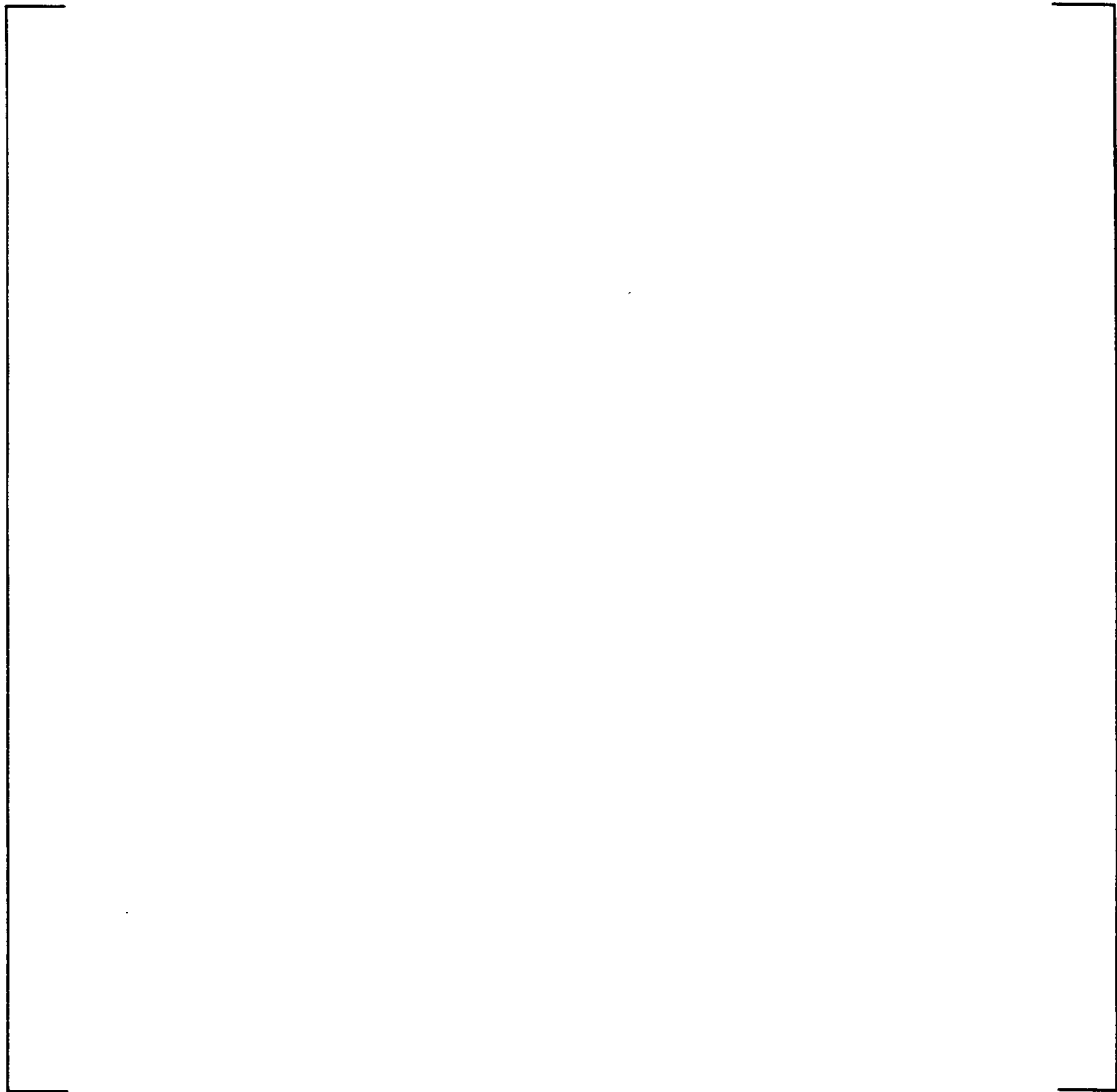
**Farley 1,2, and 4 cycle Creep Data  
(Conv. Zr-4)**



a, b, c

Figure 1.12

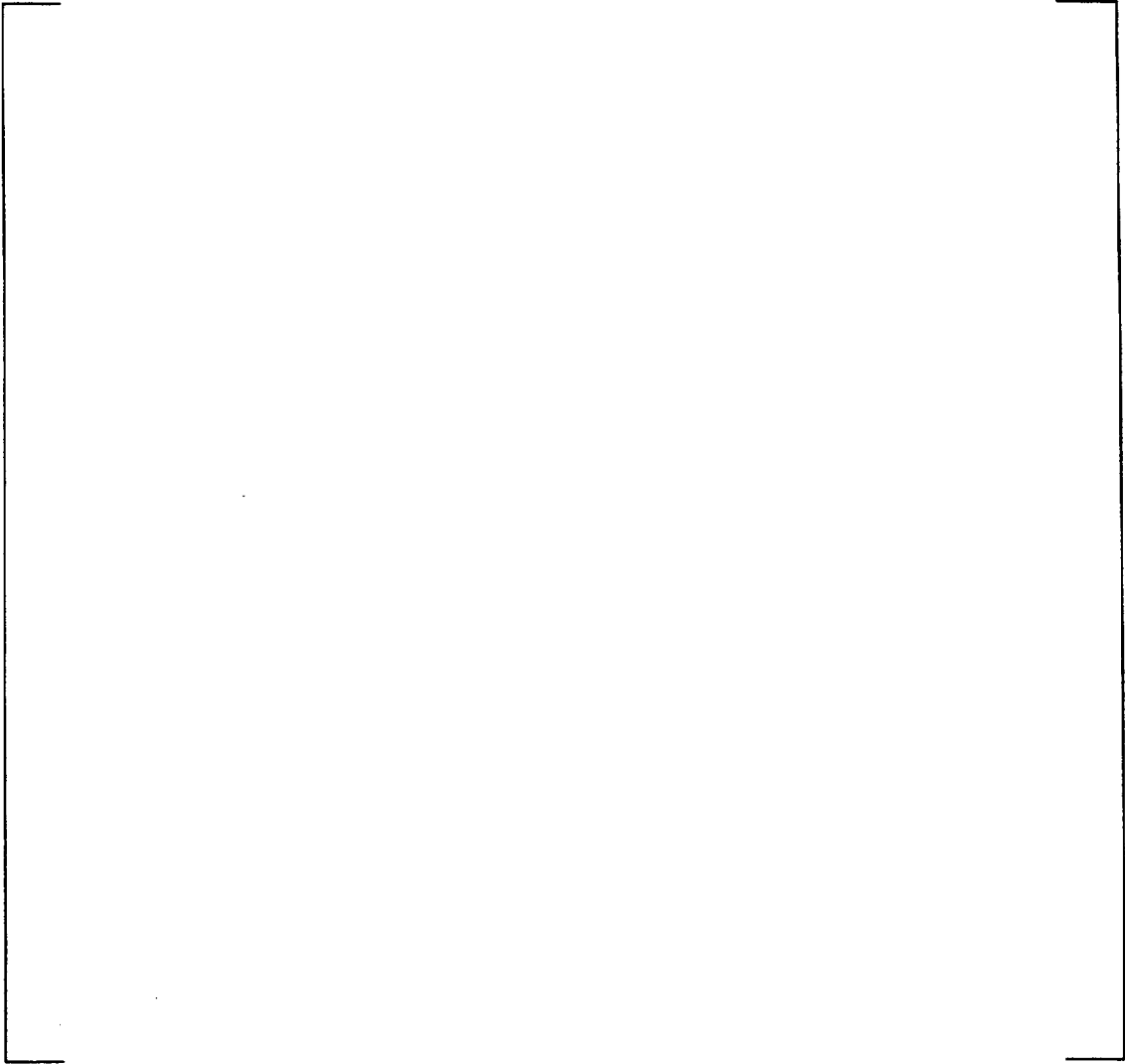
North Anna AM2 Creep Data  
(Conv. Zr-4)



a, b, c

Figure 1.13

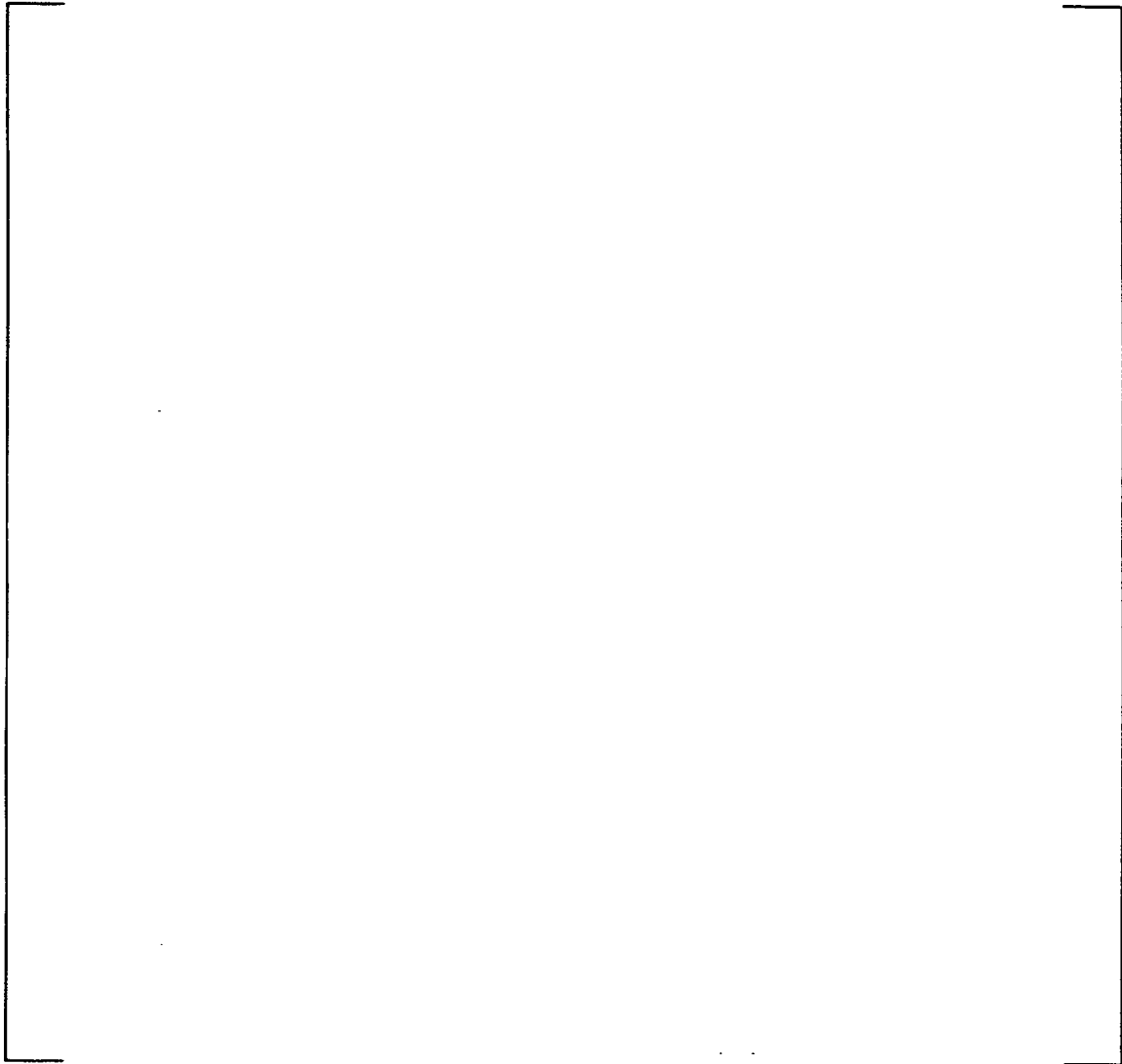
**North Anna AM2 Creep Data  
(Imp. Zr-4)**



a, b, c

Figure 1.14

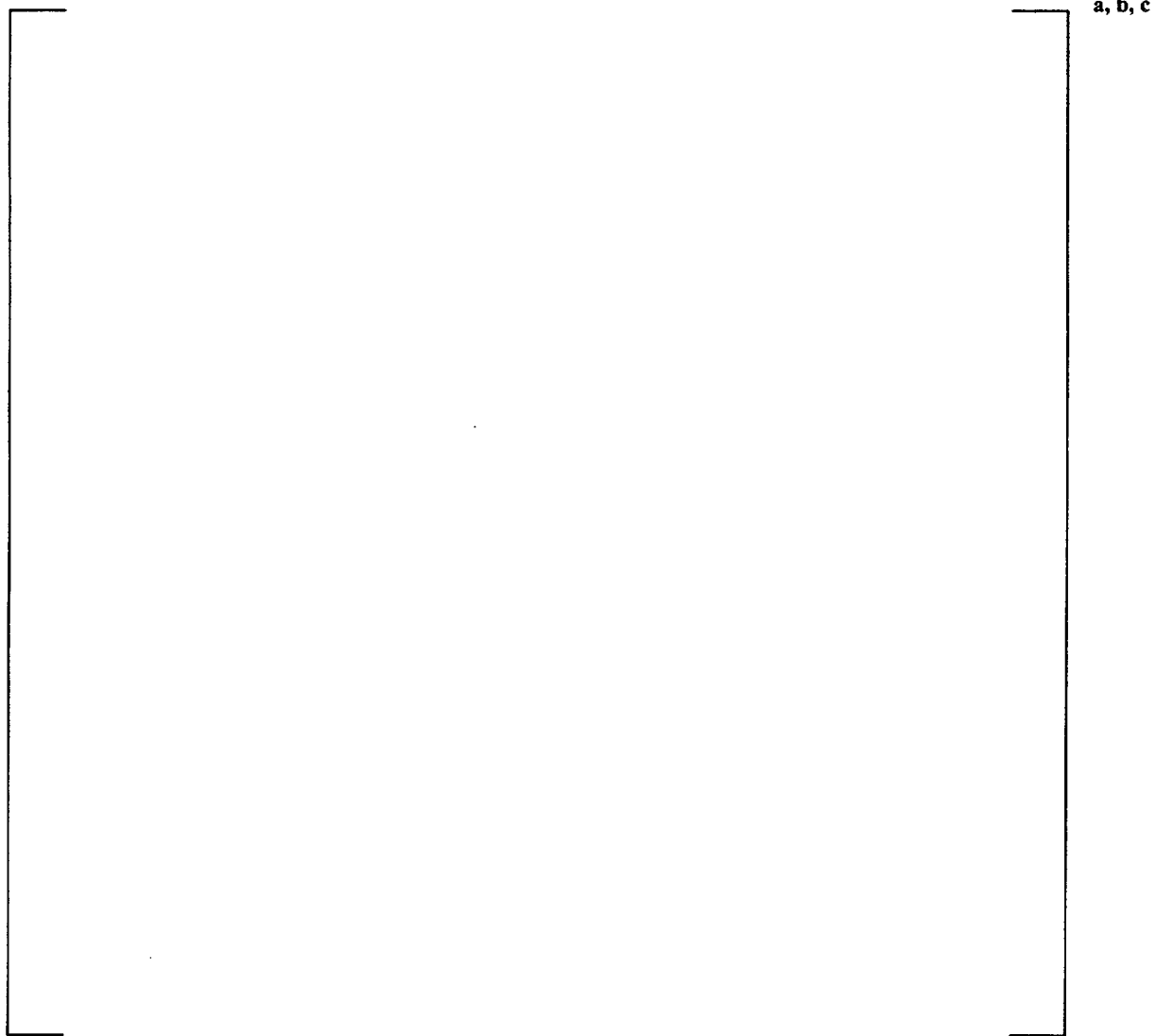
**Vandellos Creep Data  
(Imp. Zr-4)**



a, b, c

Figure 1.15

North Anna AM2 Creep Data  
(ZIRLO)





iteration of the calibration, a new value of [

] <sup>a, c</sup>.

### Thermal Model Data:

Fuel temperature data from three instrumented assemblies, IFA-431, IFA-432, and IFA-513, irradiated in the Halden reactor under NRC sponsorship, were used in this calibration. Each assembly contained six fuel rods instrumented with upper and lower thermocouples. Descriptions and pre-characterizations of the fuel are reported in References 4 and 5, and power histories and fuel temperature data are given in References 6, 7, 8, and 9.

The burnup range of the IFA-431, IFA-432, and IFA-513 data used for calibration has been limited. The calibration used thermocouple data in the burnup range of 0 to 5,000 MWD/MTU. There were several reasons for limiting the burnup range. The range of experimental variables in this burnup interval (power, gap size, fuel density, and gas composition) covers the range expected over the entire irradiation of a pressurized PWR fuel rod. Thermocouples de-calibrate as a function of the thermal neutron fluence and there is some uncertainty about the rate of de-calibration. Limiting the burnup range of the investigation also reduces the uncertainties associated with cladding creep rates, fuel densification and swelling rates, and fission gas release rates. Also, most of the high burnup data is from IFA-432 in which considerable fission gas leakage occurred in the rods at higher burnups and thus cannot be precisely modeled. However, the thermal model calibrated from this data is valid for burnups greater than 5,000 MWD/MTU in commercial LWR fuel because the ranges of the fuel variables included in the model derivation cover the range expected at much higher burnups. Furthermore, the validity of the PAD 3.4 (and thus PAD 4.0) thermal model into high burnup values (> 5,000 MWD/MTU) has been addressed in response to NRC questions in WCAP-10851-P-A, PAD 3.4<sup>(10)</sup>.

The measured data contained the following approximate ranges of conditions:

<i>Burnup:</i>	<i>0 to 5,000 MWD/MTU</i>
<i>Local Power:</i>	<i>0 to 14 kW/ft</i>
<i>Gap:</i>	<i>0 to 15 mils</i>
<i>Temperature:</i>	<i>500 to 3,200 °F</i>

Data from fifteen rods (three assemblies) from Halden were available for calibration and validation. Eleven rods were selected at random for the temperature calibration. These rods were 431-1, 431-2, 431-5, 431-6, 432-1, 432-3, 432-5, 513-2, 513-3, 513-4, and 513-6. Rods 431-3, 432-2, 513-1, and 513-5 were reserved for validation, and not included in the calibration.

### Statistical Analysis:

The PAD code was calibrated using the procedure presented above. The results of the calibration defined the [ <sup>a, c</sup>. The statistical results for the calibration, validation, and verification (total) data are shown below.

*Statistical Results of Thermal Calibration*



Figures 2.1 and 2.2 show the predicted versus measured thermal data for the calibration and validation subsets respectively. These comparisons show [

] <sup>a, c</sup>. The results are similar and consistent with those determined for the PAD 3.4 thermal model.

Figures 2.3 through 2.5 show the residual dependence of the model on rod average burnup, local power, and gap size. [

] <sup>a, c</sup>.

The thermal data has also been evaluated for rods with powers greater than 9kW/ft since these powers are most representative of normal in-reactor operation. Figures 2.6 through 2.9 show the M/P plots for each Halden fuel assembly for data with powers greater than 9kW/ft. Figures 2.10 through 2.12 show the residual dependence of the model on rod average burnup, local power, and gap size. A set of statistics for the greater than 9kW/ft data are given below:

*Statistical Results of Thermal Calibration*

*(Power > 9kW/ft)*



It can easily be seen that the thermal model tends to [

] <sup>a, c</sup>.

**Uncertainties:**

The PAD code gives best estimate fuel temperature predictions. The scatter of the differences between measurements and predictions can be due to variations in pre-irradiation physical parameters such as dimensions and densities, model inaccuracies, and instrumentation uncertainties. Since the rods were pre-characterized, it is not expected that a large fraction of the scatter is due to variations of pre-irradiation physical characteristics. However, not all parameters were either pre-characterized or documented and some assumptions were made. In these cases, the assumptions were validated by assuming certain undocumented parameters and comparing the analyzed behavior to the measured fuel. This approach ensured validity of the assumptions. Values of powers for the Halden rods are accurate to  $\pm 3\%$  to  $\pm 5\%$ <sup>(11)(12)</sup> and  $\pm 6\%$ <sup>(13)</sup> and thermocouple readings are quoted as being accurate to  $\pm 1\%$ <sup>(14)(15)(16)</sup>.

Skewness and kurtosis tests for normality were conducted on the M-P data and the P-value was determined to be [ ]<sup>a, c</sup>. The 95% upper-bound and 95% lower-bound uncertainties for the fuel centerline temperatures were calculated to bound 95% [ ]<sup>a, c</sup> and 5% of the data respectively. The computed uncertainties are shown below.

***Thermal Model Uncertainties***

--	--

a, b, c

**Conclusions:**

The thermal model has been successfully calibrated for use in PAD 4.0. The value of [ ]<sup>a, c</sup>. Associated uncertainties in the thermal model are shown above. All of the thermal model comparisons show reasonable agreement between measured and predicted data. The results for the revised PAD are consistent with those determined for the previously licensed PAD 3.4 thermal model calibration.

**Figure 2.1**

**Measured vs. Predicted Fuel Centerline Temperatures  
(calibration data)**

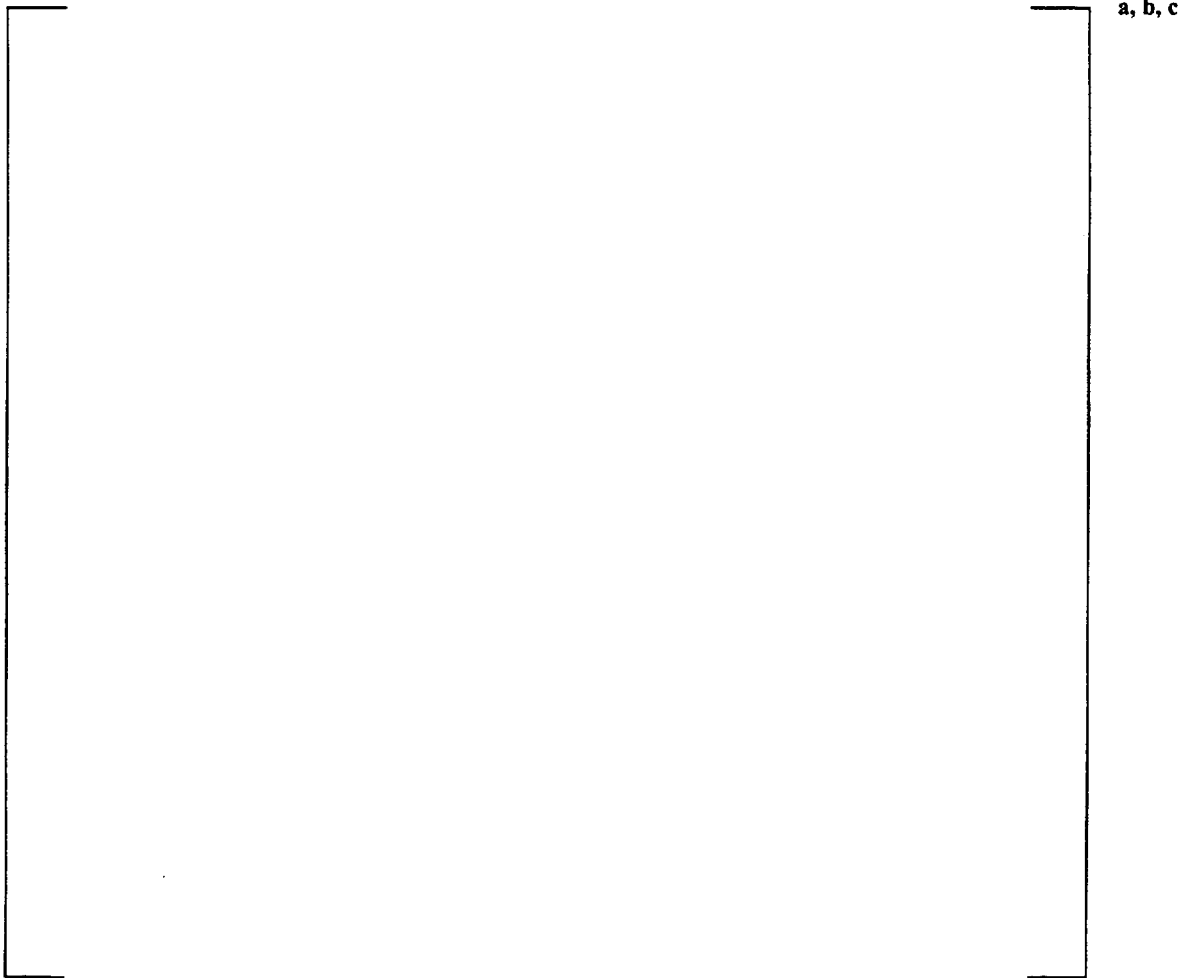


Figure 2.2

**Measured vs. Predicted Fuel Centerline Temperatures  
(validation data)**



Figure 2.3

**Measured - Predicted Fuel Centerline  
Temperatures vs Burnup  
(all data)**



a, b, c

Figure 2.4

**Measured - Predicted Fuel Centerline  
Temperatures vs Local Power  
(all data)**

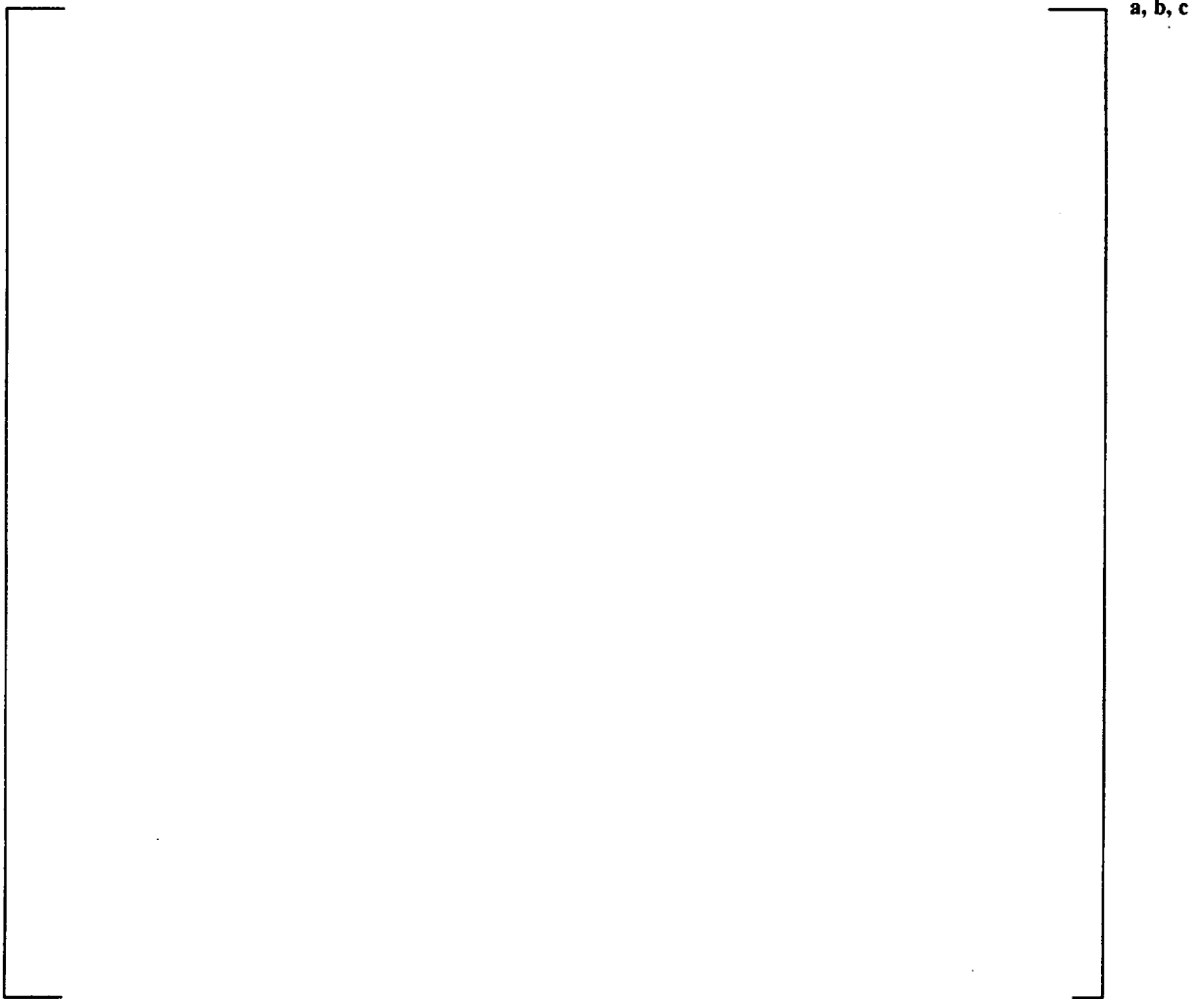


Figure 2.5

**Measured - Predicted Fuel Centerline  
Temperatures vs Fuel-to-Cladding Gap  
(all data)**



Figure 2.6

**Measured vs. Predicted Fuel Centerline Temperatures  
(Assembly 431, power > 9kW/ft)**

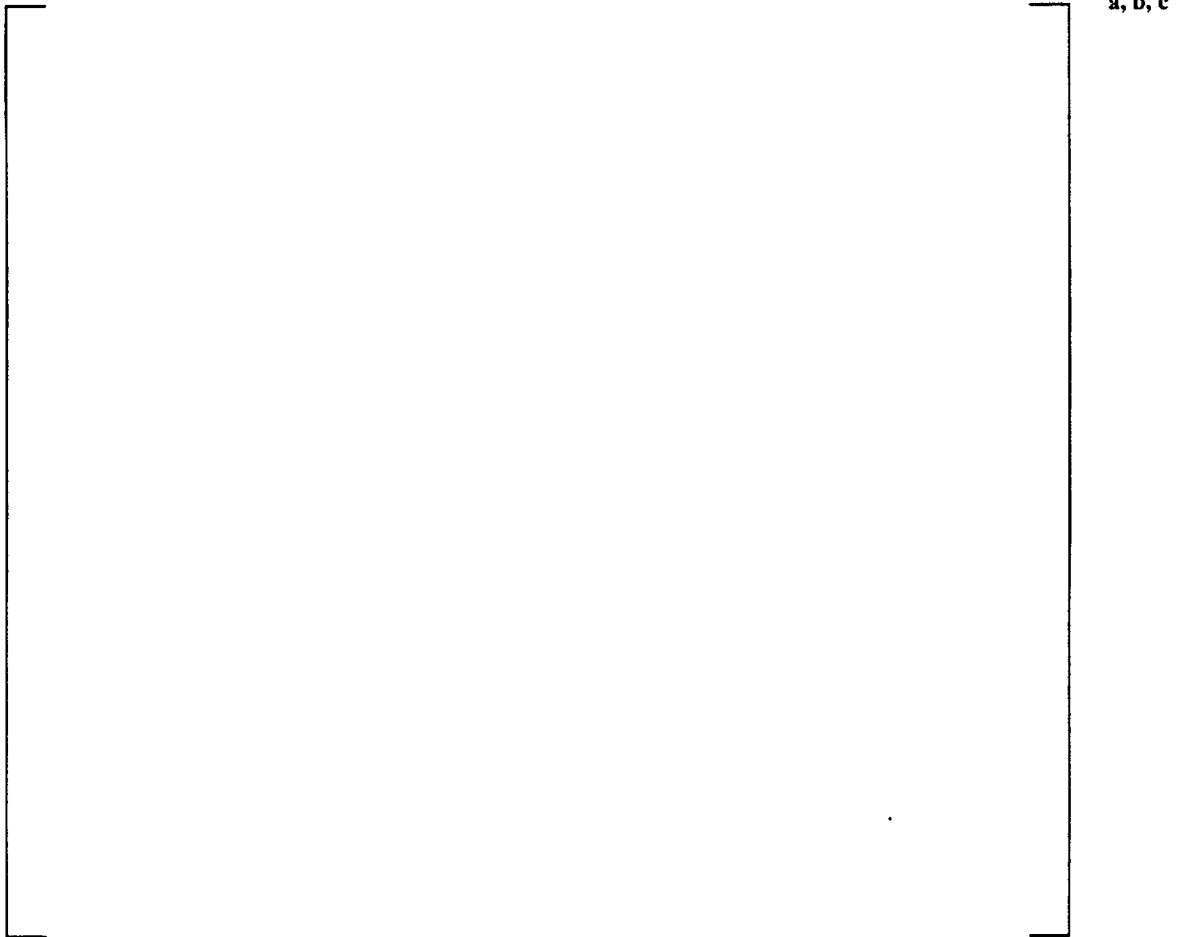


Figure 2.7

**Measured vs. Predicted Fuel Centerline Temperatures  
(Assembly 432, power > 9kW/ft)**

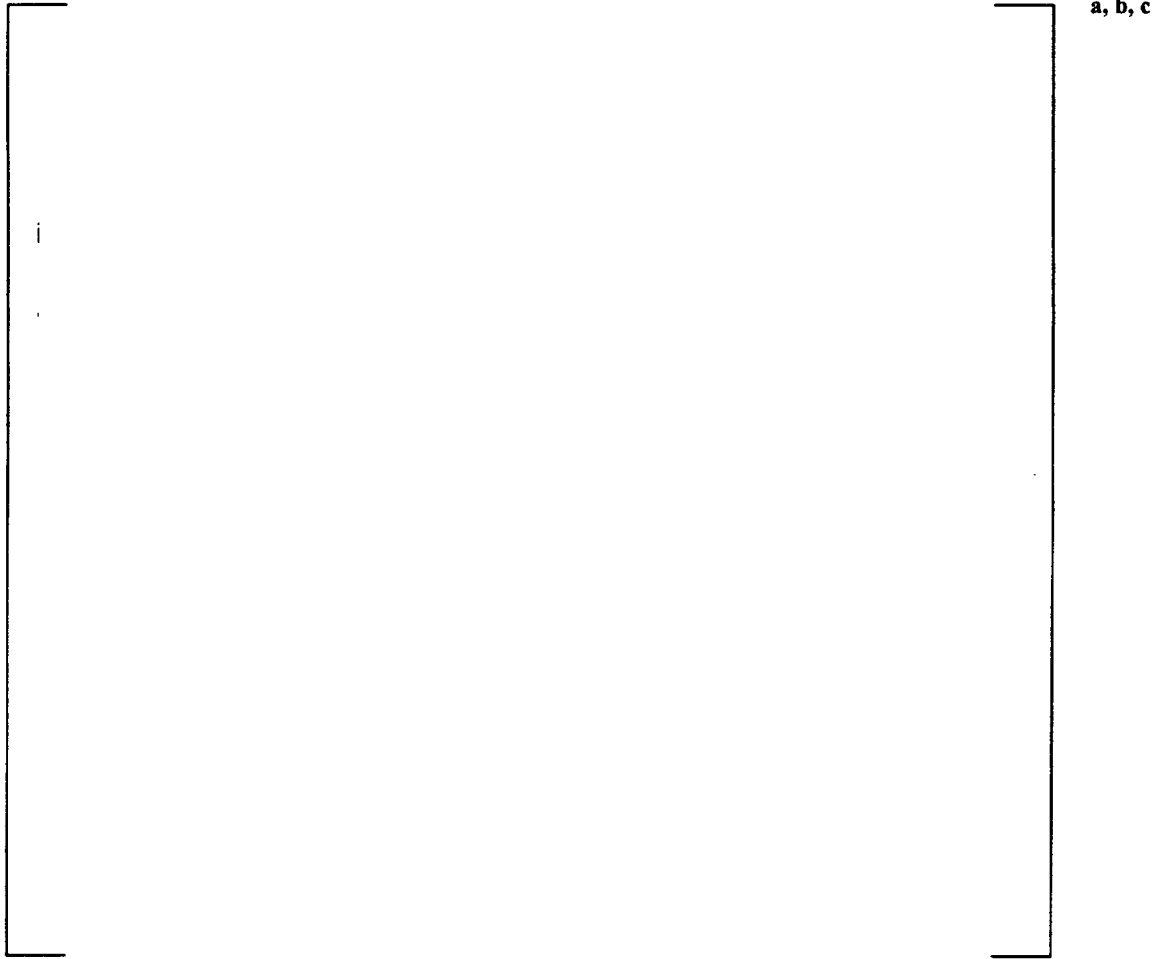


Figure 2.8

**Measured vs. Predicted Fuel Centerline Temperatures  
(Assembly 513-1,2,3, power > 9kW/ft)**



Figure 2.9

**Measured vs. Predicted Fuel Centerline Temperatures  
(Assembly 513-4,5,6, power > 9kW/ft)**

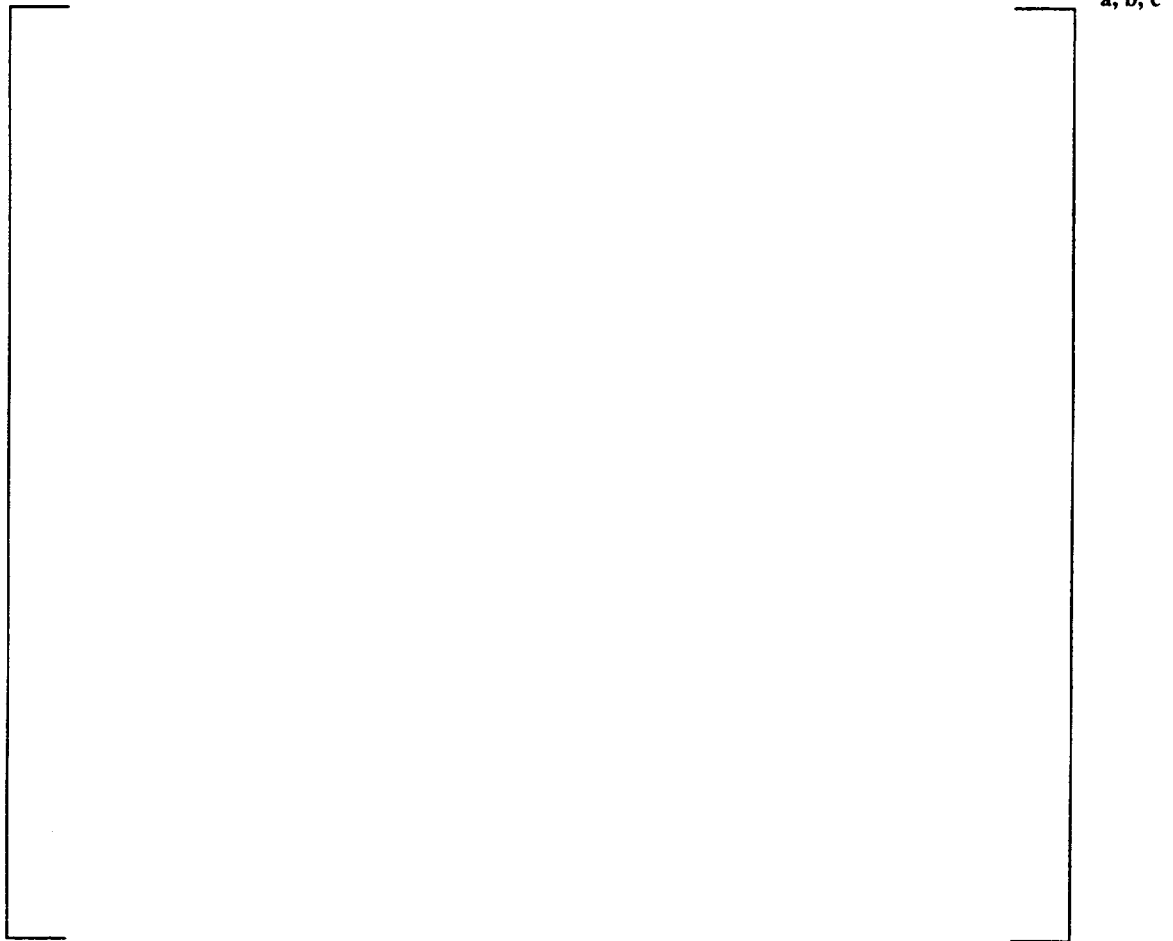


Figure 2.10

**Measured - Predicted Fuel Centerline  
Temperatures vs Burnup  
(power > 9kW/Ft)**

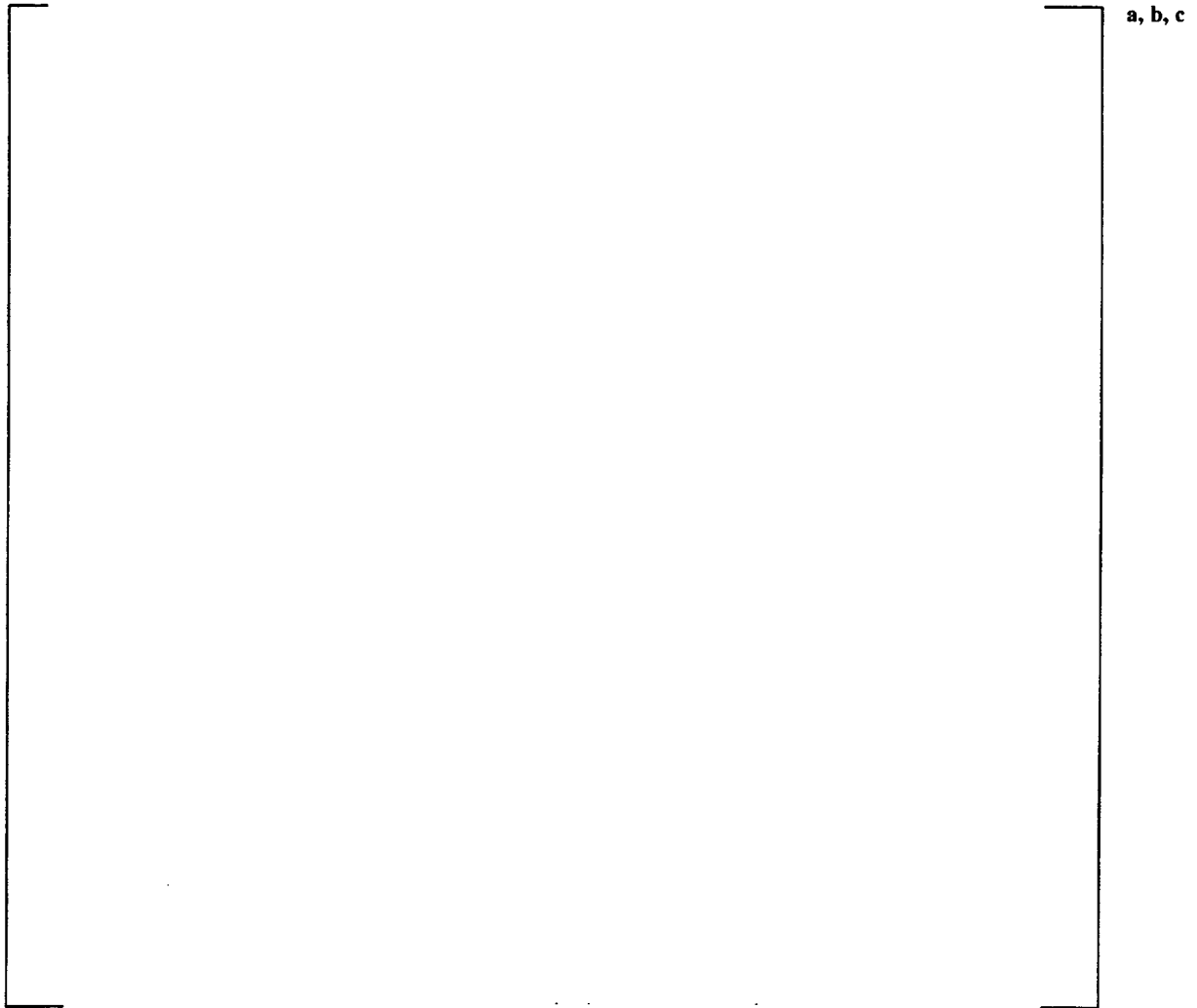


Figure 2.11

**Measured - Predicted Fuel Centerline  
Temperatures vs Local Power  
(power > 9kW/ft)**

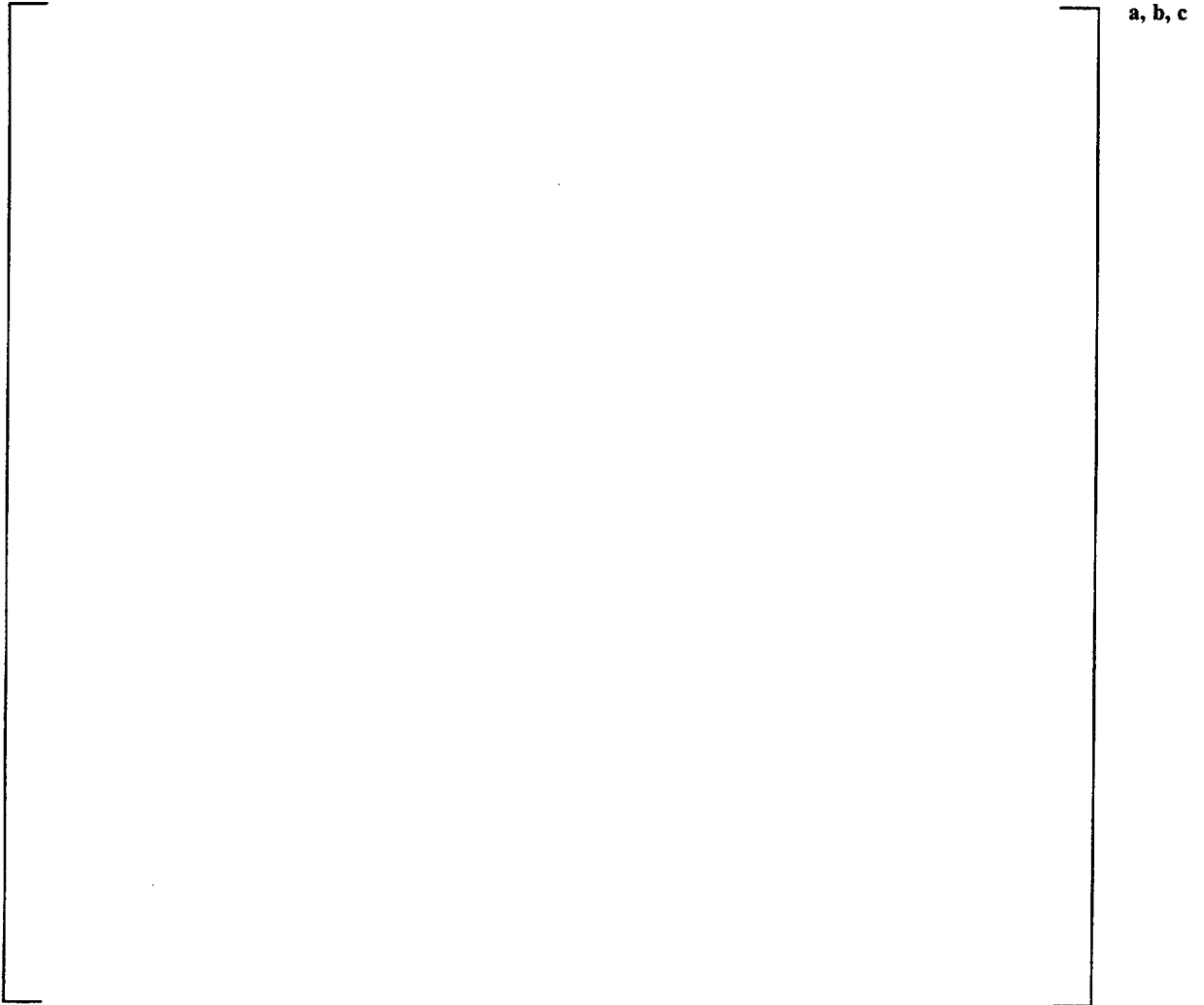
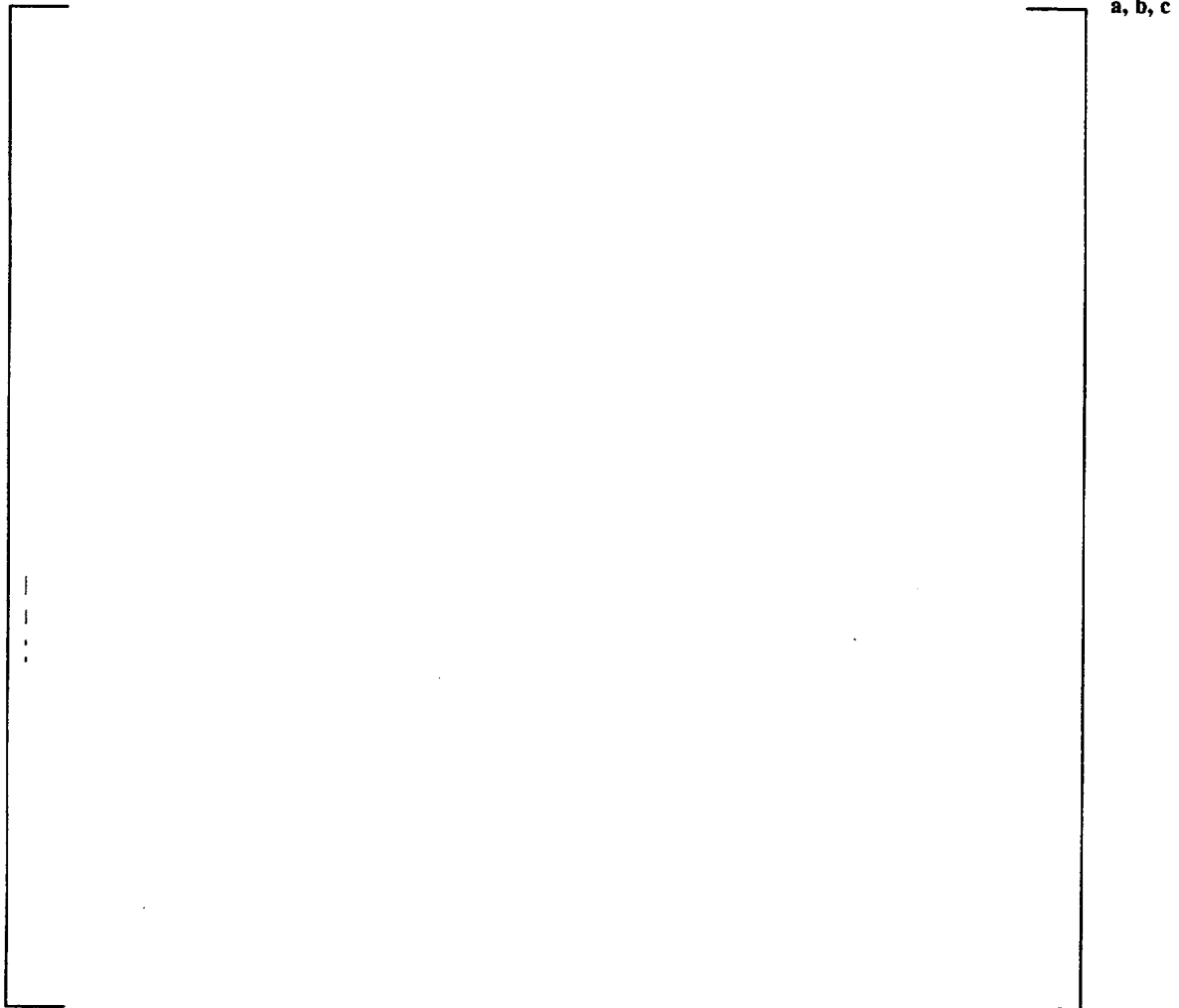


Figure 2.12

**Measured - Predicted Fuel Centerline  
Temperatures vs Fuel-to-Cladding Gap  
(power > 9kW/ft)**



## PAD 4.0

### Fission Gas Calibration and Verification Statistics

#### Introduction:

An improved in-reactor irradiation and thermal creep model has been developed and incorporated into the new PAD 4.0 code. As a result of these and other changes going into the new code, a full calibration, verification and uncertainty analysis was required for both the steady-state and transient fission gas release models.

#### Procedure:

The intent of this calibration was to compare the PAD 4.0 predicted fission gas release results to measured gas release data. The fission gas calibration was broken into two phases: [

] <sup>a, c</sup>. The process used in performing the fission gas release calibration required comparing the experimentally measured fission gas release with the PAD 4.0 predicted fission gas release.

[

] <sup>a, c</sup>.

The steady state fission gas database contains measured data other than just fission gas release. Some of the rods have associated rod growth data, void volume data, and profilometry data. Because the fission gas release model is highly dependent upon having an accurate fuel temperature prediction, it was necessary to be able to model growth, profilometry and void volume of these rods. [

] <sup>a, c</sup>.

**Fission Gas Release Model Data:**

Fission gas release data from [ ] <sup>a, c</sup> has been used to verify the steady-state fission gas release model. The range of fabrication and operating conditions covered by these rods is presented below:

[

] <sup>a, b, c</sup>

Although the results are not typically included in the statistical evaluation of the steady-state database, measured and predicted release data was reviewed for [ ]<sup>a, c</sup>.

[

] <sup>a, c</sup>.

**Rods Eliminated from PAD 3.4  
Steady-State FGR Calibration Database**

[

] <sup>a, b, c</sup>

As indicated above, it was decided to [

] <sup>a, c</sup>.

[

] <sup>a, c</sup>.

[

] <sup>a, c</sup>.



[

] <sup>a, c</sup>. Furthermore, the results are consistent with what has been predicted for these rods in past evaluations (e.g., PAD 3.4).

The statistical results for the calibration, validation, and verification (total) data are given below. [

] <sup>a, c</sup>.

*Statistical Results of Fission Gas Release Calibration*

	a, b, c
--	---------

**Uncertainties:**

Low Temperature Release Model:

[

] <sup>a, c</sup>.

[

] <sup>a,c</sup>.

High Temperature Release Model:

*Part I: Upper-Bound Uncertainty:*

[

] <sup>a,c</sup>.

[

] <sup>a,c</sup>.

[

] <sup>a,c</sup>.

*Part II: Lower-Bound Uncertainty:*

[

] <sup>a,c</sup>.

Transient Fission Gas Release Uncertainty Analysis:

[

1<sup>a, c</sup>.

**Conclusions:**

The steady-state and transient fission gas release models have been successfully calibrated for use in PAD 4.0. All of the fission gas release model comparisons show reasonable agreement between measured and predicted data. The results are similar with those determined for the PAD 3.4 fission gas release model calibration.

A summary of all calibration constants determined in this calibration are given below:

[

]

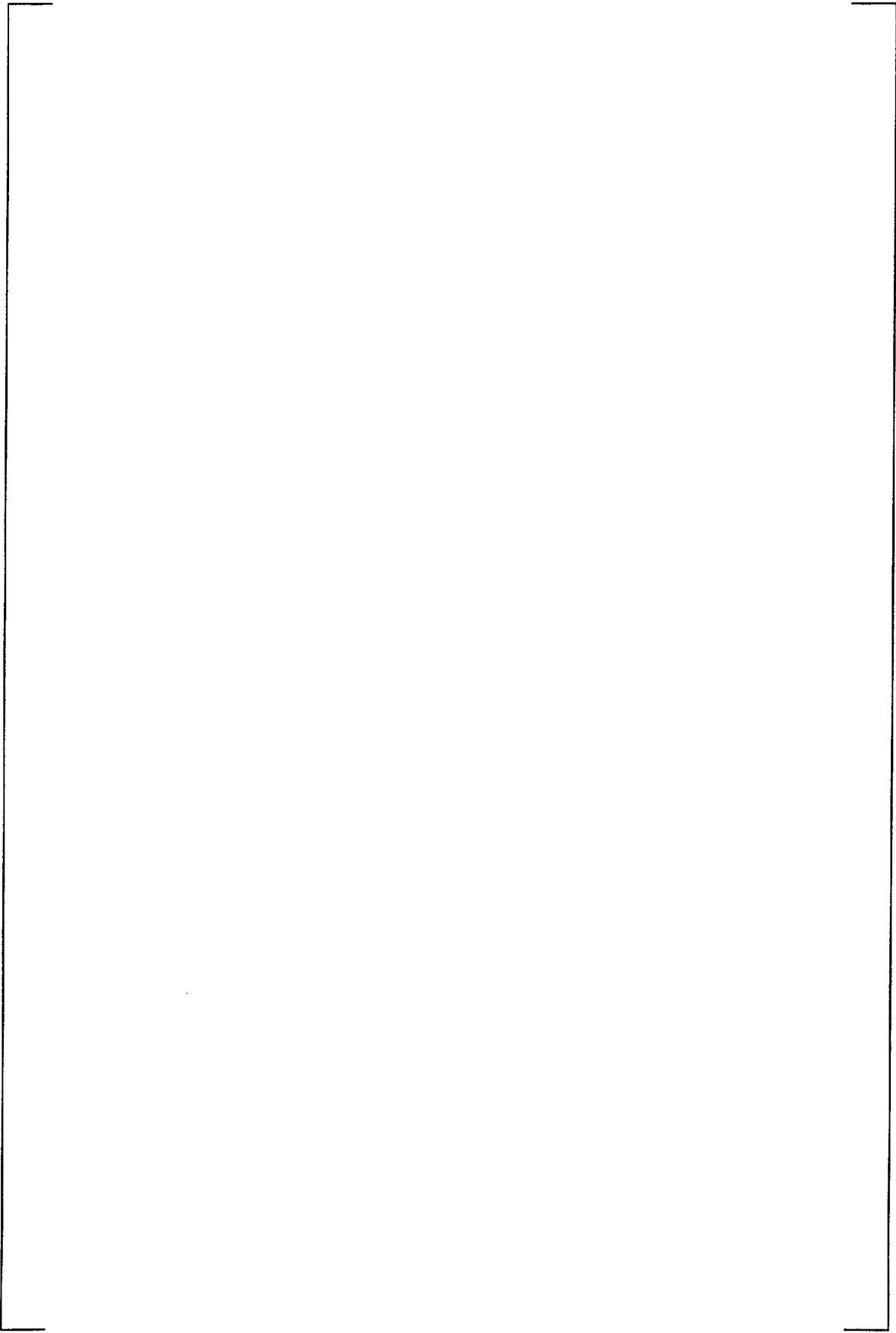
a, b, c

**List of Fission Gas Data**

a, b, c

A large, empty rectangular frame with a thin black border, occupying most of the page. It is positioned between the title and the footer, and is currently blank.

a, b, c



a, b, c

Figure 3.1

**Fission Gas Release Database  
Fuel Rod Growth Measured vs. Predicted**



a, b, c

Figure 3.2

**Fission Gas Release Database  
Fuel Rod Diametral Creep Down Measured vs. Predicted**

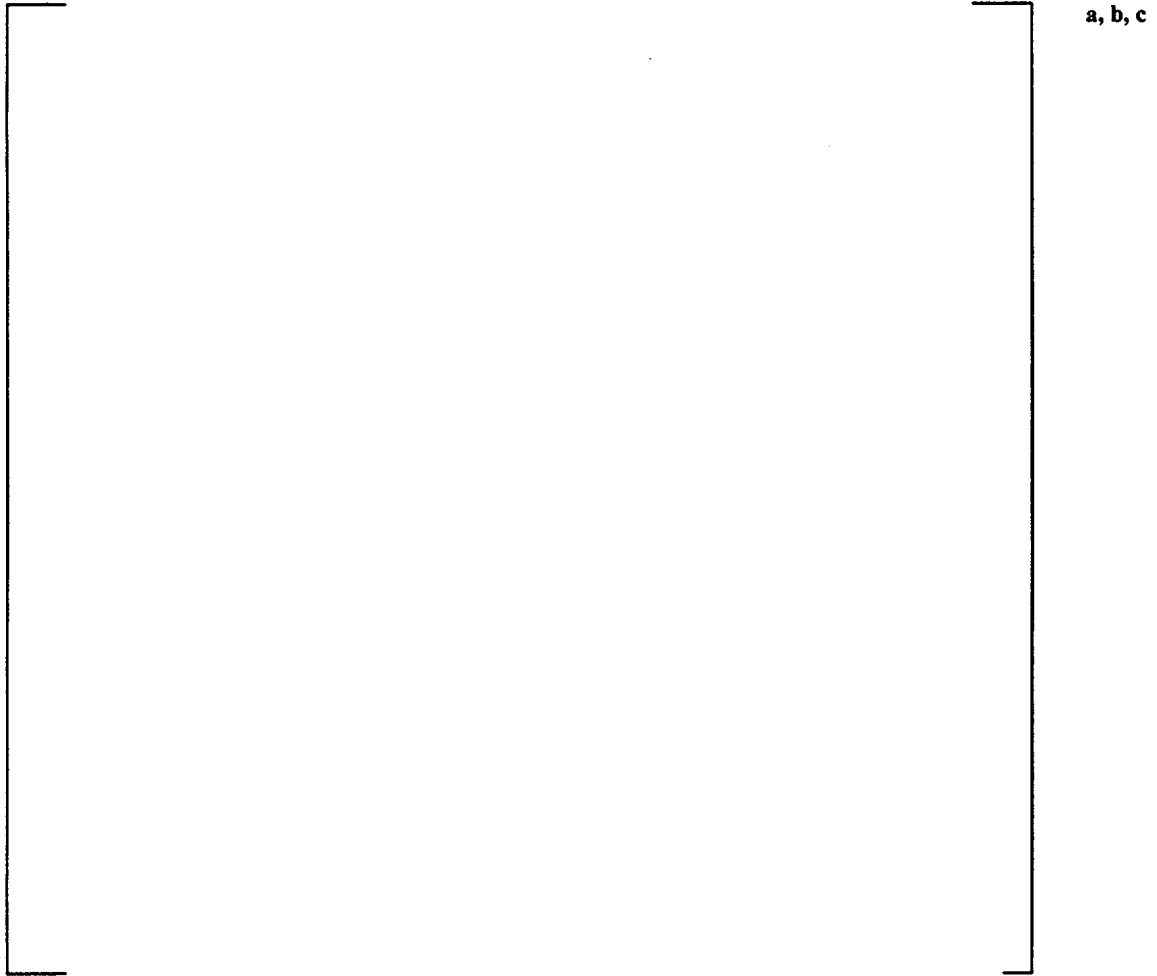
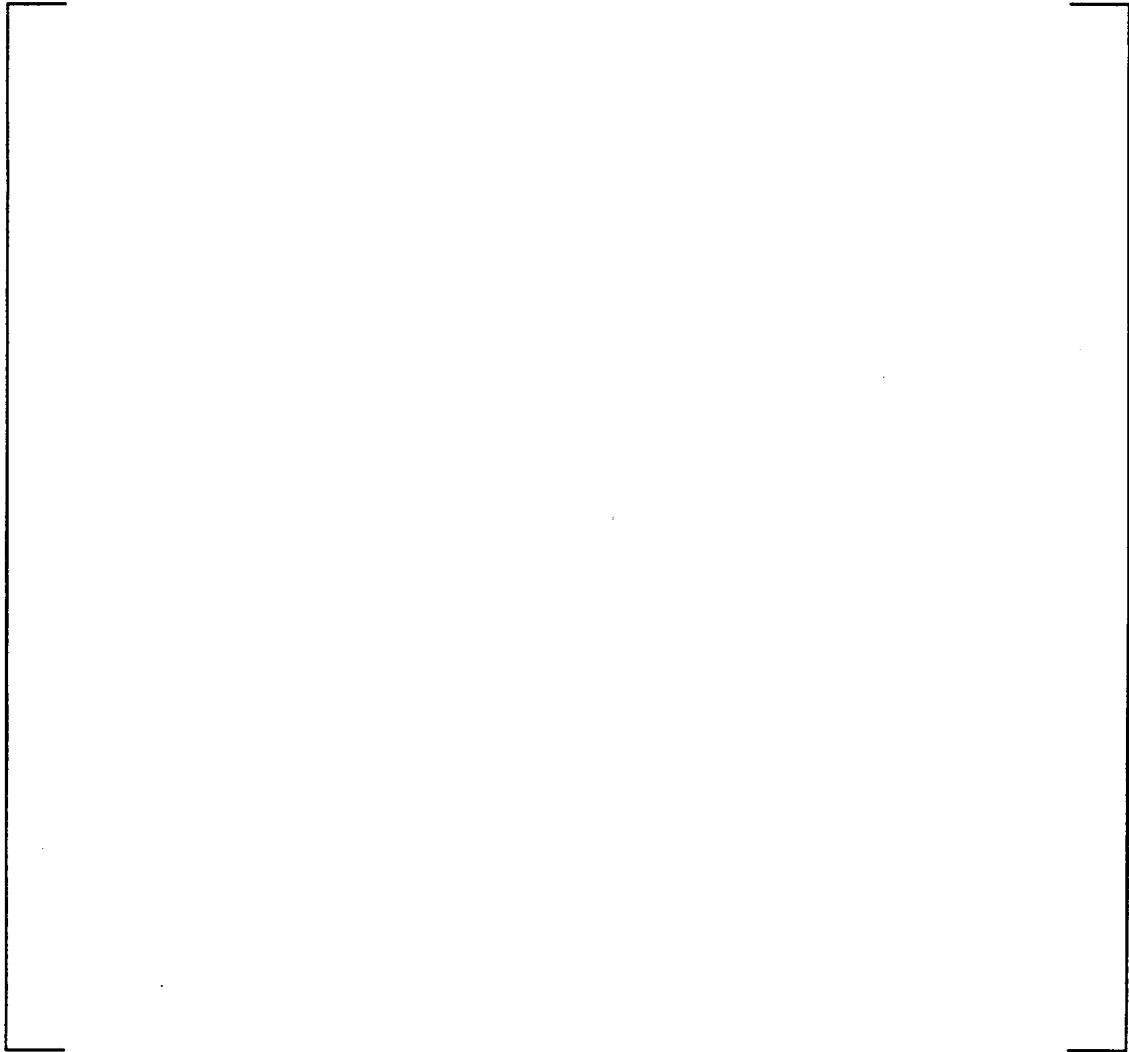


Figure 3.3

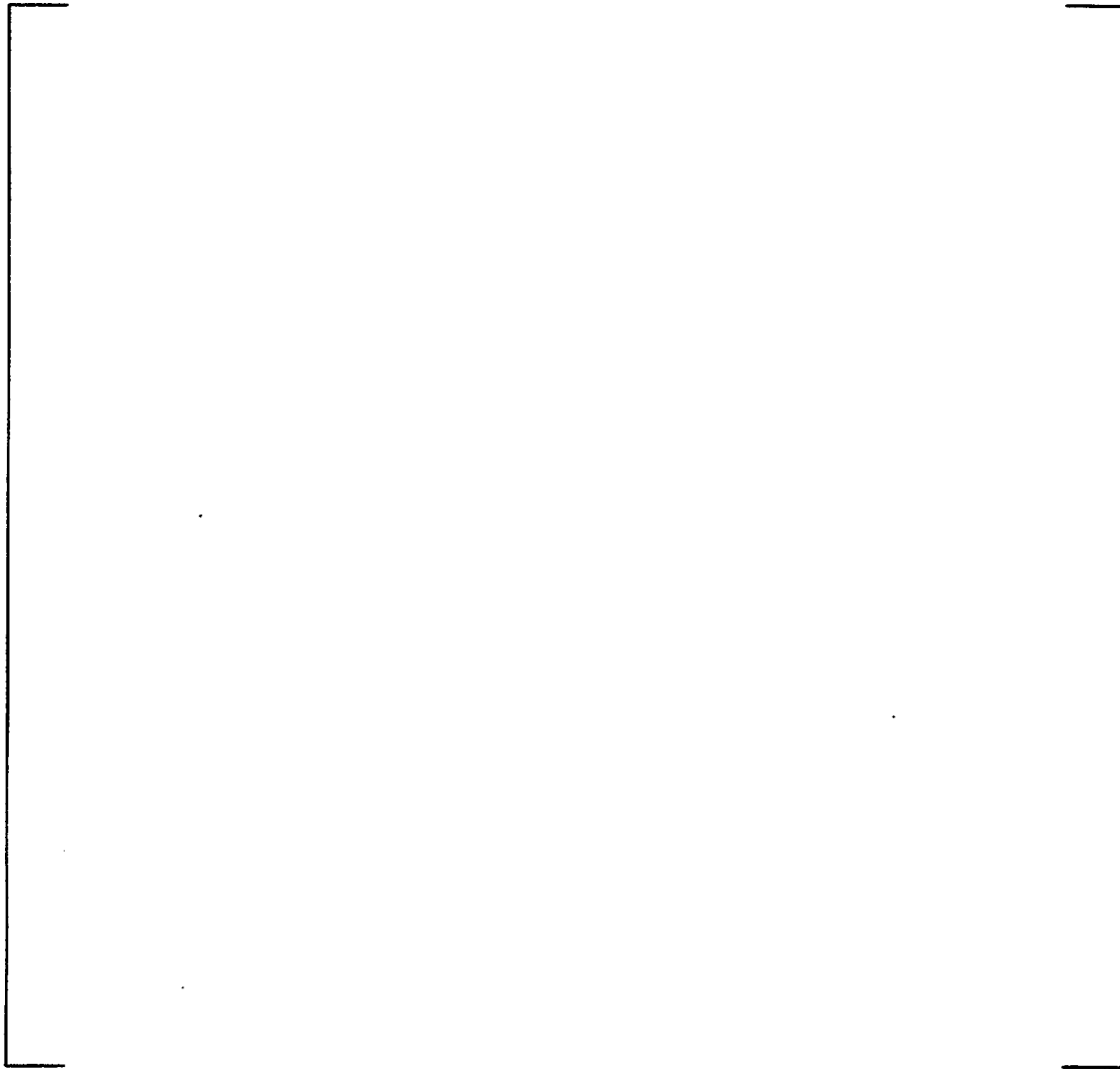
**Fission Gas Release Database  
Fuel Rod Void-Volume Measured vs. Predicted**



a, b, c

Figure 3.4

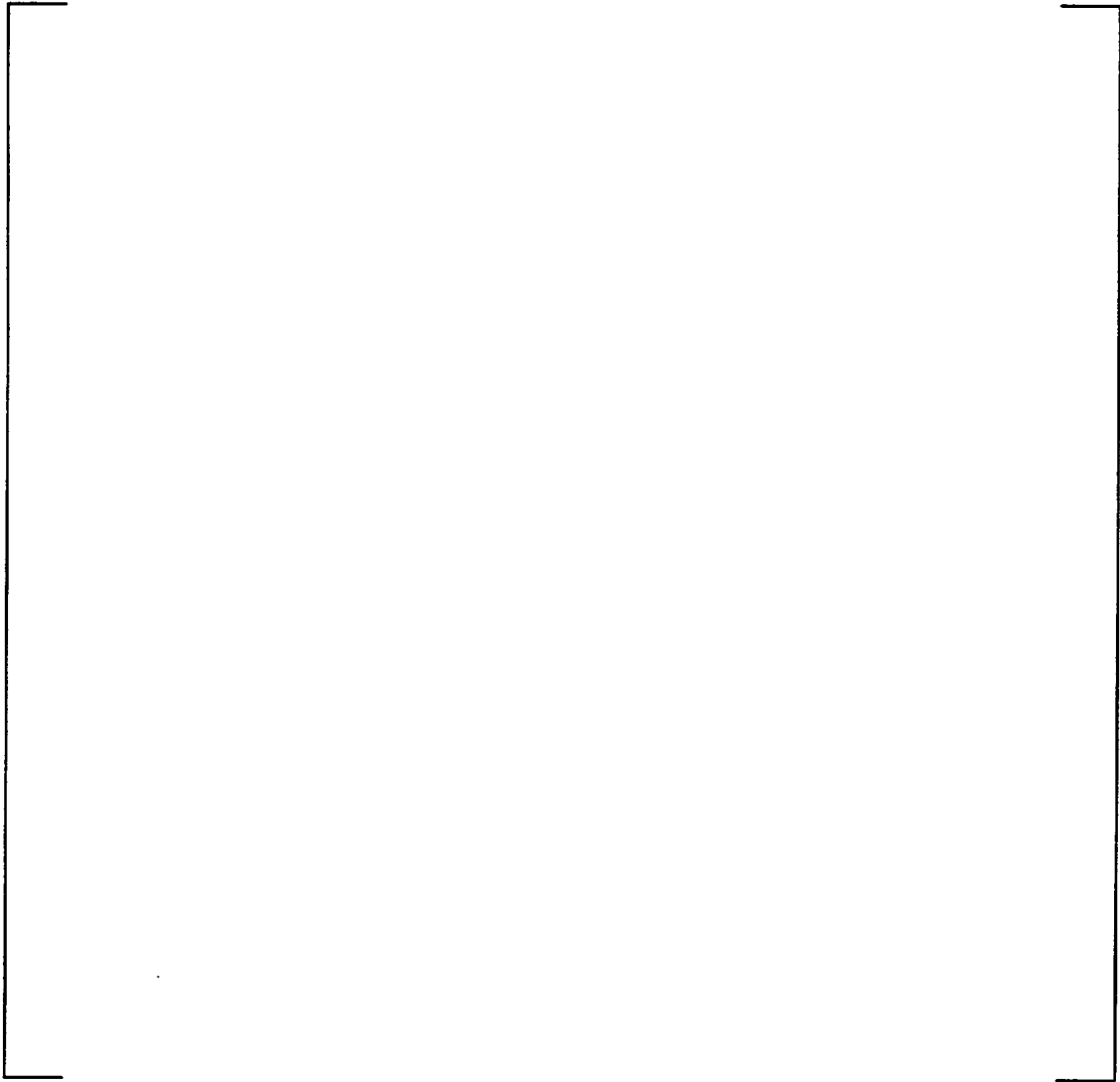
**All Fission Gas Release Data  
Predicted vs. Measured**



a, b, c

Figure 3.5

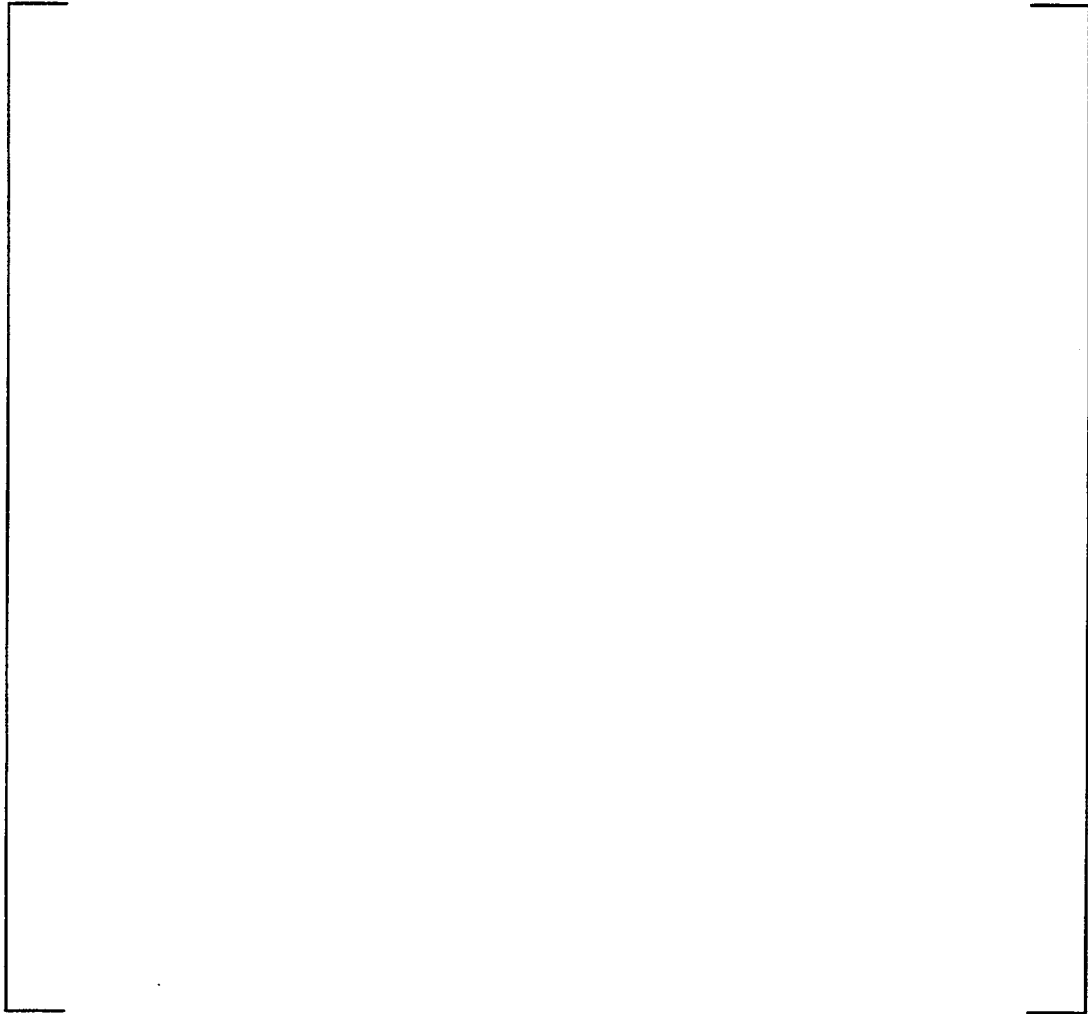
**Steady-State Fission Gas Release  
Low-Temperature Predicted vs. Measured**



a, b, c

Figure 3.6

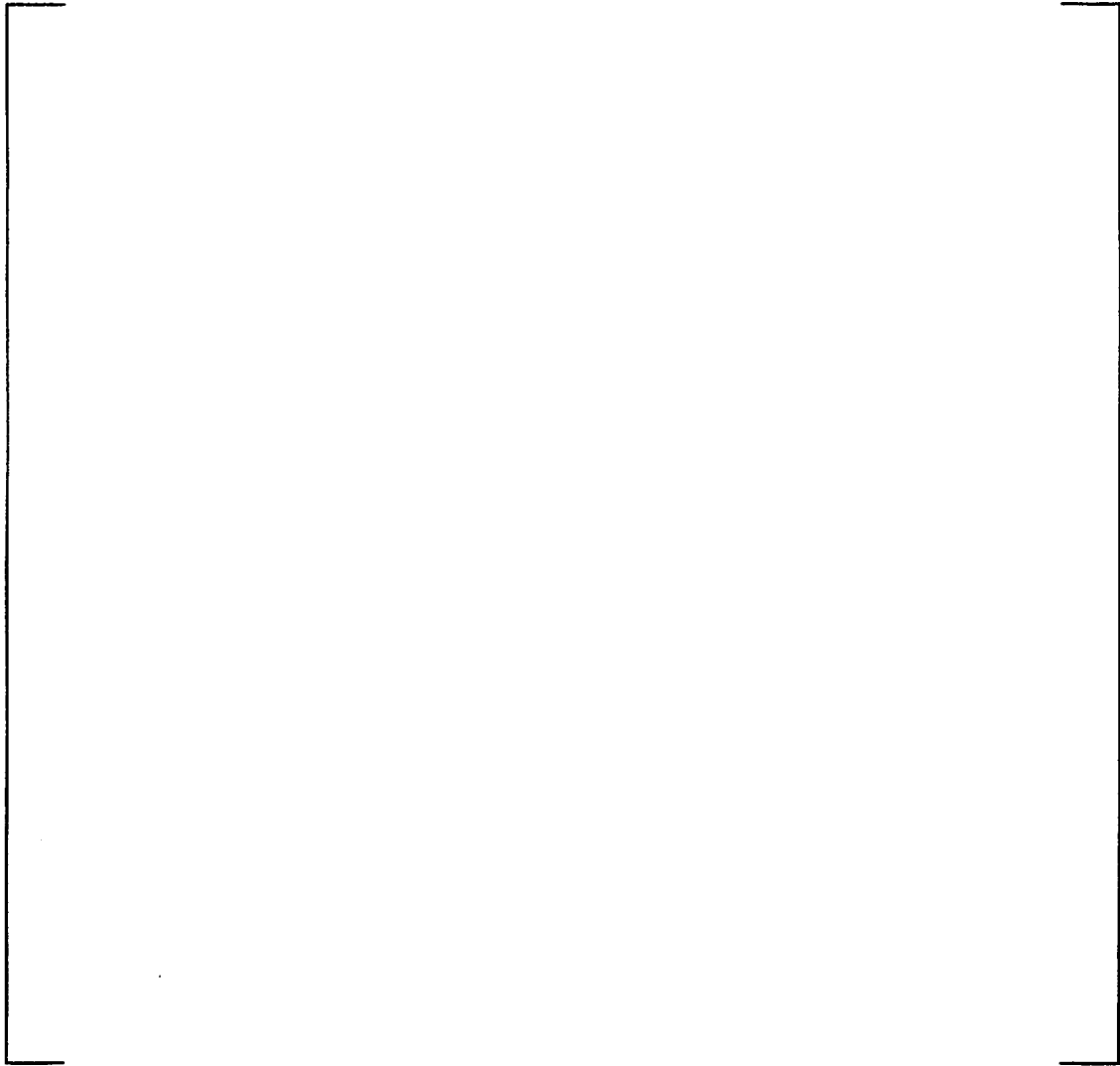
**Steady-State Fission Gas Release  
Low-Temperature Measured-Predicted vs. Burnup**



a, b, c

**Figure 3.7**

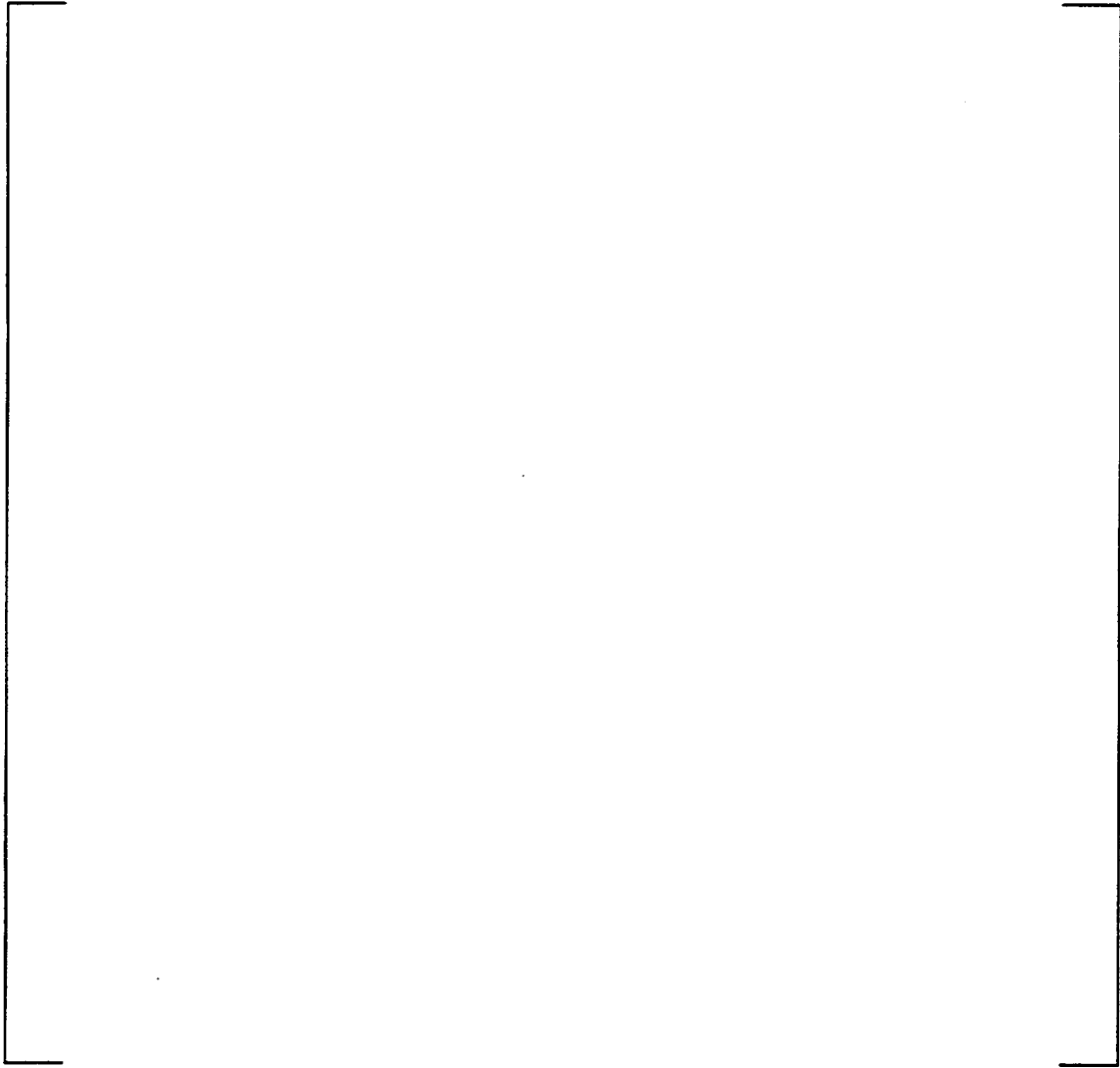
**Fission Gas Release Data (Measured 1-3 %)  
Predicted vs. Measured**



a, b, c

Figure 3.8

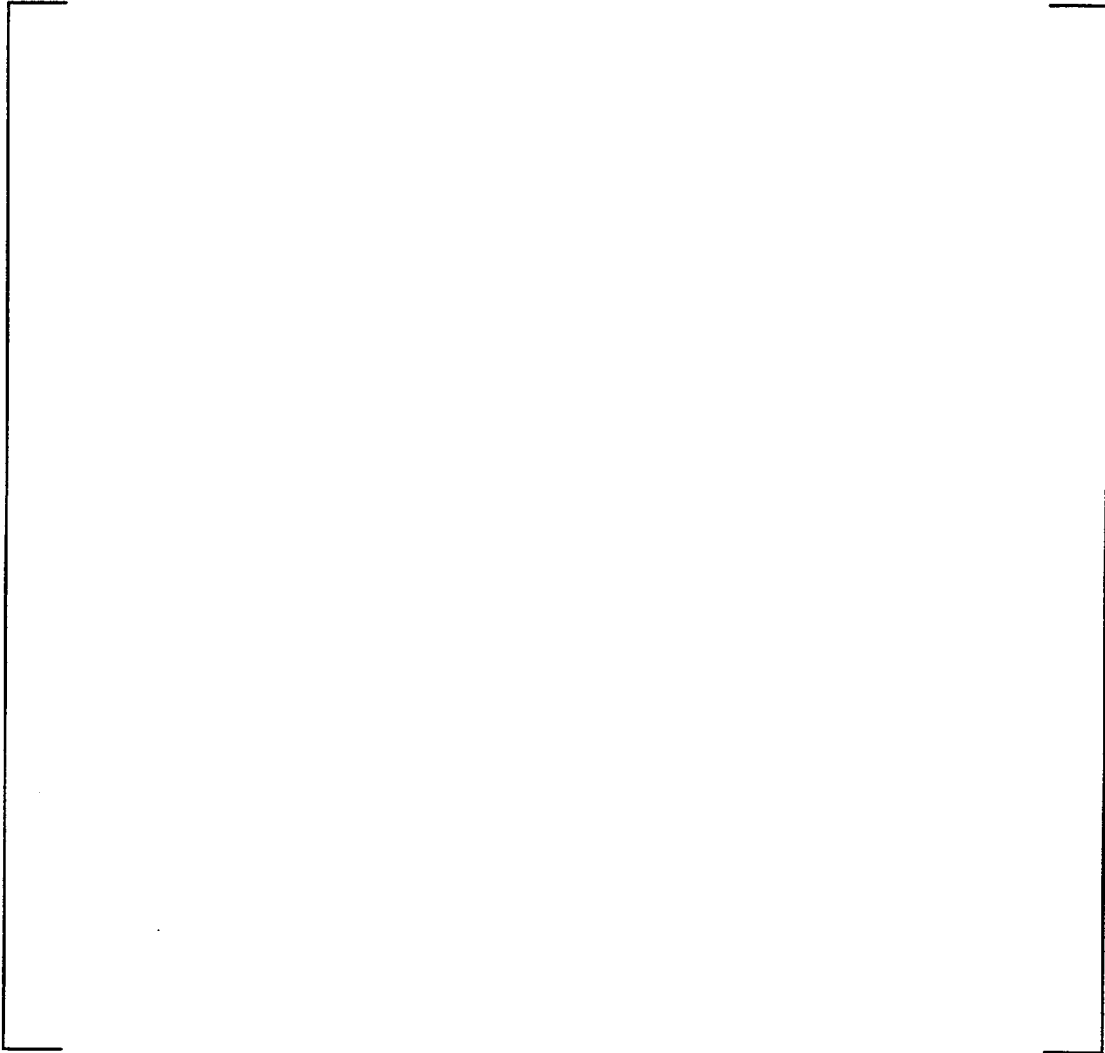
**Steady-State Fission Gas Release  
High-Temperature Predicted vs. Measured**



a, b, c

Figure 3.9

**Steady-State Fission Gas Release  
High-Temperature Predicted vs. Measured  
(measured > 10%)**



a, b, c

Figure 3.10

**Steady-State Fission Gas Release  
High-Temperature Measured-Predicted vs. Burnup**

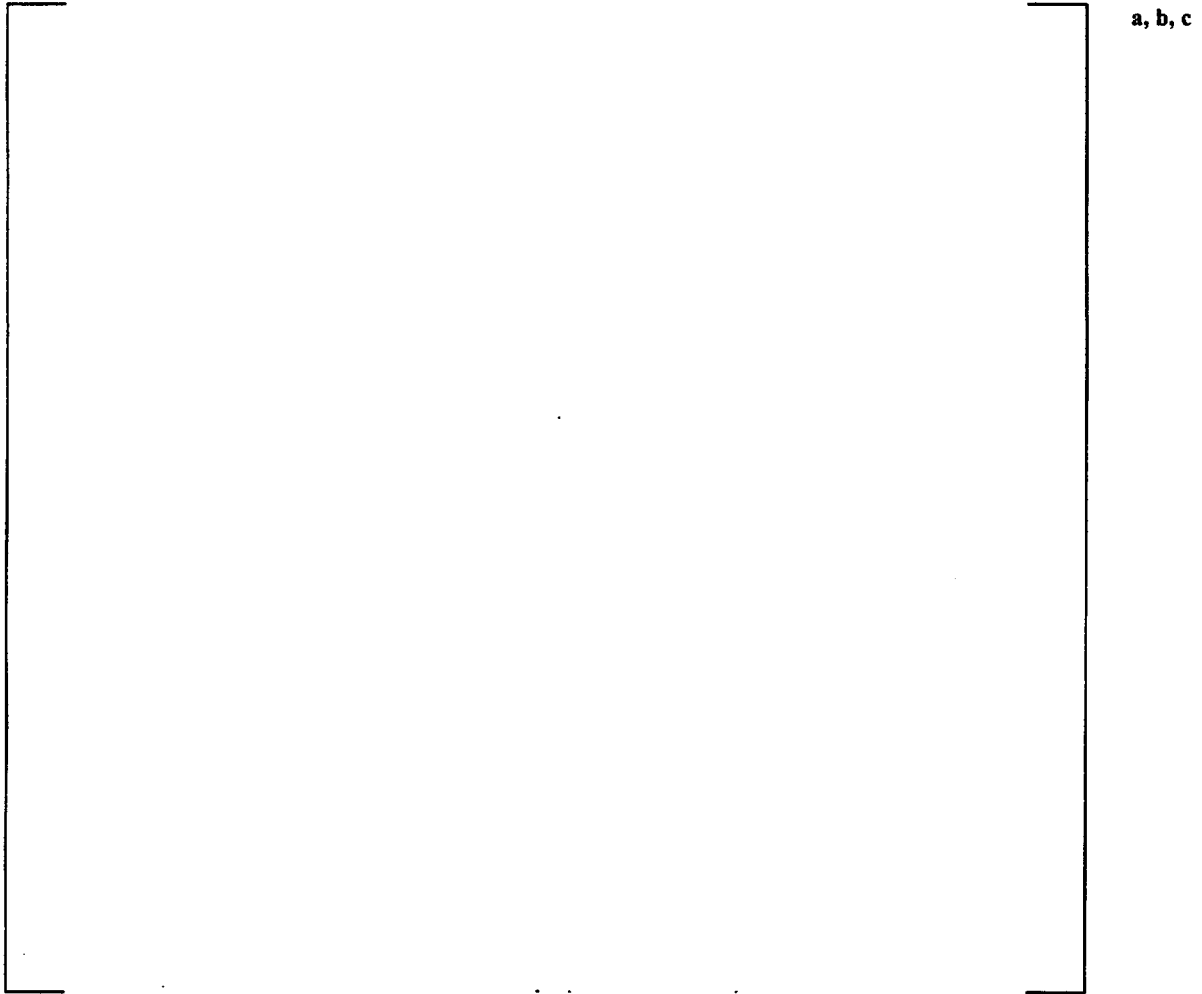


Figure 3.11

**Steady-State Fission Gas Release  
High-Temperature Measured-Predicted vs. Burnup  
(Measured > 10%)**

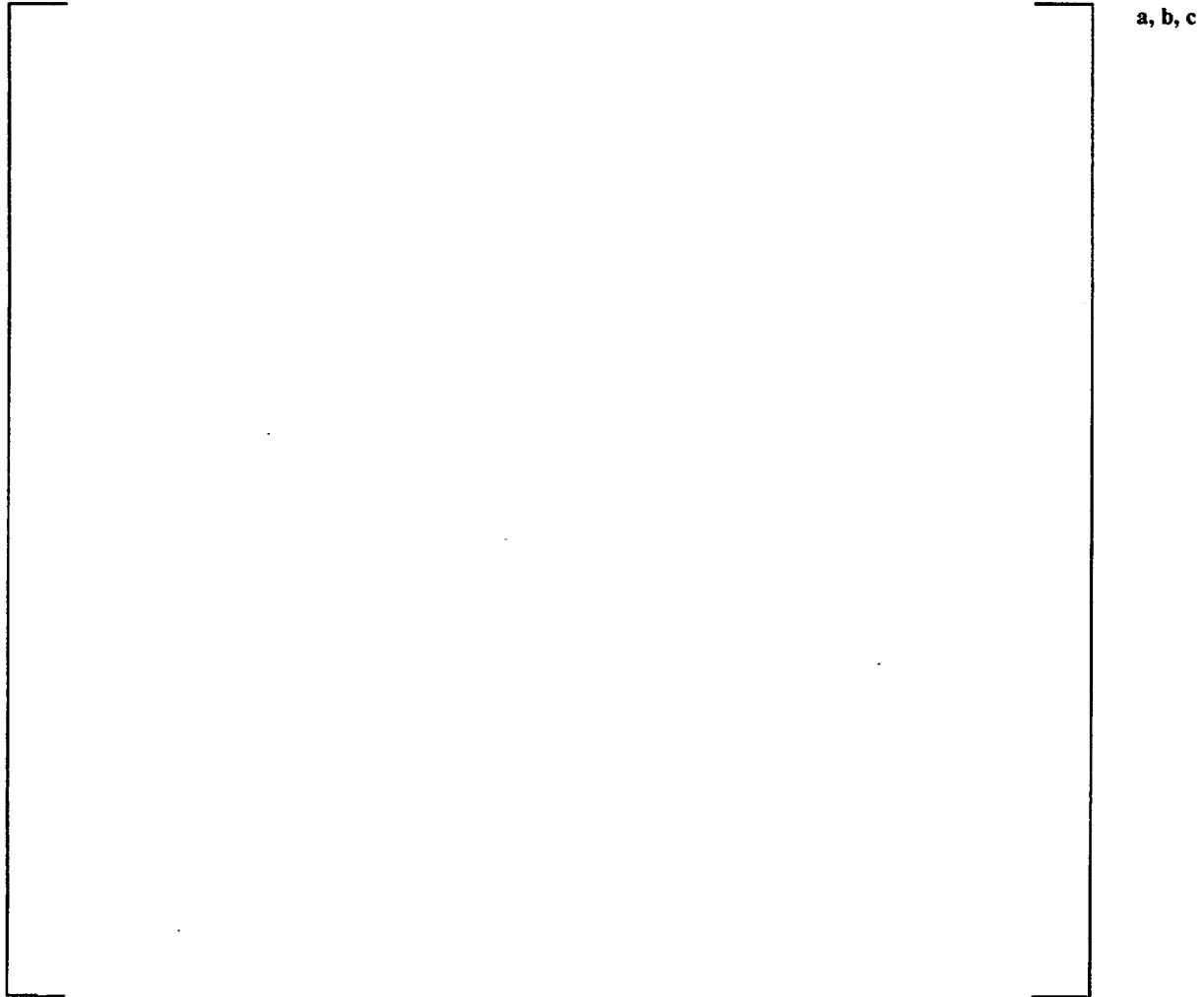
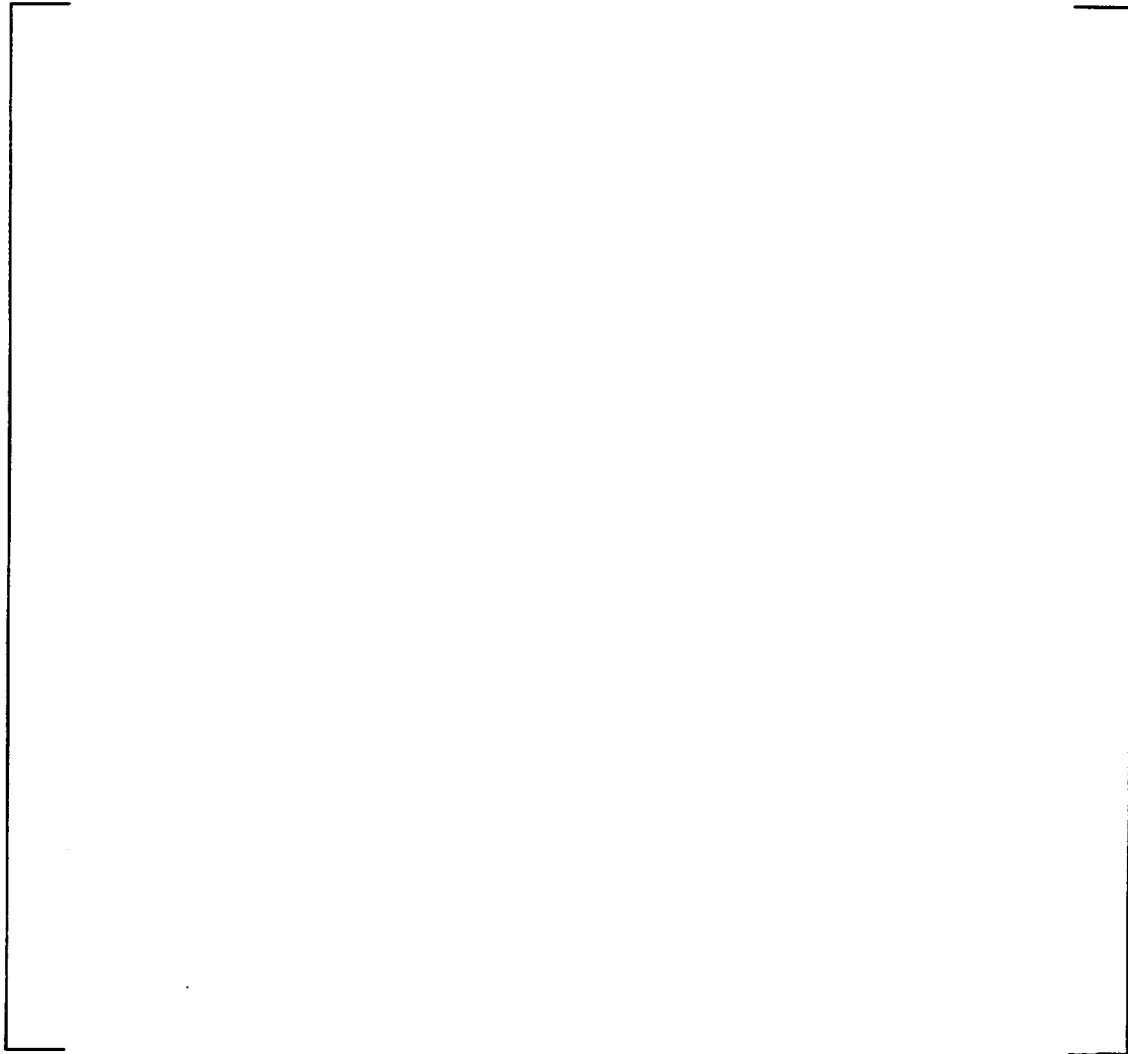


Figure 3.12

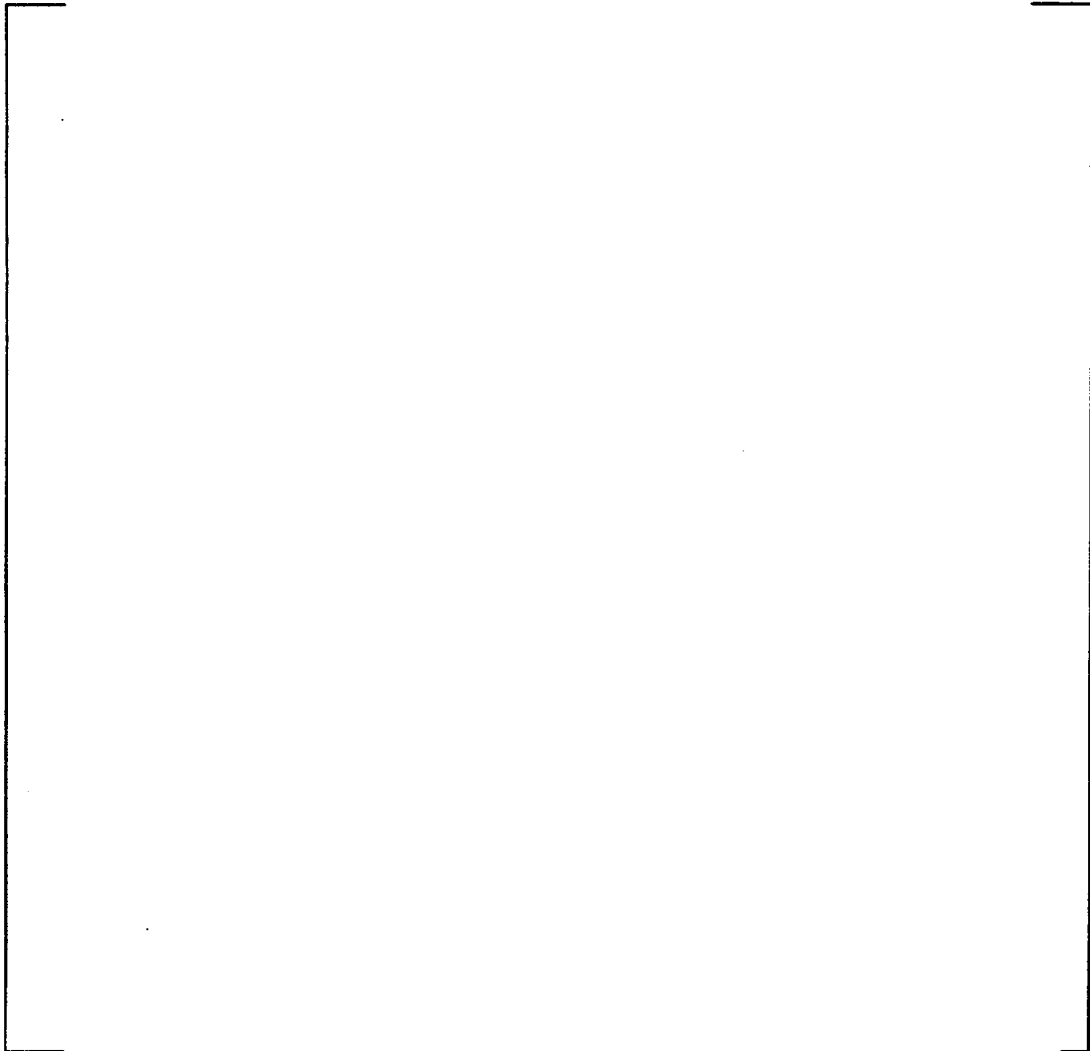
**Transient Fission Gas Release  
Predicted vs. Measured**



a, b, c

Figure 3.13

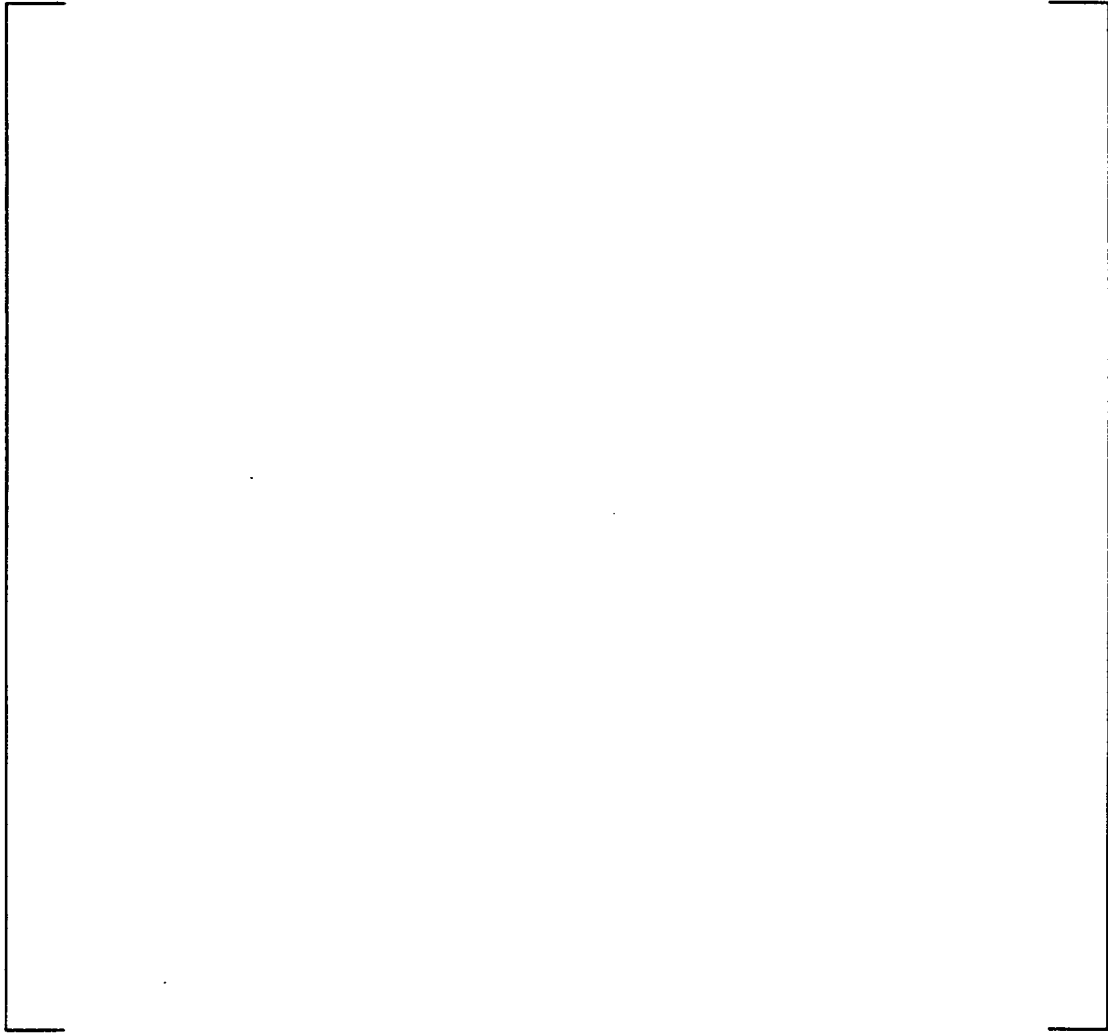
**Transient Fission Gas Release  
Predicted vs. Measured  
(Measured > 10)**



a, b, c

Figure 3.14

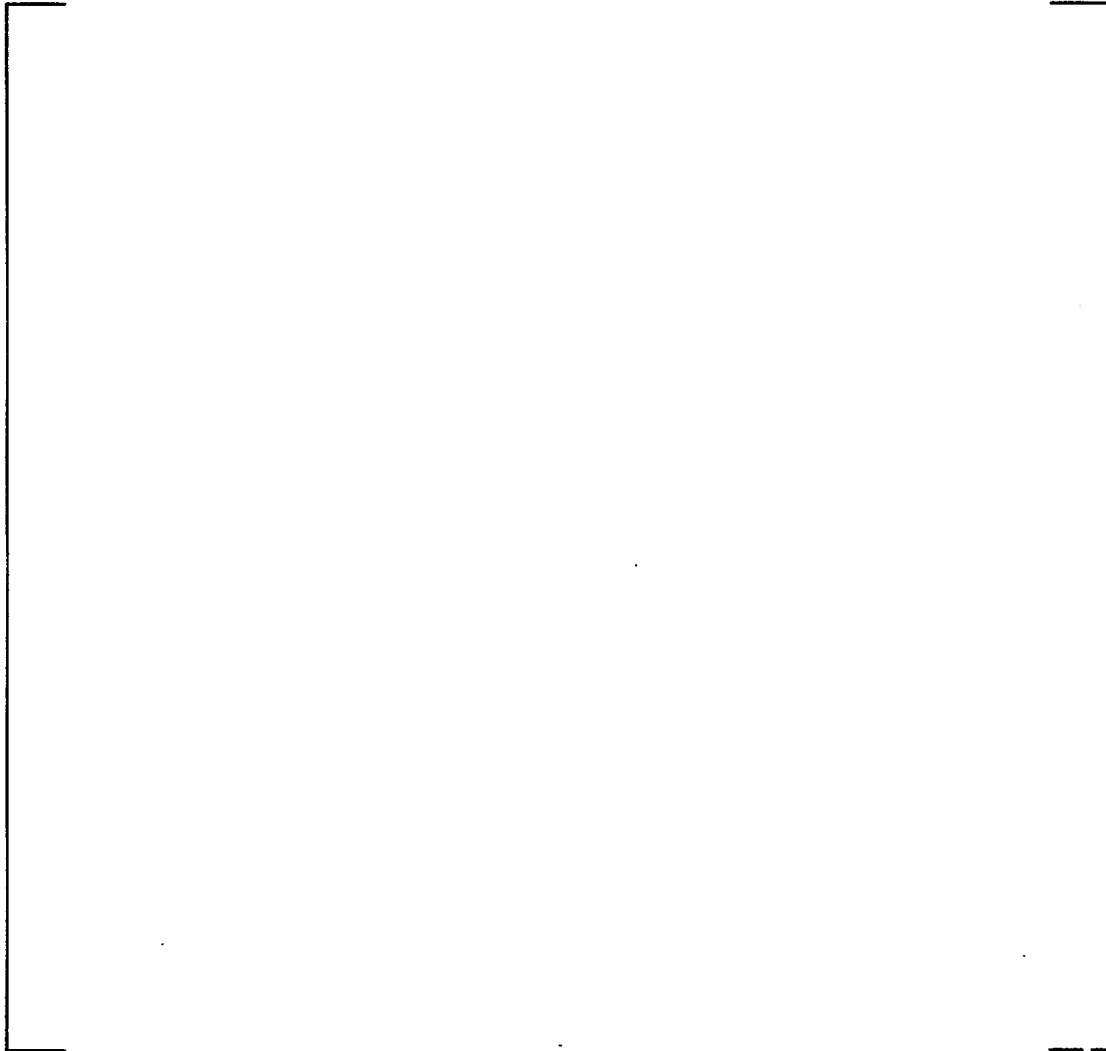
**Transient Fission Gas Release  
Measured-Predicted vs. Burnup**



a, b, c

Figure 3.15

**Transient Fission Gas Release  
Measured-Predicted vs. Burnup  
(Measured > 10%)**



a, b, c

Figure 3.16

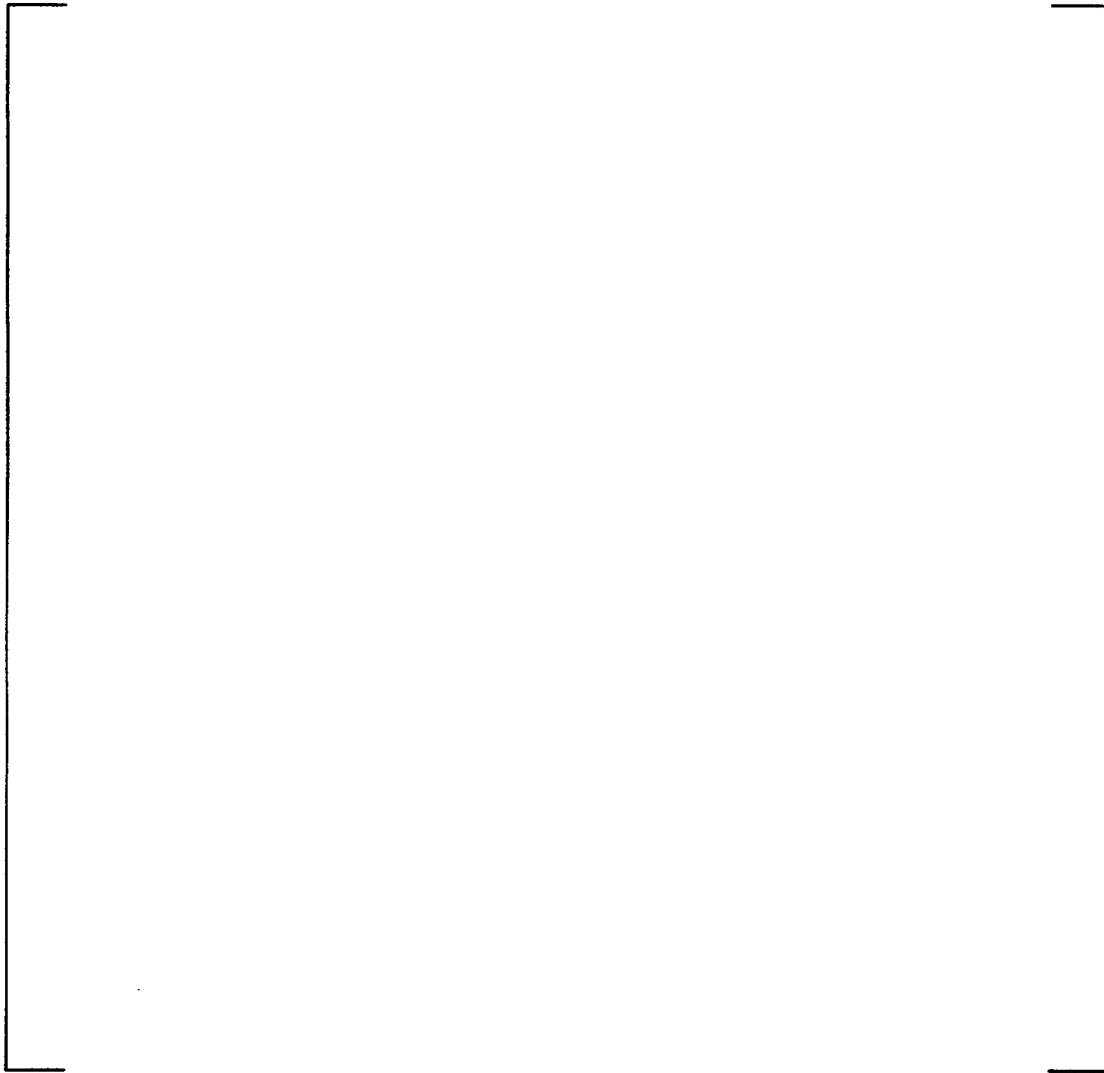
**Transient Fission Gas Release: Gadolinia Database  
Measured-Predicted vs. Burnup  
(Oconee Rods)**



a, b, c

Figure 3.17

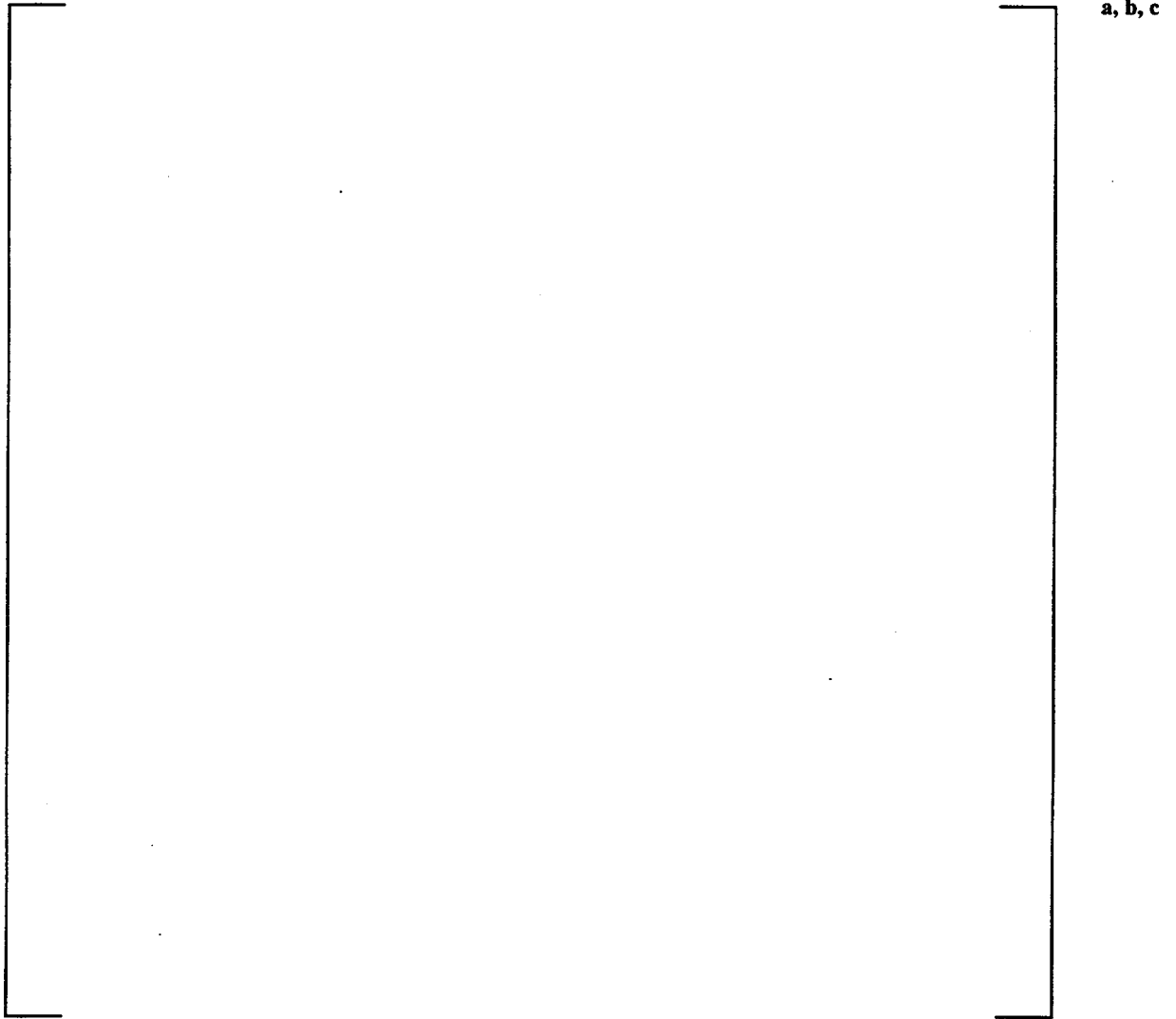
**Steady-State Data w/ AFGRL at 2.30  
Predicted vs. Measured**



a, b, c

Figure 3.18

**Steady-State Data w/ AFGRL at 0.47  
Predicted vs. Measured**



## References:

1. "Westinghouse In-Reactor Creep Model," WCAP-15063-P, June 1998.
2. "Revised PAD Code Thermal Safety Model," WCAP-8720, Addenda 2, October 1982.
3. Lanning, D. D., et al., "Irradiation History and Final Post-irradiation Data for IFA-432," NUREG/CR-4717, PNL-5971, November 1986.
4. Hann, C. R., et al., "Test Design, Pre-characterization, and Fuel Assembly Fabrication for Instrumented Fuel Assemblies IFA-431, and IFA-432," NUREG/CR-0332, BNWL-1988, R3, November 1977.
5. Bradley, E. R., et al., "Pre-characterization Report for Instrumented Nuclear Fuel Assembly IFA-513," NUREG/CR-1077, PNL-3156, R-3, November 1979.
6. Hann, C. R., et al., "Data Report for the NRC/PNL Halden Assembly IFA-431," PNL-2494, April 1978.
7. Hann, C. R., et al., "Data Report for the NRC/PNL Halden Assembly IFA-432," NUREG/CR-0560, PNL-2673, 1978.
8. Bradley, E. R., et al., "Data Report for the NRC/PNL Halden Assembly IFA-432: April 1978-May 1980," NUREG/CR-1950, PNL-3709, April 1981.
9. Bradley, E. R., et al., "Data Report for the Instrumented Fuel Assembly IFA-513," NUREG/CR-1838, PNL-3637, August 1981.
10. "Response to NRC Questions on Westinghouse Topical Report, WCAP-10851 (Proprietary), "Improved Performance Models for Westinghouse Fuel Rod Design and Safety Evaluations"," NS-NRC-86-3163, September 30, 1986.
11. Hann, C. R., et al., "Data Report for the NRC/PNL Halden Assembly IFA-431," PNL-2494, April 1978.
12. Bradley, E. R., et al., "Data Report for the Instrumented Fuel Assembly IFA-513," NUREG/CR-1838, PNL-3637, August 1981.
13. Hann, C. R., et al., "Data Report for the NRC/PNL Halden Assembly IFA-432," NUREG/CR-0560, PNL-2673, 1978.

14. Hann, C. R., et al., "Data Report for the NRC/PNL Halden Assembly IFA-431," PNL-2494, April 1978.
15. Hann, C. R., et al., "Data Report for the NRC/PNL Halden Assembly IFA-432," NUREG/CR-0560, PNL-2673, 1978.
16. Bradley, E. R., et al., "Data Report for the Instrumented Fuel Assembly IFA-513," NUREG/CR-1838, PNL-3637, August 1981.
17. WCAP-10851-P-A, "Improved Fuel Performance Models for Westinghouse Fuel Rod Design and Safety Evaluations," WCAP-10851-P-A, August 1988.